

HYDRAULIC PARAMETER ESTIMATION USING AQUIFER TESTS, SPECIFIC  
CAPACITY, OCEAN TIDES, AND WAVE SETUP FOR HAWAI'I AQUIFERS

A DISSERTATION SUBMITTED TO THE GRADUATE DIVISION OF THE  
UNIVERSITY OF HAWAI'I IN PARTIAL FULFILLMENT OF THE  
REQUIREMENTS FOR THE DEGREE OF

DOCTOR OF PHILOSOPHY

IN

GEOLOGY AND GEOPHYSICS

DECEMBER 2007

By  
Kolja Rotzoll

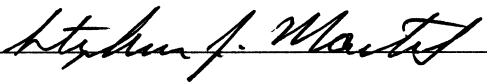
Dissertation Committee:

Aly I. El-Kadi, Chairperson  
Stephen J. Martel  
Janet M. Becker  
Chittaranjan Ray  
Ali Fares

We certify that we have read this dissertation and that, in our opinion, it is satisfactory in scope and quality as a dissertation for the degree of Doctor of Philosophy in Geology and Geophysics.

DISSERTATION COMMITTEE

  
\_\_\_\_\_  
Chairperson

  
\_\_\_\_\_

  
\_\_\_\_\_

  
\_\_\_\_\_

  
\_\_\_\_\_

## **Acknowledgments**

I would like to thank my committee members for their help and support towards graduation: Dr. Aly El-Kadi supervised me and supported me outstandingly through all the years to pursue my goals; Dr. Janet Becker taught me math and inspired me to use MATLAB; Dr. Stephen Martel helped me to fine-tune my scientific writing; Dr. Ali Fares and Dr. Chittaranjan Ray introduced me to unsaturated-zone hydraulics. All members assisted me on various aspects of my research and I am grateful for the useful discussions. Many thanks to Dr. Mark Merrifield for helpful information about tides and setup, Dr. Pål Wessel for assistance with data-analysis techniques, and Dr. Hailong Li for reviewing and considerably improving the dual-tide section.

My appreciation goes to the USGS Pacific Island Water Science Center for funding parts of the research and thereby providing the data sets that were substantial for this work. Especially, I would like to thank Stephen Gingerich, who supervised me during my internship at the USGS. I enjoyed the numerous constructive discussions with Delwyn Oki, Charles Hunt, Scott Izuka, and Jeff Perrault. I am grateful to Todd Presley and Thomas Vana for helpful comments and assistance in the data collection. Also, many thanks to Devin Galloway and Keith Halford for inspiring me to investigate aquifer-parameter estimation methods.

Further, I would like to thank Glenn Bauer and Kevin Gooding, formerly Commission on Water Resources Management, for providing access to aquifer-test data and Hawaii's state well database.

Although not related to this research, I would like to acknowledge Dan Chang from the Department of Health, Safe Drinking Water Branch for funding me for two years on the Source Water Assessment Program and Jeff Hart from The Environmental Company, Inc. for funding me for one year on the Red Hill Fuel Storage Tank Flow Model study.

I would like to recognize my fellow students: Todd Bianco and Eric Mittelstaedt for entertaining discussions and sharing the office of the Hot Spot Distinguished Academic Society; Volker Röber for many GIS questions and providing bathymetry data; Thomas Decloedt and Jonathan Weiss for their thoughts; and Jerome Aucan for providing the Kihei tide data. Special thanks go to Robert Whittier who helped me effortlessly on many occasions and who was instrumental in my career at graduate school by opening doors to agencies outside the university.

Exceptional appreciation goes to my parents, Inge and Frieder, for endless devotion and encouragement, and last but not least, Eisbär and Janosch for all the joy and love you bring in my world.

## **Abstract**

The islands of Hawaii face increasing ground-water demands due to population growth in the last decades. Analytical and numerical models are essential tools for managing sustainable ground-water resources. The models require estimates of hydraulic properties, such as hydraulic conductivity and storage parameters. Four methods were evaluated to estimate hydraulic properties for basalts on the island of Maui. First, unconventional step-drawdown tests were evaluated. The results compare favorably with those from classical aquifer tests with a correlation of 0.81. Hydraulic conductivity is log-normally distributed and ranges from 1 to 2,500 m/d with a geometric mean of 276 m/d and a median of 370 m/d. The second approach developed a simplified parameter-estimation scheme through an empirical relationship between specific capacity and hydraulic parameters that utilized Hawaii's state well database. For Maui's basalts, the analysis yields a geometric-mean and median hydraulic conductivity of 423 and 493 m/d, respectively. Results from aquifer tests and specific-capacity relationships were used to generate island-wide hydraulic-conductivity maps using kriging. The maps are expected to be of great benefit in absence of site-specific field assessments. In the third approach, ocean-tide responses in the central Maui aquifer were used to estimate an effective hydraulic diffusivity of  $2.3 \times 10^7 \text{ m}^2/\text{d}$ . The position of the study area necessitated refining the existing analytical solution that considers asynchronous and asymmetric tidal influence from two sides in an aquifer. Finally, measured ground-water responses to wave setup were used to estimate hydraulic parameters. Setup responses were significant as far as 5 km inland and dominated barometric-pressure effects during times of energetic

swell events. The effective diffusivity estimated from setup was  $2.3 \times 10^7 \text{ m}^2/\text{d}$ , matching that based on tides. Additionally, simple numerical ground-water flow models were developed to assess the accuracy of results from analytical solutions for step-drawdown tests, dual-tides and wave setup, and to evaluate sediment-damping effects on tidal propagation. The estimated mean hydraulic conductivities of the four methods range between 300 and 500 m/d for basalts in Maui. The results of different methods are consistent among each other and match previous estimates for basalts.

## Table of Contents

Acknowledgments.....	iii
Abstract.....	v
List of Tables .....	x
List of Figures.....	xii
List of Abbreviations and Symbols.....	xv
Preface.....	xix
1. Introduction.....	1
2. Site Characterization and Hydrogeology .....	4
Physical Setting .....	4
Hydrogeology .....	5
Flank Lavas .....	5
Dikes.....	6
Sediments .....	6
Ground Water .....	7
Aquifer Parameters .....	8
Flank Lava.....	8
Dike Zone.....	9
Sediment.....	9
Porosity and Aquifer Storage .....	10
3. Constant-Rate and Variable-Rate Aquifer Tests.....	11
Introduction.....	11
Methodology.....	15
Analytical Solutions .....	15
Theis Method.....	15
Cooper–Jacob Method.....	16
Theis Recovery Method .....	17
Harr Method .....	17
Zangar Method .....	18

Polubarinova Method .....	19
Thomasson Method .....	20
Data Analysis.....	22
Geostatistical Analysis .....	24
Numerical Model.....	26
Results and Discussion .....	27
Aquifer Tests .....	27
Geostatistical Analysis .....	35
Numerical Model.....	40
Chapter 3 Conclusions.....	41
4. Relationship between Hydraulic Conductivity and Specific Capacity .....	43
Introduction.....	43
Approaches .....	44
Relationship between Transmissivity and Specific Capacity.....	44
Well-Loss Correction .....	47
Aquifer-Parameter Analysis .....	48
Hydraulic-Conductivity Estimation.....	50
Geostatistical Analysis .....	51
Results and Discussion .....	51
Empirical Relationships.....	51
Hydraulic-Conductivity Estimation.....	58
Geostatistical Analysis .....	62
Chapter 4 Conclusions.....	68
5. Ocean Tides and Dual-Tide Influence .....	70
Introduction.....	70
Analytical Solution .....	73
Dual-Tide Solution.....	73
Aquifer Parameters.....	78
Approaches .....	79
Data Collection.....	79
Data Analysis.....	82
Numerical Model.....	84
Results and Discussion .....	85
Aquifer Parameters.....	85

Numerical Model.....	96
Dual Tide.....	98
Chapter 5 Conclusions.....	101
6. Wave Setup.....	103
Introduction.....	103
Study Site.....	105
Approaches.....	107
Data Collection.....	107
Data Filtering.....	108
Wave Setup.....	111
Cross-Correlation and Regression Analysis.....	112
Aquifer Parameters.....	114
Numerical Model.....	115
Results and Discussion.....	116
Regression Analysis.....	117
Aquifer Parameters.....	121
Numerical Model.....	127
Chapter 6 Conclusions.....	129
7. Summary and Conclusions.....	131
Aquifer Tests.....	131
Relationship between Hydraulic Conductivity and Specific Capacity.....	132
Ocean Tides and Dual-Tide Influence.....	133
Wave Setup.....	134
Comparison of Hydraulic-Parameter Estimation Methods.....	135
Future Research.....	137
8. Appendix A. Results of Aquifer-Test Analysis.....	140
9. References.....	144

## List of Tables

Table 3.1. Equations to estimate hydraulic parameters from constant- and variable-rate single-well aquifer tests .....	21
Table 3.2. Summary statistics of hydraulic-conductivity estimates from different analytical solutions for dike-free basalts in Maui .....	31
Table 3.3. Summary statistics of hydraulic-conductivity estimates from different analytical solutions for sediments in Maui .....	31
Table 3.4. Summary statistics of hydraulic-conductivity estimates for three geologic groups: Wailuku Basalt, Honomanu/Kula Basalt, and sediment .....	34
Table 4.1. Summary and results of previous studies that examined empirical relationships between transmissivity and specific capacity .....	46
Table 4.2. Results from the regression analysis of transmissivity and hydraulic conductivity to specific-capacity ratios for Hawaii volcanic aquifers .....	52
Table 4.3. Summary statistics of hydraulic-conductivity estimates from specific capacity for dike-free basalts in the state of Hawaii .....	62
Table 5.1. Information about ground-water monitoring points and time series .....	81
Table 5.2. Standard deviation and normalized standard deviation of the estimated tidal responses based on 32-day subsets .....	87
Table 5.3. Difference between estimated tidal response from the entire dataset and the arithmetic mean of 32-day subsets .....	88
Table 5.4. Estimated tidal responses based on the arithmetic mean of 32-day time series .....	89
Table 5.5. Estimated y-intercepts and numerically estimated sediment-damping factors of one-sided tidal-propagation scenarios .....	91
Table 5.6. Summary of one-sided tidal-propagation scenarios .....	93
Table 5.7. Estimated hydraulic diffusivities and slope factors of one-sided tidal-propagation scenarios .....	94

Table 5.8. Error summary of the different analytical solutions for the entire time series observed in Pump 7 and for the subset shown in Figure 5.8 .....	100
Table 6.1. Barometric loading efficiencies for monitoring points.....	110
Table 6.2. Estimated setup responses for $\eta_V$ and $\eta_S$ at observation points in the aquifer analyzing the entire signal .....	121
Table 6.3. Estimated wave setup responses for $\eta_V$ at observation points in the aquifer analyzing the decomposed signal .....	123
Table 6.4. Estimated wave setup responses for $\eta_S$ at observation points in the aquifer analyzing the decomposed signal .....	123
Table 6.5. Hydraulic diffusivity and conductivity estimated analytically and numerically from setup using discrete frequencies, the complete time series, and ocean tides.....	126
Table 6.6. Error summary of observed against calculated setup responses.....	128
Table 7.1. Hydraulic diffusivity and conductivity estimated from various analytical methods for dike-free basalts in Maui, Hawaii .....	135

## List of Figures

Figure 2.1. Location map of Maui, Hawaii, showing residential areas and major roads .....	4
Figure 3.1. Location of wells with aquifer-test data on Maui, as indicated by the main intersected geology .....	23
Figure 3.2. Probability distribution of hydraulic conductivity in a log-normal diagram .....	27
Figure 3.3. Log-log plot of the mean of the two hydraulic-conductivity estimates from the Harr method against the mean of the two hydraulic-conductivity estimates from traditional constant-rate tests .....	28
Figure 3.4. Log-log plot of the mean of the three hydraulic-conductivity estimates from step-drawdown tests against the mean of the two hydraulic-conductivity estimates from traditional constant-rate tests .....	30
Figure 3.5. Location and magnitude of hydraulic conductivity for (a) constant-rate aquifer tests, (b) recovery tests, (c) step-drawdown tests, and (d) all tests combined for each well.....	33
Figure 3.6. Box-and-whisker diagram for three hydrogeologic units: Wailuku Basalt, Honomanu/Kula Basalt and sediment .....	36
Figure 3.7. Experimental variogram and fitted spherical model for hydraulic conductivity on Maui.....	37
Figure 3.8. (a) Estimated hydraulic-conductivity map for Maui using ordinary kriging and (b) kriged standard error of the hydraulic-conductivity estimate.....	39
Figure 3.9. Relationship of well loss and aquifer loss to total loss in a step-drawdown test.....	41
Figure 4.1. Location of wells on Maui, as indicated by type of aquifer tests conducted.....	48
Figure 4.2. (a) Plot of transmissivity from constant-rate and step-drawdown tests against specific capacity from constant-rate and step-drawdown tests, uncorrected for well loss. (b) Plot of transmissivity from constant-rate and step-drawdown tests against specific capacity per unit aquifer penetration from step-drawdown tests, uncorrected for well loss .....	53

Figure 4.3. (a) Plot of hydraulic conductivity from constant-rate and step-drawdown tests against specific capacity from constant-rate and step-drawdown tests, uncorrected for well loss. (b) Plot of hydraulic conductivity from constant-rate and step-drawdown tests against specific capacity per unit aquifer penetration from step-drawdown tests, uncorrected for well loss .....	55
Figure 4.4. (a) Plot of hydraulic conductivity from constant-rate and step-drawdown tests against specific capacity from constant-rate and step-drawdown tests, corrected for well loss. (b) Plot of hydraulic conductivity from constant-rate and step-drawdown tests against specific capacity per unit aquifer penetration from step-drawdown tests, corrected for well loss .....	57
Figure 4.5. Hydraulic-conductivity estimates from specific capacity, and outline of dike-zone complexes (Stearns and Macdonald 1963) in the state of Hawaii .....	60
Figure 4.6. Box-and-whisker diagram for the hydraulic-conductivity estimates of dike-free volcanic rocks for five islands and for the state of Hawaii .....	61
Figure 4.7. Experimental variogram of the spatial correlation of hydraulic conductivity for Oahu and Maui, and the spherical model fit .....	63
Figure 4.8. (a) Estimated hydraulic-conductivity map of dike-free volcanic rocks for the island of Oahu. (b) Predicted standard error map for Oahu .....	65
Figure 4.9. (a) Estimated hydraulic-conductivity map of dike-free volcanic rocks for the island of Maui. (b) Predicted standard error map for Maui .....	67
Figure 5.1. Schematic cross section of an unconfined dual-tide aquifer with sediment cover at the boundary .....	74
Figure 5.2. Location of the study area and central Maui surface-geology map (modified from Stearns and Macdonald 1942) with monitoring points and tide gages .....	80
Figure 5.3. Amplitude spectra at a 5-min sampling interval (a) for a 425-day ocean-tide time series from Kahului Harbor and (b) for a 425-day observed-head time series in Pump 7 .....	86
Figure 5.4. Time lag for the monitoring points calculated from cross correlation .....	89
Figure 5.5. (a) Estimated modal attenuation and (b) phase difference against distance from Kahului .....	92

Figure 5.6. Hydraulic-diffusivity curves of $2.3 \times 10^7 \text{ m}^2/\text{d}$ for plausible ranges of aquifer thickness, hydraulic conductivity, and specific-yield values .....	95
Figure 5.7. Numerical simulation of the capping boundary effect. Plot (a) showing calculated water levels in the ocean and the cell adjacent to the capping unit at each boundary. Plot (b) showing observed and calculated water levels on the north side of the isthmus .....	97
Figure 5.8. Analytical solutions for tide-induced head fluctuations for Sc2 at Pump 7 against observed head .....	99
Figure 6.1. Cross-shore profile A-A' illustrating the effect of wave breaking, with wave setup occurring outside the breaker zone, and wave setup ( $\eta$ ) occurring inside the surf zone and at the coast.....	104
Figure 6.2. (a) Map showing the study area and offshore wave buoys. (b) Observation points in the study area, bathymetry of the coastal region, and trace of cross-shore profile A-A' shown in Figure 6.1 .....	106
Figure 6.3. (a) Barometric pressure, (b) filtered and detrended water levels, and (c) water levels corrected for barometric fluctuations for the SWELL subset .....	109
Figure 6.4. (a) Significant wave height at Waimea Buoy and estimated wave height at Kahului, (b) dominant wave period at Waimea Buoy, (c) dominant wave direction at Waimea Buoy, (d) estimated wave setups, and (e) filtered and detrended barometric pressure for the observation period.....	113
Figure 6.5. Single- and multi-variable regression of filtered water levels at CPP to setup $\eta_S$ and barometric pressure (a) for the SWELL subset and (b) for the BARO subset.....	118
Figure 6.6. Correlation coefficients of the regression analysis (a) for the SWELL subset with $\eta_V$ , and (b) with $\eta_S$ , (c) for the BARO subset with $\eta_V$ , and (d) with $\eta_S$ .....	119
Figure 6.7. Amplitude spectra of the SWELL subset for (a) setup $\eta_V$ and $\eta_S$ , and (b) observed head, corrected for barometric-pressure effects .....	122
Figure 6.8. Amplitude attenuation for setup propagation of (a) $\eta_V$ and (b) $\eta_S$ , and phase difference for setup propagation of (c) $\eta_V$ and (d) $\eta_S$ in the aquifer.....	124
Figure 6.9. Observed (symbols) and calculated (lines) water levels using 1-D MODFLOW modeling to simulate wave-setup attenuation in the aquifer.....	128

## List of Abbreviations and Symbols

$a$	tidal propagation factor ( $m^{-1}$ )
$A_1$	amplitude attenuation of the oscillation in one side of the aquifer (dimensionless)
$A_2$	amplitude attenuation of the oscillation in the other side of the aquifer (dimensionless)
amsl	above mean sea level
$b$	aquifer thickness (m)
$B$	aquifer-loss coefficient ( $d/m^2$ )
$B_e$	barometric efficiency coefficient
$\beta$	foreshore beach slope (rad)
bmsl	below mean sea level
$c$	regression exponent (dimensionless)
$C$	well-loss coefficient ( $d^2/m^5$ for $w = 2$ )
CDIP	Coastal Data Information Program
cm	centimeter
CWRM	State of Hawaii, Department of Land and Natural Resources, Commission on Water Resources Management
d	day
$d$	range (m)
$D$	complex constant
$D^*$	mean hydraulic diffusivity from $D_{amp}$ and $D_{pha}$ ( $m^2/d$ )
$D_{amp}$	hydraulic diffusivity from attenuation ( $m^2/d$ )
$D_{pha}$	hydraulic diffusivity from phase difference ( $m^2/d$ )
deg	degree
$E_1$	sediment damping coefficient at one boundary (dimensionless)
$E_2$	sediment damping coefficient at the opposite boundary (dimensionless)
$\Phi_1$	phase difference between the oscillation in the aquifer and at one boundary (rad)
$\Phi_2$	phase difference between the oscillation in the aquifer and the opposite boundary (rad)
$f_1$	regression coefficient (dimensionless)
$f_2$	regression coefficient

$F$	complex constant
$g$	acceleration due to gravity ( $\text{m/s}^2$ )
$\gamma$	variogram, degree of spatial dependence ( $\text{m}^2/\text{d}^2$ )
$\eta$	wave setup (m)
$\eta_s$	wave setup, estimated after Stockdon (2006) (m)
$\eta_v$	wave setup, estimated after Vetter (2007) (m)
$G_0$	nugget ( $\text{m}^2$ )
$G_1$	sill ( $\text{m}^2$ )
h	hour
$h$	piezometric head (m)
$H_1$	amplitude of the harmonic oscillation at the boundary (m)
$H_2$	amplitude of the harmonic oscillation at the opposite boundary (m)
$H_s$	significant wave height (m)
$H_{sK}$	significant wave height Kahului (m)
$H_{sO}$	significant wave height offshore (m)
$i$	imaginary part of the complex expression
$j$	running number of tidal constituents
$K$	hydraulic conductivity (m/d)
$K_1$	lunar-solar diurnal tidal mode
km	kilometer
$L$	active length or screened interval of the well (m)
$l$	lag or distance between the sampling points (m)
$\Lambda$	an unknown complex function
m	meter
$m$	number of tidal modes
Ma	million years
$M_2$	main lunar semidiurnal tidal mode
min	minute
MODFLOW	USGS modular ground-water flow model
$n$	sample size
$N_2$	lunar elliptic tidal mode
NCDC	National Climatic Data Center

NDBC	National Data Buoy Center
NOAA	National Oceanographic and Atmospheric Administration
$O_1$	main lunar diurnal tidal mode
$P$	dominant wave period (s)
$P_{iv}$	prediction interval
PEST	automated parameter estimation model
$Q$	discharge ( $m^3/d$ )
$R$	correlation coefficient
$r$	radius of the pumped well (m)
$r_2$	radius of influence of the pumped well (m)
rad	radian
Re	real part of the complex expression
$r_h$	hemispherical radius of pumped well (m)
$S$	storativity for confined aquifers, specific yield for unconfined aquifers (dimensionless)
$S_2$	main solar semidiurnal tidal mode
Sc1	dual-tide scenario 1
Sc2	dual-tide scenario 2
$S_C$	specific capacity ( $m^2/d$ )
sec	second
$SF$	slope factor (dimensionless)
$s_s$	steady-state well drawdown (m)
$\Delta s_s$	drawdown or recovery per log cycle
$\sigma$	standard deviation
$t$	time (d)
$T$	transmissivity ( $m^2/d$ )
TN	true north (north = $0^\circ$ , east = $90^\circ$ , west = $-90^\circ$ )
$\tau$	period of the oscillation (d)
$\theta$	dominant wave direction (degree true north)
$t_{\alpha/2}$	critical value of Student $t$ -distribution for the significance level $\alpha$ with $n-2$ degrees of freedom
USGS	United States Geologic Survey
$\varphi_1$	sediment damping phase shift at one boundary (dimensionless)

$\varphi_2$	sediment damping phase shift at the opposite boundary (dimensionless)
$v$	dependent variable of the prediction interval
$\hat{v}$	predicted value of the dependent variable using the regression
$w$	well-loss exponent
$W(u)$	Theis well function
$\omega$	angular frequency ( $d^{-1}$ )
$x$	distance from the boundary (m)
$X$	aquifer length (m)
$\psi$	phase lag of ocean tides on opposite sides of the aquifer
$z$	independent variable of the prediction interval
$\hat{z}$	predicted independent variable of the prediction interval
$\bar{z}$	arithmetic mean of the independent variable of the prediction interval

## Preface

The dissertation is organized as follows: A brief introduction covers the purpose, scope, and motivation for the work. The second chapter includes a description of the study area in Maui, Hawaii, and a summary of its hydrogeological aspects. The research consists of four different approaches to estimate hydraulic properties for Hawaii aquifers. Each chapter starts with a brief introduction of the method, literature review, the approach, results, and a summary. The third chapter is published in the Journal of the American Water Resources Association, 2007, 43(2):334-345 with the title "*Estimating hydraulic properties for volcanic aquifers using constant-rate and variable-rate aquifer tests*". Chapter 4 is tentatively accepted for publication in the Hydrogeology Journal with the title: "*Estimating hydraulic conductivity from specific capacity for Hawaii aquifers*". The fifth chapter is accepted for publication in the Journal of Ground Water with the title: "*Analysis of an unconfined aquifer subject to asynchronous dual-tide propagation*". The sixth chapter is submitted to Journal of Hydrology with the title: "*Estimating hydraulic properties for coastal aquifers using wave setup*". Article one and three are co-authored with A.I. El-Kadi and S.B. Gingerich and article two and four with A.I. El-Kadi. Chapter 7 is a summary and compares results from the different methods.

## **1. Introduction**

Many factors can affect water levels in coastal aquifers. Changes can be secular, seasonal, and on shorter time scales. Among the factors responsible for periodic water-level fluctuations are seasonal recharge patterns, seasonal and daily evapotranspiration, semidiurnal atmospheric pressure variations at the surface, diurnal and semidiurnal ocean tides, and earth tides. Aperiodical stresses include local recharge events, pumping, barometric pressure fluctuations as air masses move over land, strong winds (i.e., hurricanes), earthquakes, external loading (i.e., passing trains), and land subsidence (e.g., Fetter 2000; Todd and Mays 2004). Wave setup associated with large swell events is an additional factor, which generally is overlooked.

The need to identify and quantify contributions from all factors is crucial for hydrogeologic assessments. Removal of background noises, such as factors mentioned above that are not of interest in the investigation, is critical for a successful water-level analysis (i.e., analysis of an aquifer test in a tidal-influenced area). Additionally, any perturbation of an aquifer can potentially be used to estimate its hydraulic properties, such as hydraulic conductivity and storage parameters. Estimating hydraulic parameters is the central objective of this dissertation, because essentially all hydrogeologic assessments require estimates of hydraulic parameters to investigate water-supply or water-quality issues (Butler 2005).

As is the case in many parts of the United States and the world, water problems in Hawaii are related to the availability of drinking water and to its contamination by

organic or inorganic chemicals due to land-use activities (El-Kadi and Moncur 2006). Ground water, which is mostly contained in volcanic-rock aquifers, provides about 99% of domestic water use and about 50% of other freshwater uses in Hawaii (Gingerich and Oki 2000). Although all the main islands have large amounts of ground water, the quality may not be appropriate for all applications. While there is a great need to identify new sources for potable water, better management of existing resources is as important (El-Kadi and Moncur 2006).

Aquifer management in Hawaii is based on the concept of aquifer sustainable yield, which is defined as the maximum allowable total daily pumping without compromising storage and water quality. When such a yield is exceeded an increase in salinity may result (e.g., Visher and Mink 1964; Oki 2005). Moreover, water-quality profiles in Hawaii show that the salinity of ground water has increased over the years and the transition zone is undergoing a steady rise (e.g., Meyer and Presley 2000; Oki 2005) due to increasing water demands. The population has increased significantly on all main islands in the last few decades, and residential development plans would continue this trend. Between 1950 and 2000, the population in the state of Hawaii has increase more than 140%. The recent growth is more significant on the islands of Kauai, Maui, and Hawaii. For example, between 1970 and 2000, the population on Maui increased more than 200% (State of Hawaii 2000). Hence, better management of the aquifers is essential to ensure sustainability of Hawaii's ground-water resources.

Aquifer sustainable yield and resource management in Hawaii rely on analytical (Mink 1981; Liu 2006) and numerical models (e.g., Oki 1998; Oki 1999; Izuka and Oki

2002; Oki 2002, 2005, 2006). Both models require values of hydraulic-flow parameters to characterize the formations. Therefore, hydraulic parameters are essential elements for models used to manage ground-water availability and quality. Uncertainty in these parameters results in erroneous model estimates and potentially mismanagement of drinking-water supplies.

Although hydraulic properties of basalts have been investigated for the neighboring island of Oahu (see Hunt 1996), large-scale estimates for Maui are lacking. In this study, four methods were evaluated to estimate hydraulic properties for volcanic rocks on the island of Maui. Unconventional step-drawdown tests were tested against classical constant-rate aquifer tests. To simplify parameter estimation, empirical relationships between specific capacity and hydraulic parameters were developed and applied to the well database of the state of Hawaii. The point estimates from the aquifer tests and the specific-capacity relationship were used to generate island-wide hydraulic-conductivity maps using kriging, which provide an estimate of effective parameters. Ocean tide responses were used to estimate hydraulic diffusivity in the central Maui aquifer. Existing analytical solutions considering tidal forcing were modified to include asynchronous effects from two opposite sides. Finally, measured ground-water responses to wave setup were used to estimate hydraulic parameters. Additionally, simple numerical ground-water flow models were developed to evaluate the accuracy of results from analytical solutions applied to step-drawdown tests, sediment-damping effects at the boundary in tidal propagation, and wave setup responses in the aquifer. Finally, the results from the four different aquifer-parameter estimation methods were compared.

## 2. Site Characterization and Hydrogeology

### Physical Setting

The island of Maui is part of the main islands of Hawaii, which are located almost in the center of the North Pacific Ocean. Maui is the second largest island in the state of Hawaii and covers an area of 1,884 km<sup>2</sup> with 193 km of coastline (Fierstein and Fletcher 2004). The topography is formed by eroded remnants of two shield volcanoes: West Maui Volcano and East Maui Volcano. An isthmus connects the two volcanoes where lava flows coalesced (Figure 2.1).

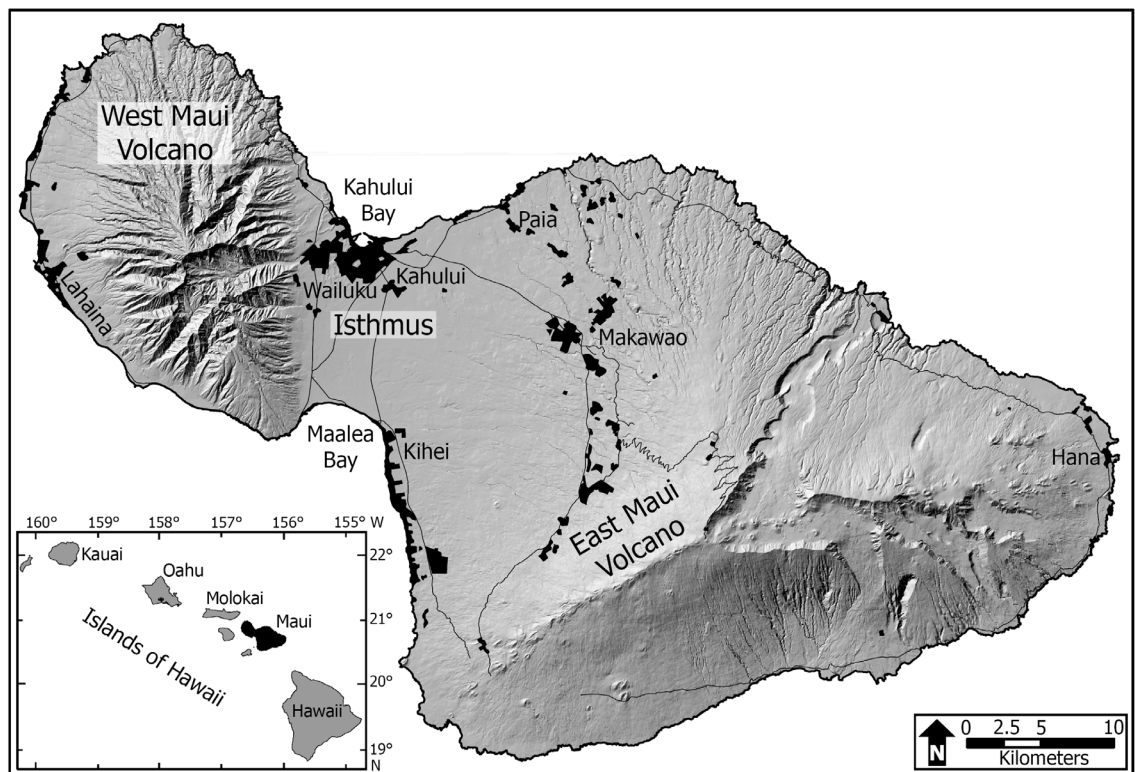


**Figure 2.1.** Location map of Maui, Hawaii, showing residential areas and major roads.

The highest elevation on East Maui Volcano is 3,055 m above mean sea level (amsl); West Maui Volcano ascends to 1,764 m amsl, and the center of the isthmus

reaches to about 40 m amsl. The population of Maui was 117,664 in 2000 (State of Hawaii 2000). The land use is currently in transition from large-scale agricultural practices (sugarcane and pineapple) to diversified cultivation and rapidly expanding urban developments. The main study area is located on the isthmus in central Maui including the eastern edge of West Maui Volcano and the western part of East Maui volcano, although the entire island also is considered for aspects of the research.

### **Hydrogeology**

Stearns and Macdonald (1942) provided a comprehensive description of Maui's geology, while Takasaki (1972) reviewed the hydrogeology of central Maui. Of the two main volcanoes, West Maui Volcano is older than East Maui Volcano. Potassium-argon analyses indicate an age of  $1.32 \pm 0.04$  Ma for basalts from West Maui Volcano (McDougall 1964), and  $0.75 \pm 0.04$  Ma for East Maui Volcano basalts (Naughton et al. 1980).

### ***Flank Lavas***

Thin-bedded shield-building lava flows form most of the flanks of the volcanoes. Flows typically dip about 10 degrees (Stearns and Macdonald 1942). West Maui Volcano is composed primarily of Wailuku Basalt. The west side of East Maui Volcano is comprised primarily of Honomanu Basalt, which is overlain by thicker postshield-stage Kula Volcanics (Langenheim and Clague 1987). The flows of Honomanu Basalt are mainly characterized by thin ( $< 10$  m) pahoehoe flows (Gingerich 1999b). In the Kula Volcanics, on the other hand, massive ( $\sim 20$  m, often  $> 70$  m) aa flows of relatively low permeability that are interbedded with permeable clinker zones dominate over pahoehoe

flows (Takasaki 1972). Since lithologic information is scant, the contact between Honomanu and Kula Basalt in the study area is not well defined. However, the latter formation is potentially thicker on the south than on the north side of the isthmus (Stephen Gingerich, USGS, written commun., 2007).

### ***Dikes***

Rift zones radiate from the calderas of the volcanoes. The rift zone in West Maui Volcano is characterized by a radial pattern within the collapsed caldera and East Maui Volcano has two distinct primary elongated rift zones running southwest to east and from the center towards the north (Macdonald et al. 1983). Numerous near-vertical dikes mark the rift zones. Dikes are thin sheets of massive, low-permeability rock that intrude existing rocks and have cooled beneath the surface. The thickness of individual dikes generally is less than 3 m. Dikes can extend vertically and laterally for several kilometers. Within a dike complex, dikes intersect at various angles. The number of dikes across a rift zone can exceed 600 per kilometer in the center, but decreases sharply in the outer part. However, individual, widely-scattered dikes can extend beyond a dike complex (Takasaki and Mink 1985).

### ***Sediments***

Holocene marine and terrestrial sedimentary deposits cover the flank lavas in the coastal regions and across central Maui. The sediments on the north side of central Maui consist of calcareous dune deposits that are mostly consolidated and well sorted. The sediments on the south side of the isthmus and on the southwest side of West Maui are comprised of poorly-sorted alluvium, which includes calcareous beach sand and talus fan

deposits (Stearns and Macdonald 1942). The thickness of the sediments ranges from 5 m in the center of the isthmus to about 25 m at the coast. The sediments are significantly less conductive than the basalts and can form a caprock at some places along the coast.

### **Ground Water**

Ground water in Hawaii primarily occurs in a basal freshwater lens in dike-free volcanic rocks and in dike-impounded systems in the rift zones, and secondarily in valley fill and coastal sediments (Gingerich and Oki 2000). The basal freshwater lens floats on top of the saltwater due to the density contrast. Currently, water-table measurements in the basal freshwater lens generally do not reach ten meters amsl. Ground-water elevations are lowest at the coast and the natural flow gradient is typically  $\sim 0.2$  m/km (Lau and Mink 2006). However, aquifer heterogeneities, discharging springs, heavily pumped wells, valley-fill barriers, and perched water can cause local ground-water table variations (Oki 2005). Ground water in a dike-zone complex can be as high as 1,000 m amsl on Maui and Hawaii and 500 m amsl on Oahu (Gingerich and Oki 2000).

The aquifers in the study area are unconfined (Takasaki 1972), except for the Wailuku Basalt aquifer on the east side of West Maui Volcano; this aquifer is confined by alluvium (Meyer and Presley 2000). The depth of aquifers in Hawaii is not physically defined due to missing geologic information. Souza and Voss (1987) considered 1,800 m below mean sea level (bmsl) as a reasonable aquifer depth, which coincides with a seismic velocity unconformity in south Oahu (Furumoto et al. 1970).

## **Aquifer Parameters**

Values of hydraulic properties, such as hydraulic conductivity, transmissivity, porosity, and aquifer storage, control ground-water flow and solute transport. The aquifers in Hawaii are characterized by heterogeneity at various scales. Although basalts are among the most permeable rocks on earth, local variations in permeability are common (Peterson 1972). For most applications, it is more useful to estimate effective aquifer parameters due to the lack of information about the heterogeneous aquifer system at field scales. A heterogeneous aquifer can be reduced to a homogeneous one by using effective parameters, while preserving the identical physical and chemical behavior of the system (e.g., El-Kadi and Brutsaert 1985; Yeh 1989). In the absence of detailed subsurface information, effective parameters provide estimates that are practical to initialize applications. Numerous studies have been conducted on aquifer parameters on the neighbor island of Oahu (see, e.g., Nichols et al. (1996), Hunt (1996), and Oki (1998)). Large-scale estimates for Maui, however, are lacking.

## ***Flank Lava***

Void spaces in lava flows and along contacts contribute to the permeability of the formation. Hydraulic conductivity of flank lavas depends on such features as the thickness of the flows; the thickness of clinker zones associated with aa flows; the frequency, extent and connectedness of fractures; and the occurrence of lava tubes and gas vesicles associated with pahoehoe flows (Peterson 1972; Oki 2005). Hydraulic conductivity in flank lavas ranges from several hundred to several thousands meters per day (Wentworth 1951; Soroos 1973; Williams and Soroos 1973; Mink and Lau 1980;

Hunt 1996). The hydraulic conductivity in dike-free flank lavas on Oahu ranges from 150 to 1,500 m/d, although smaller and larger values are common (Nichols et al. 1996). The lava flows generally are anisotropic in three dimensions. Horizontal hydraulic conductivity tends to be several times greater parallel to lava flows than perpendicular to the flows (e.g., Peterson 1993). Souza and Voss (1987) estimated the ratio of vertical to horizontal hydraulic conductivity to be 0.05.

### ***Dike Zone***

Intrusive volcanic rocks, such as dikes and sills, have a significantly lower permeability than flank lavas. Therefore, dikes impede ground-water flow and generally channel flow parallel to the dikes. Hydraulic conductivity in the dike zone is greater along the strike of the dike zone than perpendicular to the strike and the average conductivity decreases as the number of dikes increases towards the center of the rift zone (Takasaki and Mink 1985). The effective horizontal hydraulic conductivity of an entire dike complex can range between 0.05 and 0.1 m/d (Hunt 1996), considering that the hydraulic conductivity of individual dikes was estimated to be several orders of magnitude lower (Meyer and Souza 1995).

### ***Sediment***

The hydraulic conductivity of sediment spans several orders of magnitude due to the diversity of materials composed in this formation. The hydraulic conductivity of the older alluvium, including fine-grained muds and saprolite, ranges from 0.01 to 0.3 m/d (Wentworth 1938). Sands have an estimated hydraulic conductivity ranging from 0.3 to 300 m/d (Nichols et al. 1996). The most conductive units are the coral gravels and reef

limestones that have hydraulic conductivities of several thousands of meters per day (Oki 1998). Although the permeability of the components is diverse, the overall permeability of the caprock is low (Visher and Mink 1964). In general, the sediments are significantly less conductive than the basalts, with effective horizontal hydraulic conductivities from 1 to 60 m/d (Hunt 1996).

### ***Porosity and Aquifer Storage***

The total porosity of basaltic rocks is controlled by void spaces in the rock, vesicles, cracks, separations at contacts between flows, and lava tubes (Oki 2005) and ranges between 5 and 51 percent in Hawaii (Wentworth 1938, 1951). However, effective porosity may be up to an order of magnitude lower because not all existing pores are hydraulically interconnected and provide a pathway for ground-water flow (Oki 2005). Common values used for effective porosity and specific yield in Hawaii aquifers are 0.1 (Oki 1997), 0.05 (Oki 1998; Whittier et al. 2004) and 0.04 (Oki 2005) and 0.03 (Rotzoll and El-Kadi 2007). In the Pearl Harbor area on Oahu, specific storage was estimated to range from  $3 \times 10^{-4}$  to  $3 \times 10^{-7} \text{ m}^{-1}$  (Williams and Soroos 1973). Using the compressibility of water and the rock matrix, as well as an effective porosity of 0.05 yields a specific storage of  $2.5 \times 10^{-5} \text{ m}^{-1}$  (Oki 2005).

### **3. Constant-Rate and Variable-Rate Aquifer Tests**

#### **Introduction**

The objectives of this chapter are to characterize aquifer parameters at different scales on Maui using single-well aquifer tests, to examine the usefulness of the Harr method and the step-drawdown tests, and to evaluate aquifer-parameter results from step-drawdown tests with a numerical model. Seven analytical methods were applied to drawdown or recovery data obtained from constant- and variable-rate single-well aquifer tests. This allowed a comparison of estimated hydraulic properties for the same well. On a larger scale, hydraulic-conductivity estimates were correlated to geology. The point estimates were used in a geostatistical technique to estimate hydraulic-conductivity maps using ordinary kriging. The validity of step-drawdown test analysis was assessed by a numerical inversion method.

Numerous methods permit estimates of hydraulic properties of an aquifer. Among the most popular methods are aquifer-test analyses (Kruseman and de Ridder 1991). Traditional approaches involve analytical solutions. Recently, the use of numerical models is gaining popularity because more site-specific details can be included, such as aquifer heterogeneity (e.g., Lebbe and De Breuck 1995; Kollet and Zlotnik 2005; Wu et al. 2005). In this chapter, alternative analytical solutions to interpret aquifer-test data were tested against conventional curve-matching techniques. This approach, if successful, would provide parameter values that serve as a reference for other hydraulic estimation methods in the following chapters.

Aquifer tests impose artificial stress on a hydrologic system by pumping water from a well and measuring the changes in water levels in the pumped well and nearby observation wells. The response of the hydraulic head in the aquifer can be used to estimate transmissivity or hydraulic conductivity. In the absence of observation wells, estimating storage properties using analytical methods can be troublesome. However, numerical methods can be used to estimate storage properties (e.g., Pavelko 2004; Burbey 2006; Rotzoll and El-Kadi 2007).

Traditional methods used to estimate transmissivity from constant-rate aquifer tests include Theis-curve fitting (Theis 1935), recovery fitting (Theis 1935), and Cooper–Jacob straight-line fitting (Cooper and Jacob 1946). An important limitation of methods that provide estimates of transmissivity is that knowledge about aquifer thickness is required to determine hydraulic conductivity. Williams and Soroos (1973) assessed the suitability of a aquifer tests with observation wells using traditional methods on Hawaii volcanic aquifers in eight case studies. However, the small number of tests is not sufficient for parameter estimations on a large scale.

Variable-rate or step-drawdown aquifer tests relate steady-state drawdown to steps of increasing discharge. They are conducted as production tests, generally to establish the depth at which the pump is set or to define drawdown-yield relations. They are frequently ignored for evaluation of hydraulic properties. Jacob (1947) expressed the relationship between steady-state drawdown in the well and discharge as

$$s_s = BQ + CQ^w \quad (3.1)$$

where  $s_s$  is the steady-state drawdown in the well (m);  $Q$  is the discharge ( $\text{m}^3/\text{d}$ );  $B$  is the aquifer-loss coefficient ( $\text{d}/\text{m}^2$ );  $C$  is the well-loss coefficient ( $\text{d}^2/\text{m}^5$  for  $w = 2$ ); and  $w$  is the well-loss exponent. The aquifer-loss term includes all laminar losses in the aquifer, while the well-loss term comprises all turbulent losses in the well.

Ample work has been done on the determination of the well-loss part of Equation (3.1). Jacob (1947) proposed  $w = 2$ , which was adopted by many authors, mainly to simplify the analysis. He relied upon an analogy with turbulent flow in pipes, where drawdown varies proportional with fluid velocity to some power and the square being an approximate upper limit (Mogg 1969). Eden and Hazel (1973) strongly doubted whether any relationship other than quadratic is justified. They stated that results for  $w > 2$  should be interpreted with extreme caution due to the possibility that results were based on inaccurate data. They suggested that  $w = 2$  is an acceptable approximation for most step-drawdown tests under field conditions.

Rorabaugh (1953) disagreed on the quadratic exponent proposed by Jacob (1947) and suggested that  $w$  be evaluated individually for each test. The parameter  $w$  compensates partially for the transition from laminar to turbulent flow with increasing pumping rates (Uhl et al. 1975). Lennox (1966) reported values for  $w$  as high as 3.5. Soroos (1973) used step-drawdown tests to estimate hydraulic conductivity for 72 wells on Oahu. He found that well-loss exponent values ranged from 1.1 to 8.9, with a mean value of 2.4. Although fitting  $w$  may occasionally give a better match with the data,

Soroos attributed the higher values to errors in the field data or to the limited number of steps in the test and suggested using  $w = 2$ . Soroos (1973) did not include a broad comparison between hydraulic-conductivity estimates obtained by traditional methods and step-drawdown results for the tested wells.

The advantage of step-drawdown tests is that they provide a direct estimate of hydraulic conductivity, thereby avoiding uncertainties related to aquifers thickness. Furthermore, the analysis of step-drawdown tests includes a correction for well loss, which makes it suitable for aquifer test without an observation well. Moreover, the analysis does not depend on the subjectivity of the analyst in ignoring or incorporating wrong points. Usually early-time complications due to wellbore storage and partial penetration are avoided by ignoring the first drawdown measurements in a constant-rate test. Other advantages are that step-drawdown tests are faster to complete than constant-rate tests and that data from step-drawdown tests are readily available in Hawaii.

Based on available point measurements, the spatial distribution of hydraulic conductivity may be predicted using a geostatistical estimation approach. The concept of kriging has been widely used in connection with aquifer properties (e.g., Ahmed and de Marsily 1987; Ahmed et al. 1988; Fabbri 1997; Bissell and Aichele 2004; Razack and Lasm 2006). Ordinary kriging was used in this study to predict hydraulic conductivity on a larger scale than available for single-well aquifer tests in central Maui. Ordinary kriging was favored over other kriging methods because ordinary kriging assumes that spatial correlation among hydraulic-conductivity estimates exists and that local means (clustering of similar values) are not necessarily closely related to the population mean.

Ordinary kriging also relies on a relaxed assumption of stationary, which means that predictions are less affected by extremely heterogeneous data than predictions from other kriging algorithms would be (Bissell and Aichele 2004). A detailed description of kriging methods can be found in geostatistical text books, e.g. Clark and Harper (2000), and a comprehensive review is beyond the scope of this work.

## **Methodology**

### ***Analytical Solutions***

Several analytical solutions were used for single-well aquifer tests in this study. For estimating transmissivity, traditional methods used for constant-rate aquifer tests were Theis-curve fitting (Theis 1935), Theis recovery (Theis 1935), and Cooper–Jacob straight-line fitting (Cooper and Jacob 1946). A solution that was independently developed by Harr (1962) and Polubarinova–Kochina (1962) was used to estimate two hydraulic-conductivity values from constant-rate tests and one value from step-drawdown aquifer tests. Step-drawdown tests were analyzed with the equation of Zangar (1953) to estimate hydraulic conductivity and with the method of Thomasson et al. (1960) to estimate transmissivity. Details of the methods are provided below.

### **Theis Method**

The traditional methods for constant-rate aquifer tests were strictly used as described by Kruseman and de Ridder (1991). The Theis method (Theis 1935) was developed for aquifer tests with an observation well and applies to confined infinite aquifers that are homogeneous and isotropic. However, if aquifer drawdown is insignificant compared with aquifer thickness, it also may be applied to single-well tests

in unconfined aquifers (Gingerich 1999a). Transmissivity is estimated by matching a log-log plot of drawdown against time ( $t$ ) with the theoretical curve of the Theis well function  $W(u)$ , which is plotted against  $1/u$ . Obtaining a match point from the coordinate system of the Theis type-curve and  $s_s$  and  $W(u)$  allows the use of the following equation:

$$T = \frac{Q}{4\pi s_s} W(u), \quad (3.2)$$

where  $T$  is the transmissivity ( $\text{m}^2/\text{d}$ ).

#### Cooper–Jacob Method

The Cooper–Jacob straight-line fitting method (Cooper and Jacob 1946) was developed for aquifer tests with an observation well and applies to confined infinite aquifers that are homogeneous and isotropic. For the case of relatively small drawdown, the Cooper–Jacob method also may be applied to single-well tests in unconfined aquifers. The method estimates transmissivity by fitting a straight line to aquifer drawdown against the time since the pumping was started on a semi-logarithmic scale. Transmissivity is given by:

$$T = \frac{2.3Q}{4\pi \Delta s_s}. \quad (3.3)$$

in which  $\Delta s_s$  is the drawdown per log cycle.

In case a significant change in slope appeared in the semi-log plot of the Cooper–Jacob test (after ignoring the early-time drawdown), only the first slope was considered in

the analysis to eliminate boundary effects associated with the dike-zone complex. Halford et al. (2006) claimed that transmissivity values from the Cooper–Jacob method in unconfined aquifers were overestimated by a factor of 2 due to subjectivity of the analyst, especially when late-time drawdown values were ignored. No evidence of leakage was observed in aquifer tests used in this study, which suggests that transmissivity estimates are reliable.

#### Theis Recovery Method

The Theis recovery method (Theis 1935) applies to aquifer tests in confined infinite aquifers that are homogeneous and isotropic. Again, the method applies to unconfined aquifers if drawdowns are relatively small. The method fits a straight line to residual drawdown against the time since pumping stopped on a semi-logarithmic scale with emphasis on the late-time data. The amount of recovery per log cycle,  $\Delta s_s$ , is substituted in Equation (3.3) to estimate transmissivity.

#### Harr Method

Polubarinova–Kochina (1962) and Harr (1962) independently presented a solution that can be applied to constant-rate and variable-rate aquifer tests, even though it is not commonly used this way. The solution estimates hydraulic conductivity of a thick unconfined aquifer that is partially penetrated by a pumped well. For simplicity, the method for analyzing constant-rate tests is hereafter referred to as the Harr method. The solution assumes a homogeneous and isotropic aquifer of infinite thickness. Spherical flow develops underneath the well bottom and the elliptic equipotentials of the well surface resemble an ellipsoid with the volume of a cylinder (Harr 1962; Polubarinova-

Kochina 1962). The method combines information on well construction and head responses to pumping to estimate hydraulic conductivity with the following equation:

$$K = \frac{Q}{2\pi L s_s} \ln\left(\frac{1.6 L}{r}\right), \quad (3.4)$$

where  $K$  is the hydraulic conductivity (m/d);  $L$  is the active length or screened interval of the well (m); and  $r$  is the radius of the pumped well (m). Although the solution requires a condition of steady-state drawdown, neither Polubarinova–Kochina (1962) nor Harr (1962) do provide a suitable criterion for such a condition. The approach by Gingerich (1999a) was adapted by assuming that this condition is fulfilled when the drawdown per unit time becomes relatively small compared to early-time drawdown. According to Gingerich (1999a), the drawdown per unit time is relatively small after  $1 \times 10^3$  min for wells with high hydraulic conductivity. For wells with relatively low conductivity, the drawdown per unit time can still be significant after  $1 \times 10^4$  min. The steady-state drawdown was estimated from a Cooper-Jacob straight line that is arbitrarily extended to  $1 \times 10^4$  min and  $1 \times 10^6$  min (Gingerich 1999a). This yields two hydraulic conductivity estimates that define a range of possible values from this method.

#### Zangar Method

Zangar (1953) proposed an equation to estimate hydraulic conductivity based on the ratio of steady-state drawdown to discharge. He determined the equivalent hemispherical radius of a partially penetrating cylindrical well in a homogeneous and

isotropic aquifer of infinite thickness and incorporated well construction information.

Zangar's estimate of hydraulic conductivity is

$$K = \frac{Q}{2\pi r_h s_s}, \quad (3.5)$$

where  $r_h$  is the hemispherical radius of pumped well (m), which is defined as

$$r_h = \frac{L}{\ln\left(\frac{L}{r}\right)}. \quad (3.6)$$

Soroos (1973) used Equation (3.1) to separate well-head losses from aquifer-head losses in step-drawdown tests. Where the active length of the well is less than 20% of the aquifer thickness, the aquifer loss term from Equation (3.1) equals the steady-state drawdown (Soroos 1973). Thus, Equation 3.5 may be written as

$$K = \frac{1}{2\pi L B} \ln\left(\frac{L}{r}\right). \quad (3.7)$$

#### Polubarinova Method

Isolating the aquifer-head loss from step-drawdown tests may be used in the same way for the Harr method (Harr 1962; Polubarinova-Kochina 1962). By using the same assumptions regarding the well and the aquifer and by replacing specific drawdown ( $s_s/Q$ ) in Equation (3.4) with the aquifer-loss coefficient, the solution reads:

$$K = \frac{1}{2\pi L B} \ln\left(\frac{1.6 L}{r}\right). \quad (3.8)$$

This method is hereafter referred to as the Polubarinova method to avoid confusion with the Harr method for constant-rate aquifer tests, even though the solution was independently derived by both authors.

The Thiem (1906) equilibrium equation for confined aquifers with a pumping well reads:

$$T = \frac{2.3 Q}{2 \pi s_s} \ln\left(\frac{r_2}{r}\right), \quad (3.9)$$

where  $r_2$  is the radius of influence of the pumped well (m). Thomasson et al. (1960) reported that empirical values for the log-ratio of the radius of influence of the well to the effective well radius range from 2.5 to 4.2, with a mean of 3.2. The use of this mean ratio simplifies Equation (3.9). Logan (1964) reported a similar value of 3.3, which is valid for 98 aquifer tests made in sand-and-gravel wells in Illinois.

#### Thomasson Method

Starting with Razack and Huntley (1991), numerous studies targeted empirical relationships between transmissivity and specific capacity ( $Q/s_s$ ). Due to the comparable high hydraulic conductivity in coarse sediment and in basaltic rocks, the value of 3.3 for the log-ratio of radii mentioned above has not been altered for this analysis. The empirical relationship between specific capacity and hydraulic parameters for Hawaii

aquifers will be investigated in Chapter 4. Well losses are neglected in Equation (3.9) (see Clark 1977) but may be incorporated by replacing the specific drawdown with the aquifer-loss coefficient determined from step-drawdown tests. Combining the constants in Equation (3.9), the equation that estimates transmissivity then reads:

$$T = \frac{1.2}{B} \quad (3.10)$$

This method is hereafter referred to as the Thomasson method. The six equations to estimate hydraulic parameters using aquifer tests are listed in Table 3.1.

**Table 3.1.** Equations to estimate hydraulic parameters from constant- and variable-rate single-well aquifer tests

Test type	Method name	Reference	Equation
Constant-rate	Theis	Theis (1935)	$T = \frac{Q}{4\pi s_s} W(u)$
	Cooper-Jacob Theis Recovery	Cooper-Jacob (1946) Theis (1935)	$T = \frac{2.3Q}{4\pi \Delta s_s}$
	Harr	Harr (1962) Polubarinova-Kochina (1962)	$K = \frac{Q}{2\pi L s_s} \ln\left(\frac{1.6L}{r}\right)$
Step-drawdown	Zangar	Zangar (1953)	$K = \frac{1}{2\pi L B} \ln\left(\frac{L}{r}\right)$
	Polubarinova	Harr (1962) Polubarinova-Kochina (1962)	$K = \frac{1}{2\pi L B} \ln\left(\frac{1.6L}{r}\right)$
	Thomasson	Thomasson et al. (1960)	$T = \frac{1.2}{B}$

### ***Data Analysis***

Aquifer-loss and well-loss coefficients for step-drawdown tests were determined by fitting the observed drawdown in the well to Equation (3.1). An iterative procedure minimized the error for  $w$ , and constrained its range from 1.1 to 10, with increasing steps of 0.001. The coefficients  $B$  and  $C$  for each exponent were determined by least-square regression. Cases where the test produced a nonphysical hydraulic conductivity (i.e., negative values) were disregarded. Reasons for these cases are most likely associated with measurement errors in the field.

In total, 238 single-well aquifer tests were analyzed using the seven different solutions listed in Table 3.1. Most of these tests were performed during pump installation and are documented in the files of the Hawaii Department of Land and Natural Resources' Commission on Water Resource Management (CWRM). Useful data were available for 72 constant-rate tests from 62 wells, for 74 recovery tests from 54 wells, and for 92 step-drawdown tests from 66 wells. The large number of step-drawdown tests is notable. Figure 3.1 shows locations of the aquifer tests and the geologic unit tested. When data from multiple tests of the same kind at the same well were available, the arithmetic mean for each method was used.

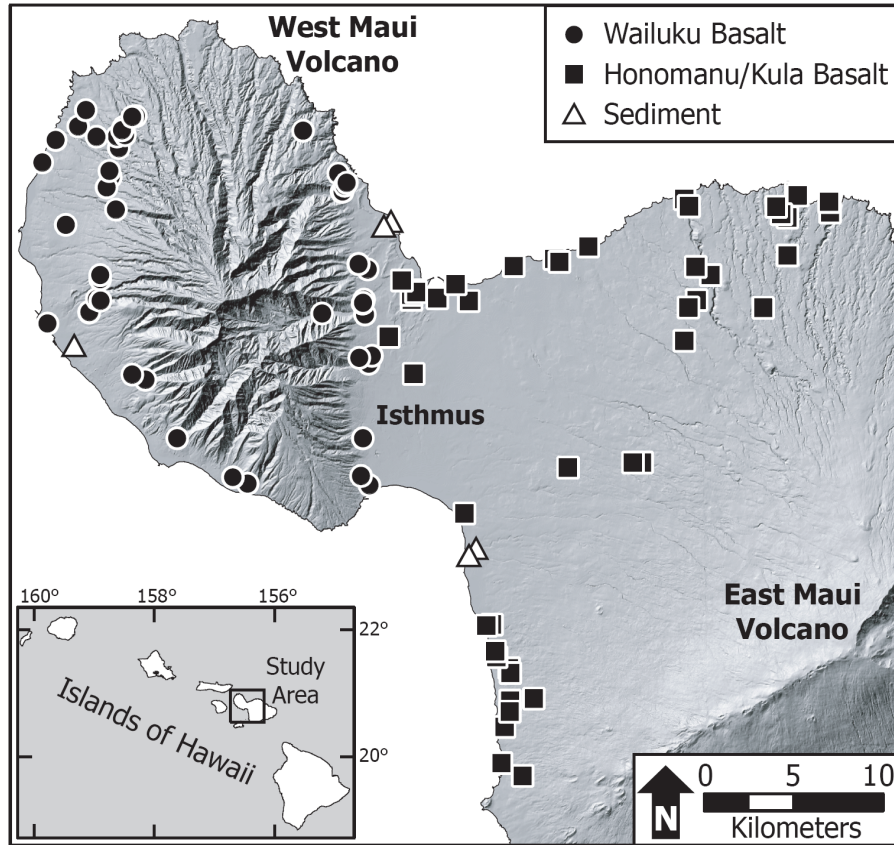


**Figure 3.1.** Location of wells with aquifer-test data on Maui, as indicated by the main intersected geology.

As previously mentioned, the exact thickness of Hawaii aquifers is not physically defined. However, an estimate of the aquifer thickness is necessary to convert transmissivity to hydraulic conductivity using

$$T = Kb, \tag{3.11}$$

where  $b$  is the aquifer thickness (m). Halford et al. (2006) found that hydraulic conductivity is better estimated with aquifer thickness rather than screen length in the case of partially penetrating wells in unconfined aquifers. However, the conversion from transmissivity to conductivity remains difficult for Hawaii aquifers. Thus, either the

aquifer is regarded of semi-infinite extent or only parts of it can be considered to contribute to its effective thickness. For the aquifer-test analysis, the approach of Gingerich (1999a) was adapted, whereby thickness is taken as the distance from the well base to the water table. It was assumed that all wells are fully saturated from the water table above sea level to the bottom of the well. The thickness used here is the minimum thickness contributing water from the aquifer, because even though the aquifer extends deeper, supporting lithologic information at depth is unavailable to quantify the aquifer thickness. In addition, although the wells penetrate multiple layers of basalt flows and sedimentary deposits, a single aquifer was assumed because available lithologic information is insufficient to define the individual layers.

### ***Geostatistical Analysis***

For statistical comparison, a t-test was used to determine whether the hydraulic-conductivity means of the two flank-lava populations are different. The test assumes that the samples come from normal distributions with unknown and possibly unequal variances. A two-sample Kolmogorov–Smirnov test was used to compare two samples, as it is sensitive to differences in both location and shape of the empirical cumulative distribution functions of the estimated hydraulic conductivity. The null hypothesis is that samples of hydraulic-conductivity estimates come from the same population.

The geostatistical analyst, a toolbox in ESRI's ArcMap software package, was used for the geostatistical approach. A normal distribution of the variable improves the prediction (Ahmed et al. 1988). However, the logarithmic transformation of hydraulic conductivity used in kriging is problematic. Bissell and Aichele (2004) as well as Razack

and Lasm (2006) indicated that the unbiasedness of the estimated value is lost when the logarithmic  $K$ -prediction is backtransformed to hydraulic conductivity. The latter authors therefore questioned the necessity of a normal distribution in geostatistical analysis. Hence, the non-transformed conductivity values were preferred. Investigation of statistical anisotropy with directional variograms was difficult in this study area. Horizontal hydraulic conductivity tends to be several times greater parallel to lava flows than perpendicular to the flows (e.g., Nichols et al. 1996). Since the study area encompasses two volcanoes with flows propagating from the caldera in all directions, the experimental variogram was expected to be omni-directional. To reduce complexity, only the spherical model to fit the experimental variogram was used in this study. The equation of the spherical model is

$$\gamma(l) = \begin{cases} G_1 \left( \frac{3l}{2d} - \frac{l^3}{2d^3} \right) + G_0 & l \leq d \\ G_1 + G_0 & l > d \end{cases}, \quad (3.12)$$

where  $\gamma$  is the degree of spatial dependence of the estimated variable ( $K$ );  $l$  is the lag or distance between the sampling points (m);  $G_1$  is the sill ( $m^2$ );  $G_0$  is the nugget ( $m^2$ ); and  $d$  is the range (m) (e.g., Fabbri 1997; Clark and Harper 2000). A wide comparison of different kriging methods and different fitting models is beyond the scope of this study.

### ***Numerical Model***

The validity of the analytical solutions of step-drawdown tests was evaluated with a numerical ground-water flow simulation using MODFLOW-2000 (Harbaugh et al. 2000). A simple cylindrical three-dimensional finite-difference domain, representing an unconfined aquifer, was constructed. The radius of the homogeneous cylinder was taken as 1 km to avoid drawdown effects at the outer boundary. The grid size was refined toward the center of the domain, equaling the well diameter in the center and gradually increasing to 50 m at the edge of the cylinder. The model contains ten layers to account for vertical flow due to the partial penetration of the well. The thickness of the layers increased at depth. The well penetrated 20% of the depth of the modeled aquifer to satisfy the assumption of partial penetration for step-drawdown tests (Zangar 1953). The well diameter, the length of the open interval, and the aquifer thickness were adjusted based on well-construction properties for each model. The ratio of vertical to horizontal hydraulic conductivity is set as 0.1, within the range of reported values (Nichols et al. 1996). The withdrawal from the well corresponding to each step was used to produce a transient model. The hydraulic conductivity and storage parameters, i.e., specific storage and specific yield, were numerically estimated using the automated parameter estimation algorithm PEST (Doherty 2004). PEST is a non-linear parameter estimator that iteratively minimizes the error between observed and computed water levels by adjusting selected aquifer parameters. The calculated aquifer loss in the well, based on Equation (3.1) was used for the automated calibration.

## Results and Discussion

### *Aquifer Tests*

The values of hydraulic conductivity for all wells range between 1 and 2,500 m/d, characterizing a highly heterogeneous system. The variability of the highly permeable basalt is caused by fracture flow on different scales. Detailed results of the aquifer tests for each well are provided in Table A1. A normal probability plot of the log-transformed data is shown in Figure 3.2. The linear fit, shown as the gray line, reflects a log-normal distribution of hydraulic conductivity, especially for the robust data between 0.1 and 0.9. The deviation from the fitted line in the lower part is attributed to the geologic origin of that specific data and will be discussed later.

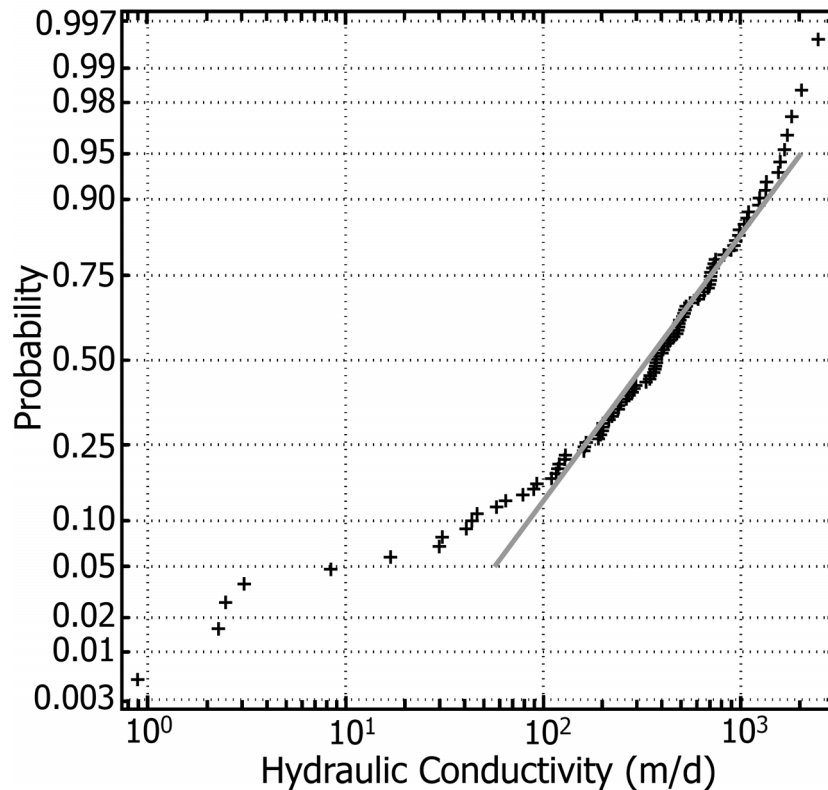


**Figure 3.2.** Probability distribution of hydraulic conductivity in a log-normal diagram. The gray line is a best-fit regression to the data.

The validity of non-traditional methods was evaluated by comparing the results of the Harr method and the step-drawdown tests to traditional methods. First, the arithmetic mean hydraulic conductivity based on Theis and Cooper–Jacob methods is plotted against the mean conductivity of the two Harr estimates (Figure 3.3). The correlation coefficient ( $R$ ) is given for the log-transformed values. The  $R$ -value of 0.86 shows a good relationship between hydraulic conductivity from traditional methods and the Harr method for constant-rate tests. The 1:1 black line in Figure 3.3 represents perfect match of results from both methods. The data points are scattered on both sides along that line, and deviations are within half an order of magnitude, indicating the usefulness of the Harr method.

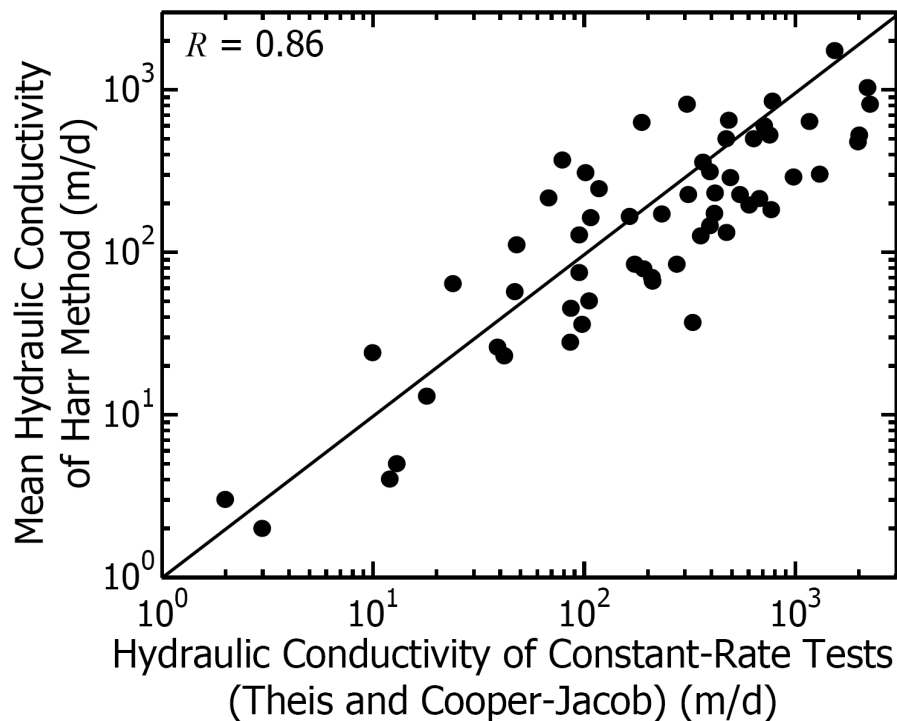


**Figure 3.3.** Log-log plot of the mean of the two hydraulic-conductivity estimates from the Harr method against the mean of the two hydraulic-conductivity estimates from traditional constant-rate tests. The 1:1 match is plotted as the black line.

The results of the step-drawdown test analysis indicate that fitting the well-loss exponent gives a better match to the observed data than using the quadratic exponent. The error between observed and calculated total loss is reduced for some wells by up to 100% and on average by 37%. Values for the exponent  $w$  range from 1.1 to 6.2, with a mean of 2.9 and a median of 2.6. This raises the question whether a result with high values of  $w$  is physically realistic. Projecting the curve further at higher pumping rates for such a large exponent would mean that a small increase of discharge results in an unrealistic large increase in drawdown. A higher exponent means more aquifer loss and less well loss, as indicated by a greater slope  $B$ , and this translates into a lower hydraulic-conductivity estimate. One reason for large exponents is the low number of steps. The range of  $w$  and the standard deviation ( $\sigma$ ) drops gradually with increasing number of steps. While tests with three steps cover the full range of values for  $w$  up to 6.2 with  $\sigma = 2.0$ , tests with seven or more steps do not exceed an exponent of 2.7 with  $\sigma = 0.6$ , which is consistent with the findings of Soroos (1973). Due to the high uncertainty at higher exponents, the results reported in this study are all based on  $w = 2$ .

The hydraulic-conductivity estimates based on step-drawdown tests were compared with those based on constant-rate tests. Figure 3.4 shows the relationship between the arithmetic-mean constant-rate hydraulic conductivity and the mean conductivity for three step-drawdown methods: Zangar, Polubarinova, and Thomasson. Step-drawdown tests tend to overestimate hydraulic conductivity compared to the results based on constant-rate methods. However, as can be seen in Figure 3.4, the overestimation does not exceed 0.15 log cycles. Summary statistics of the results from

different methods for basalt are provided in Table 3.2. The arithmetic mean of the five geometric means from constant-rate tests is 200 m/d and from the three step-drawdown tests it is 330 m/d. The difference between the two averages of the mean is 0.2 log cycles. This is within acceptable scatter of hydraulic-parameter estimation, considering that  $K$  values range over three log cycles and that, in general, values are only reliable to one significant figure (Keith Halford, USGS, oral commun., 2005). Additionally, the  $R$ -value of 0.81 on a log-log scale indicates a good correlation. This suggests that step-drawdown methods can also provide results of accuracy comparable to those based on traditional constant-rate tests. In conclusion, the Harr method and step-drawdown tests provide a useful way to estimate aquifer parameters from single-well tests in volcanic aquifers.

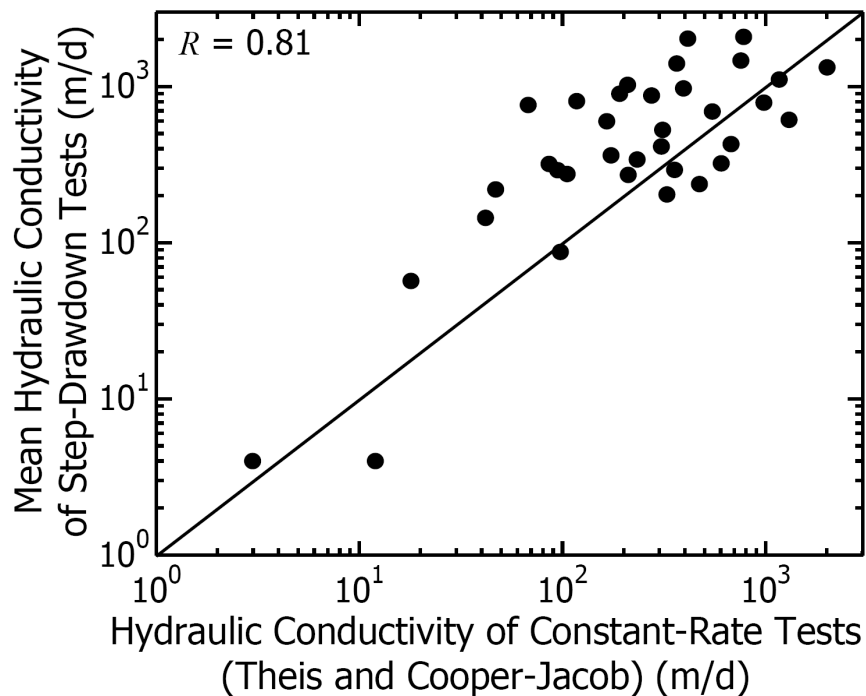


**Figure 3.4.** Log-log plot of the mean of the three hydraulic-conductivity estimates from step-drawdown tests against the mean of the two hydraulic-conductivity estimates from traditional constant-rate tests. The 1:1 match is plotted as the black line.

**Table 3.2.** Summary statistics of hydraulic conductivity estimates (m/d) from different analytical solutions for dike-free basalts in Maui

	Constant-rate test				Step-drawdown test			
	Theis	Cooper– Jacob	Harr $t = 10^4$	Harr $t = 10^6$	Reco- very	Zangar	Polubar- inova	Thom- asson
Geometric mean	217	238	176	139	242	298	329	358
Median	310	320	210	170	295	380	420	470
Mean - std. dev.	45	55	42	32	54	71	77	79
Mean + std. dev.	1,046	1,038	740	612	1,083	1,256	1,408	1,626

Summary statistics of the results for sediments from different methods are provided in Table 3.3. The arithmetic mean of the five geometric means from constant-rate tests is 40 m/d, and from the three step-drawdown tests the arithmetic mean is 50 m/d.

**Table 3.3.** Summary statistics of hydraulic conductivity estimates (m/d) from different analytical solutions for sediments in Maui

	Constant-rate test				Step-drawdown test			
	Theis	Cooper– Jacob	Harr $t = 10^4$	Harr $t = 10^6$	Reco- very	Zangar	Polubar- inova	Thom- asson
Geometric mean	25	44	58	36	42	33	49	63
Median	40	45	30	20	80	60	70	110
Mean - std. dev.	4	23	16	11	4	6	14	12
Mean + std. dev.	145	81	217	112	446	181	174	322

Figures 3.5a, 3.5b, and 3.5c show hydraulic conductivity values obtained from constant-rate tests, recovery tests, and step-drawdown tests, respectively. Figure 3.5d shows the combined results for all methods used for each well. When more than one method was used, the arithmetic mean is displayed in the figure. The analysis provides values of hydraulic conductivity for 103 wells in central Maui, and evidently, the values

estimated from the aquifer tests are characterized by significant spatial variability. In the northwestern part of the isthmus, for example, low conductivity values are shown next to contrasting high conductivity values. This can be attributed to the heterogeneity of the formation or the existence of different geologic units that are intersected by the well. Another reason could be the proximity of the dike zone, which does not have a well-defined boundary. Single dikes may occur beyond the marginal dike zone, causing boundary effects to drawdown cones. Another source of uncertainty is clogging or deterioration the well screen of once highly conductive wells over time. Some aquifer tests have been performed 60 years ago. This factor is not considered in this analysis, because comparisons to recent aquifer tests at the same well are not available.

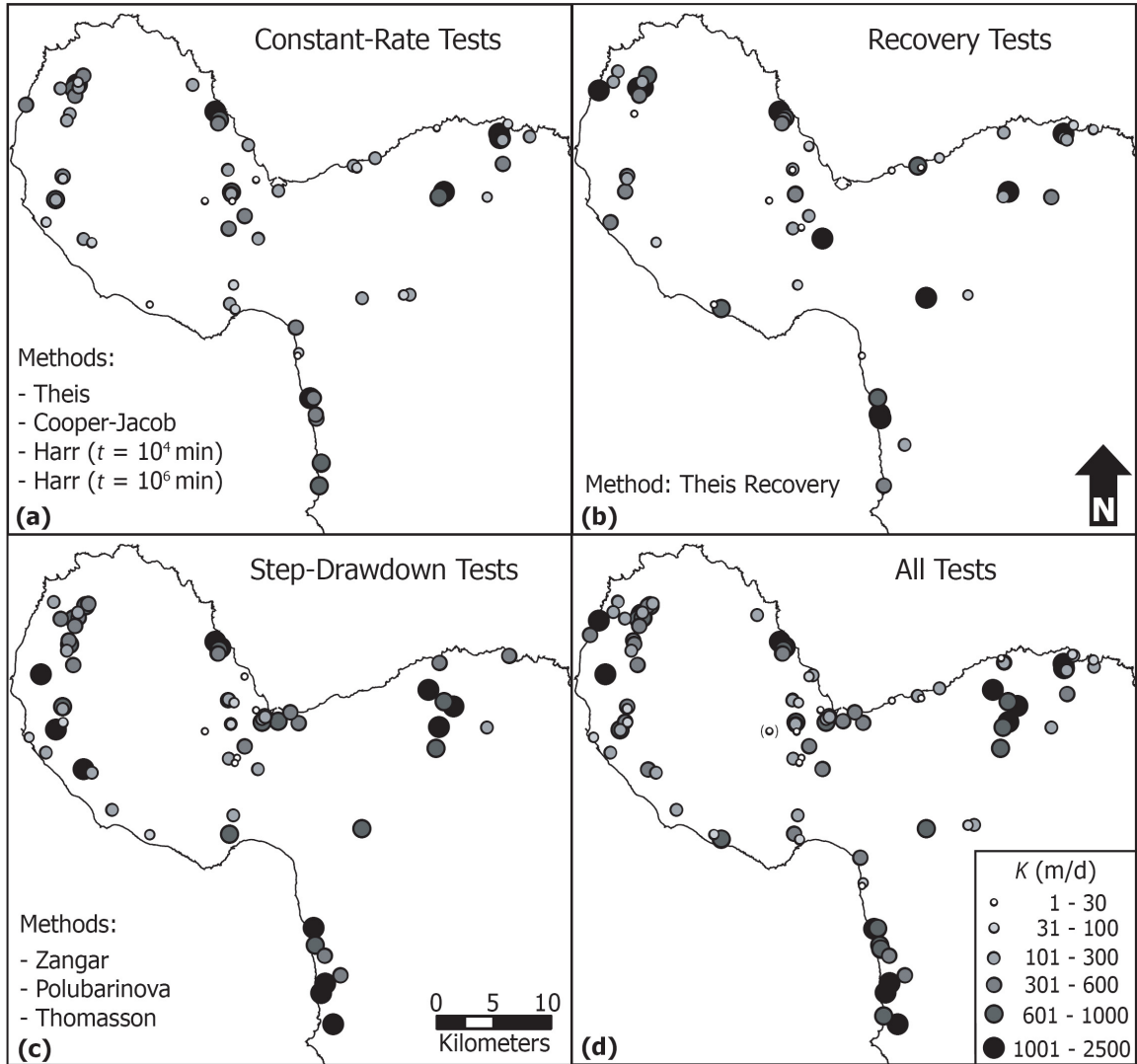


**Figure 3.5.** Location and magnitude of hydraulic conductivity for (a) constant-rate aquifer tests, (b) recovery tests, (c) step-drawdown tests, and (d) all tests combined for each well. The well in parenthesis (d) is excluded from the Wailuku flank lava because it is located within the dike complex.

Since hydraulic conductivity is log-normally distributed, the geometric mean is more accurate when compared against the arithmetic mean. The geometric standard deviation is an asymmetric interval that represents variations of the log-transformed values around the geometric mean. The hydraulic conductivity for wells that penetrate basalts ranges from 1 to 2,500 m/d, with a geometric-mean value of 276 m/d, a median

value of 370 m/d (Table 3.4). The asymmetric interval of the standard deviation is between 62 and 1,240 m/d. The results are within the known range for dike-free lava on other Hawaiian islands. Only five shallow wells penetrate the sediment layer, for which hydraulic conductivity estimates range from 10 to 210 m/d. The geometric mean of 46 m/d and the median of 30 m/d are also within the expected limit. The interval of the standard deviation is between 14 and 153 m/d.

**Table 3.4.** Summary statistics of hydraulic-conductivity estimates (m/d) for three geologic groups: Wailuku Basalt, Honomanu/Kula Basalt, and sediment

	Basalt			Sediment
	Wailuku	Honomanu/Kula	Both	
<i>n</i>	51	46	97	5
Geometric mean	247	312	276	46
Median	400	370	370	30
Mean - std. dev.	56	68	62	14
Mean + std. dev.	1,094	1,435	1,240	153

The deviation from the linear trend in Figure 3.2, mentioned earlier, is attributed to the inclusion of wells from the sediment unit. In addition, some wells that may be located in the marginal dike are included. Water-level responses in wells in the vicinity of dikes show a major change in slope based on the Cooper–Jacob test, which is associated with ground-water flow barriers related to dikes. However, no significant spatial trend can be observed from wells that show evidence of a boundary. In the absence of observation wells, it is difficult to locate these boundaries.

### ***Geostatistical Analysis***

In order to link estimated hydraulic-conductivity values to the underlying geology, the Wailuku Basalt, Honomanu/Kula Basalt, and the sediments are examined individually. One well in the Iao Valley, indicated with parenthesis in Figure 3.5d, has a very low hydraulic conductivity (6 m/d) and a measured water table of 206 m above sea level. This well is clearly located in the dike-zone complex and therefore excluded from the Wailuku Basalt flank lava group. A detailed statistical description of each group is shown in a box and whisker diagram (Figure 3.6). The bottom of the box is the lower quartile value, the white line is the median value, and the top of the box is the upper quartile value. The whiskers are lines extending from each end of the box to show the minimum and maximum values of the data. The plot provides more insight into the distribution of the data. The sediment group is obviously distinct from the flank lavas. Sediment hydraulic conductivities are one order of magnitude lower. The flank lava conductivities for Wailuku Basalt and Honomanu/Kula Basalt seem to be similar. The values for Honomanu/Kula Basalt are slightly higher than those for Wailuku Basalt. The main difference is the wider interval of the Honomanu/Kula Basalt standard deviation (Table 3.4).

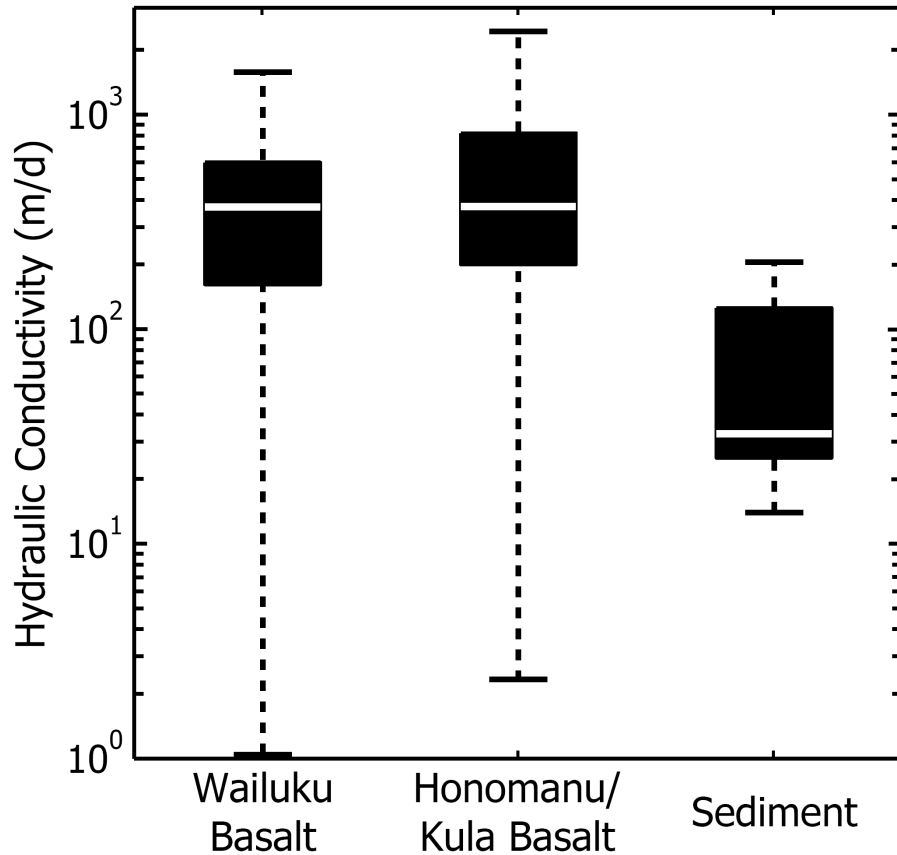


**Figure 3.6.** Box-and-whisker diagram for three hydrogeologic units: Wailuku Basalt, Honomanu/Kula Basalt and sediment.

Does a significant hydrologic difference exist between the Wailuku and Honomanu/Kula formations? As previously noted, the arithmetic mean can be misleading, considering the values of hydraulic conductivity span several orders of magnitude and are log-normally distributed. The t-test reveals that the means of both samples are indistinguishable at the 99% confidence interval for the log-transformed conductivity and the non-transformed variable. The two-sample Kolmogorov–Smirnov test shows that samples come from the same population at the 99% confidence interval. Therefore, the two basalt groups can be treated as one population.

The wells that tap the sediment and one well in the dike zone are excluded from the flank lava grouping. The experimental variogram shown in Figure 3.7 illustrates spatial dependence of flank-lava conductivity values. The parameters for the spherical model from Equation (3.12) are  $G_0 = 139,320$ ,  $G_1 = 94,683$ ,  $d = 9,571$ , and  $l = 1,000$ . The plateau of the maximum spatial autocorrelation is reached at a distance of 9.6 km. Beyond this, no significant spatial correlation exists between points.

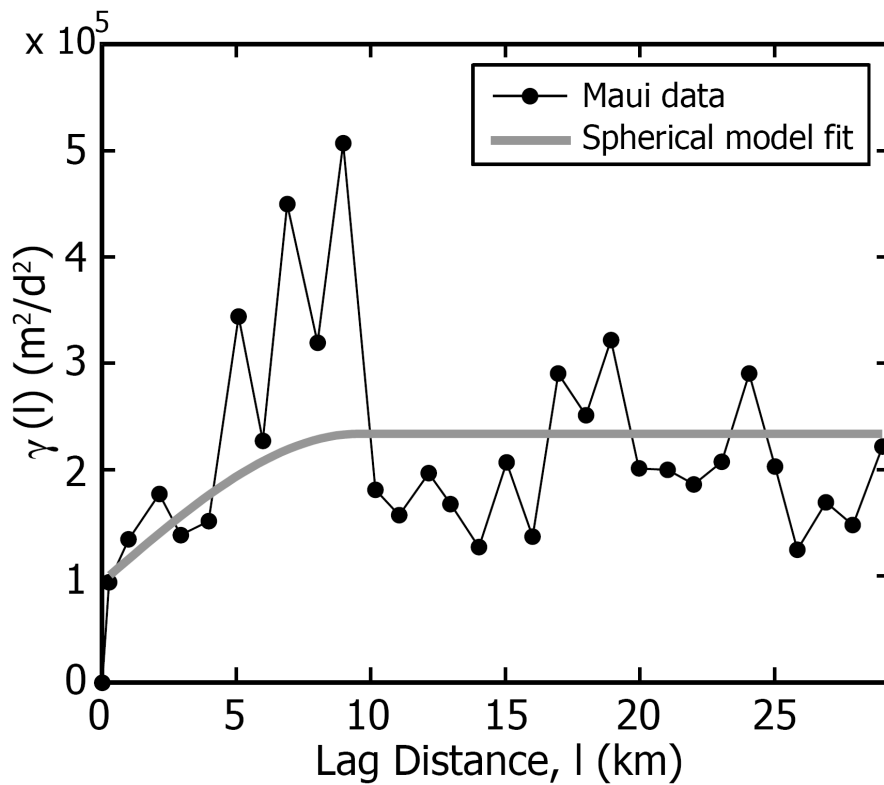


**Figure 3.7.** Experimental variogram and fitted spherical model for hydraulic conductivity on Maui. The distance between sampling points is divided into lags of 1 km.

The estimated hydraulic conductivity map using ordinary kriging is shown in Figure 3.8a. The distribution is contoured to simplify the illustration, considering that aquifer test results are generally reported to one significant figure. In West Maui, two

small areas of higher conductivity are apparent on both sides of the volcano. The area of the dike complex is masked, because no correlation between hydraulic conductivity in the flank lava and in the dike complex can be drawn. With only one sample from the dike complex, predictions are nonexistent. The isthmus has relatively low conductivity values, possibly because some wells that already belong to the West Maui marginal dike zone are mixed within the flank lava group. The flanks of East Maui Volcano show considerably higher conductivity values, with two larger clusters in the south and the north. The kriged standard error is illustrated in Figure 3.8b. As expected, the error is relatively small where the sample population is denser. The area of higher conductivity identified on the west side of West Maui Volcano has a larger standard error. This can be attributed to the fact that this area is influenced by only one sample point. The three other areas that show higher conductivity, mentioned earlier, come from a cluster of wells with consistently higher values. The map in Figure 3.8a provides an estimate of the spatial distribution of effective hydraulic conductivity, which can be useful as initial values of aquifer parameters used in hydrogeologic assessments in the absence of more detailed measurements.

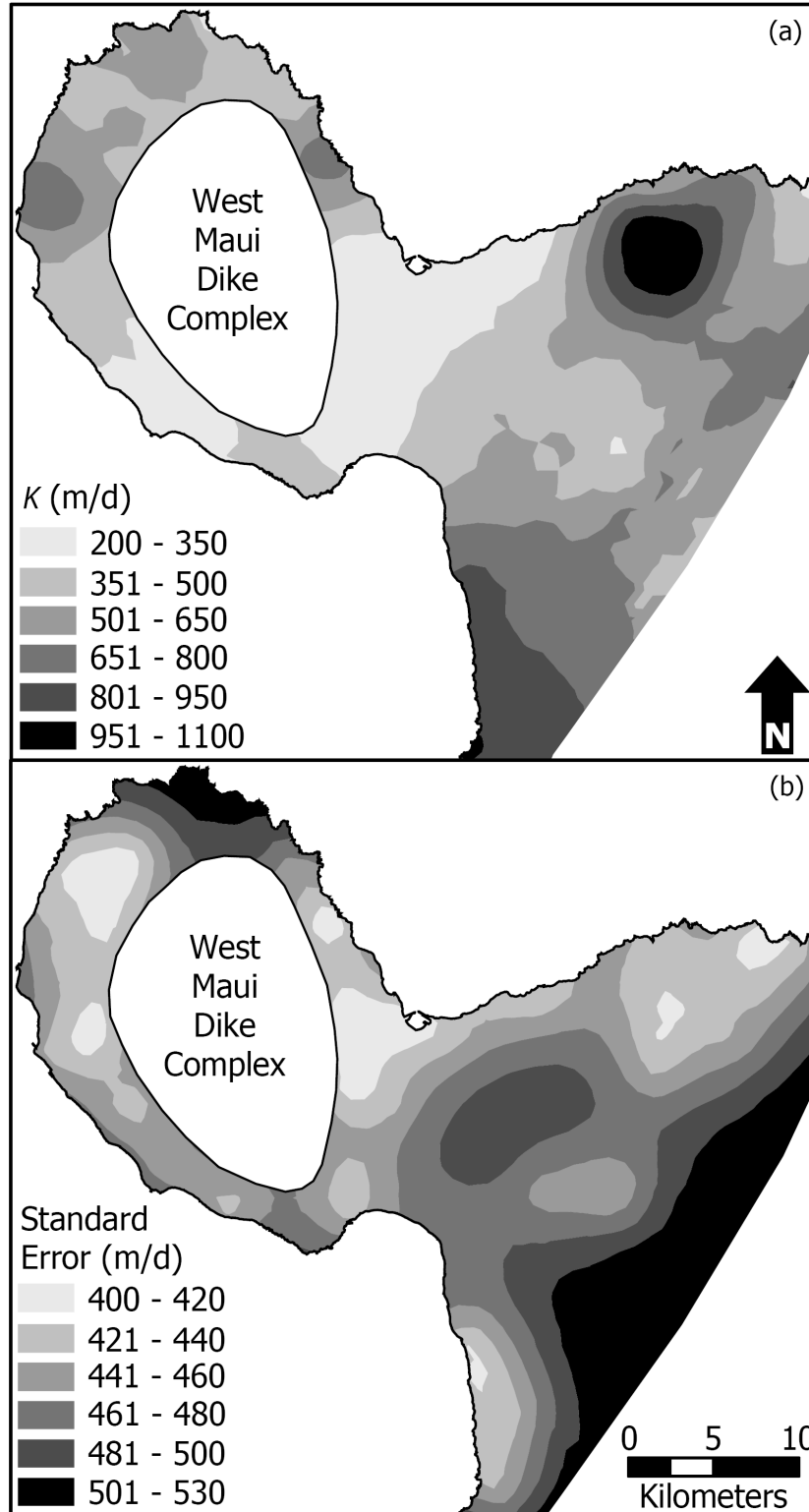


**Figure 3.8.** (a) Estimated hydraulic-conductivity map for Maui using ordinary kriging and (b) kriged standard error of the hydraulic-conductivity estimate.

### *Numerical Model*

Several step-drawdown tests were used to evaluate the results from the analytical step-drawdown analysis against hydraulic conductivity based on a calibrated numerical model. One well, which is typical for the dataset, was used to demonstrate the results. The separation of aquifer loss and well loss is shown in Figure 3.9. The figure also shows the aquifer-loss values obtained from the numerical model. The three hydraulic conductivity estimates for this well are 85, 92, and 84 m/d for the Zangar, Polubarinova, and Thomasson method, respectively. Using PEST, the conductivity was estimated within that range, with a value of 85 m/d. The absolute mean difference between observed and calculated drawdown and the sum of squared differences were 0.03 m and  $0.006 \text{ m}^2$ , respectively. When compared to analytical methods, numerical methods have the advantage of providing estimates of storage parameters for single-well tests. PEST estimates for the specific storage and the specific yield were  $6.4 \times 10^{-6} \text{ m}^{-1}$  and 0.073, respectively, which are typical values for Hawaii's unconfined aquifers. It can be concluded that comparable values for hydraulic conductivity are obtained by using analytical and numerical models. The numerical model has the extra advantage of providing values for storage parameters.

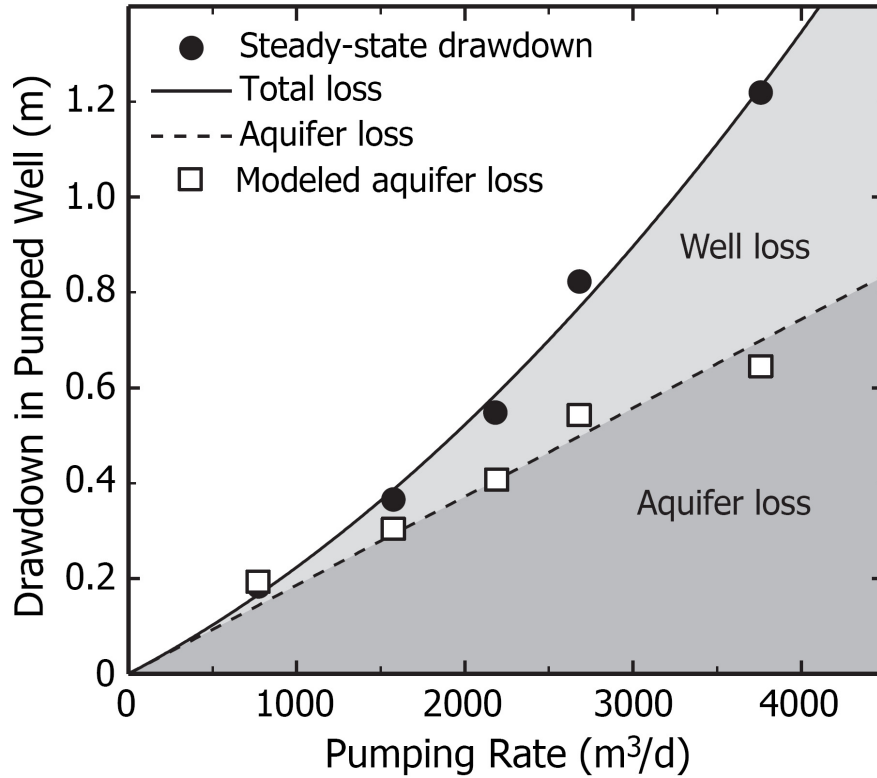


**Figure 3.9.** Relationship of well loss and aquifer loss to total loss in a step-drawdown test. The quadratic fit represents the total loss. Numerical modeled aquifer loss for this particular well is consistent with the predicted aquifer loss from the regression analysis.

### Chapter 3 Conclusions

The analysis provides values of transmissivity and hydraulic conductivity for a large area in Maui that are consistent with estimates published for other Hawaii islands. Hydraulic conductivity is log-normally distributed. The Harr method and the often-disregarded step-drawdown tests are valuable tools for estimating hydraulic conductivity from single-well tests in volcanic island aquifers. The correlation coefficients for tests compared with traditional methods are 0.86 for the Harr method and 0.81 for step-drawdown tests.

Aquifer conductivities, which range over several orders of magnitude from 1 to 2,500 m/d, match expected values in dike-free volcanic rocks and the sediment. The geometric mean and median values of hydraulic conductivity are respectively 276 and 370 m/d for basalt and 46 and 30 m/d for sediment. The two flank lava groups, Wailuku and Honomanu/Kula Basalts, are statistically from the same population. The sediment group is clearly distinct due to its geological nature, with hydraulic conductivities that are one order of magnitude lower than that of the basalts.

Hydraulic conductivity is spatially correlated, and ordinary kriging provides an estimated hydraulic conductivity map on Maui for a larger scale compared to individual aquifer tests. The kriged standard error is lower, and confidence in estimated values is higher in areas of higher sample density. Numerically estimated step-drawdown test values agree with those estimated by analytical solutions. Numerical solutions have the advantage of estimating storage properties for single-well tests. The combination of different analytical solutions applied to 238 aquifer tests successfully yield hydraulic properties on a regional scale.

## 4. Relationship between Hydraulic Conductivity and Specific Capacity

### Introduction

Traditional methods to estimate aquifer properties rely on aquifer tests, which provide effective hydraulic properties over a large area (Butler 2005). However, spatial variations of aquifer parameters are common, yet appropriate data that densely cover a study area are generally lacking. Therefore, simple and inexpensive parameter-estimation methods with extensive coverage of the study area are necessary. One hydraulic parameter that is easy to measure is the specific capacity ( $S_C$ ) of a well, which is the ratio of pumping rate to drawdown in the well. The fact that  $S_C$  is correlated with hydraulic flow properties (e.g., Todd 1980; Fetter 2000) can simplify parameter estimations. In many places around the world, well drillers are required to establish the depth-of-pump setting and to define drawdown-yield relations at well completion. Generally, measurements of  $S_C$  or a step-drawdown test are used for this purpose. Thus,  $S_C$  values are more abundant in ground-water databases than values of transmissivity ( $T$ ) or hydraulic conductivity ( $K$ ), and offer another approach to estimate hydraulic parameters.

This chapter examines the relationship between  $S_C$  and both  $T$  and  $K$  for the volcanic rock aquifers of Maui. The relationships were tested to investigate the effects of well-loss correction and consideration of aquifer penetration. The Maui relationship was used to estimate  $K$  for the aquifers of the state of Hawaii. Finally, a geostatistical interpolation was applied to generate  $K$  maps for the islands of Maui and Oahu. The two islands were chosen because their aquifers are among the most stressed in the state, and

regional values of hydraulic properties are extremely useful for ground-water management efforts.

## **Approaches**

### ***Relationship between Transmissivity and Specific Capacity***

Numerous studies have been conducted to simplify aquifer-parameter estimation methods by developing empirical relationships between  $T$  and  $S_C$  (e.g., Razack and Huntley 1991). Approaches are based on the Thiem (1906) equilibrium equation for confined aquifers (Equation 3.9). The Thiem equation may be applicable to unconfined aquifers when aquifer drawdown is insignificant compared with aquifer thickness (Gingerich 1999a).

Thomasson et al. (1960) simplified Equation (3.9) using theoretical values for the log-ratio term. Combining a mean value for the log-ratio term with the other constants, the relationship between  $T$  and  $S_C$  reduces to

$$T = f_1 S_C \quad (4.1)$$

where  $S_C$  is specific capacity,  $Q/s$  ( $\text{m}^2/\text{d}$ ). The dimensionless constant  $f_1$  ranged from 0.9 to 1.52, with a mean of 1.18 (Thomasson et al. 1960). Logan (1964) reported a similar empirical value of 1.22.

Starting with Razack and Huntley (1991), several investigators described empirical relationships between  $T$  and  $S_C$  for fractured rock aquifers (Huntley et al. 1992; Choi 1999; Jalludin and Razack 2004; Hamm et al. 2005; Razack and Lasm 2006) and

limestone aquifers (Eagon and Johe 1972; Wolansky and Corall 1985; Fabbri 1997; Mace 1997). Usually, the correlation is better between log-transforms of  $T$  and  $S_C$ , and the linear relationship of the log-transformed variables can thus be expressed as

$$T = f_2 S_C^c \quad (4.2)$$

where  $f_2$  and  $c$  are regression coefficients of the power relationship. Inaccuracies of such simplification originate mostly because well-construction details (depth of well, well diameter, and length of screened interval) are overlooked in the calculations. A better way to represent  $S_C$  was suggested by Takasaki and Mink (1982), who divided  $S_C$  by the depth of aquifer penetration, which is the uncased interval of a well. For dike-free flank lava flows on Oahu, the authors estimated values for  $S_C$  greater than 1,800 m<sup>2</sup>/d, and for  $S_C$  per unit uncased meter of aquifer penetration greater than 90 m/d.

Table 4.1 provides information about studies completed in fractured aquifers including methods to determine  $S_C$  and  $T$ , the coefficients of the empirical relationship between the two variables, and correlation coefficients ( $R$ , when available). Obviously, the empirical relationships vary for different hydrogeologic settings. The expressions are also different in similar geologic environments, indicating that the relationships are truly site specific (Razack and Lasm 2006). The relationships further depend on the methods used to identify  $S_C$  and  $T$ . For example, when estimating  $T$  for the same volcanic island aquifer, a different relationship was obtained with the Cooper–Jacob method (Choi 1999) than with the leaky Moench solution (Hamm et al. 2005). Considering variations in

hydrogeologic settings, relationships derived for other volcanic aquifers might not apply to the Hawaii islands.

**Table 4.1.** Summary and results of previous studies that examined empirical relationships between transmissivity and specific capacity (corrected and uncorrected for well losses)

Study	Aquifer	Location	Methods to determine hydraulic parameters		Regression coefficients <sup>a</sup>		<i>R</i> Non-trans-formed	<i>R</i> Log-trans-formed
			Specific capacity	Transmissivity	$f_2$	$c$		
Thomasson et al. (1960)	Valley-fill sediment	Solano County, California	Constant-rate test (uncorrected)	Aquifer test, method not specified	1.18	1.00	—	—
Logan (1964)	Sand & gravel	Illinois	Constant-rate test (uncorrected)	Aquifer test, method not specified	1.22	1.00	—	—
Razack and Huntley (1991)	Heterogeneous alluvium	Haouz plain, Morocco	Constant-rate test (uncorrected)	Cooper–Jacob	15.30	0.67	0.40	0.63
Huntley et al. (1992)	Fractured rock	San Diego, California	Constant-rate test, all steps from step test (uncorrected)	Cooper–Jacob (Neuman), Gringarten	0.12	1.18	0.72	0.89
Jalludin and Razack (2004)	Sediment, fractured basalt	Djibuti, Horn of Africa	Step-drawdown test (corrected)	Cooper–Jacob, Boulton, Theis Recovery	3.64	0.94	0.59	0.91
Razack and Lasm (2006)	Fractured rock	Man Danane, Ivory Coast	Step-drawdown test (corrected)	Theis Recovery	0.33	1.33	—	0.94
Eagon and Johe (1972) <sup>b</sup>	Karst	NW-Ohio	Constant-rate test (corrected)	Cooper–Jacob	3.24	0.81	—	—
Wolansky and Corall (1985) <sup>b</sup>	Karst	Florida	Constant-rate test (uncorrected)	Theis, Cooper–Jacob, Hantush (leaky)	1.23	1.05	—	—
Mace (1997)	Karst	Edwards, Texas	All steps from step test (uncorrected)	Theis, Cooper–Jacob, Theis Recovery	0.76	1.08	—	0.79
Fabbri (1997)	Karst	Veneto, NE-Italy	Constant-rate test (uncorrected)	Dupuit–Thiem	0.85	1.07	0.95	0.97
Choi (1999)	Volcanic island	Jeju, Korea	Constant-rate test (uncorrected)	Cooper–Jacob	0.45	1.05	—	—
Hamm et al. (2005)	Volcanic island	Jeju, Korea	Constant-rate test (uncorrected)	Moench (leaky)	0.99	0.89	0.60	0.94

<sup>a</sup>Regression coefficients are for  $S_C$  in  $m^2/d$

<sup>b</sup>in Mace (1997)

Previous studies estimated  $T$  from  $S_C$  (Table 4.1). However, an estimate of  $K$  is generally more useful for many applications in that it avoids the need for an estimate of aquifer thickness when using the empirical relationships to estimate aquifer parameters. Although estimates of  $K$  are of primary concern in this study, the relationship between  $T$  and  $S_C$  was also determined to facilitate comparison of results with those from previous studies.

### ***Well-Loss Correction***

$S_C$  can be determined from field data in various ways. Any corresponding pumping rate and drawdown measurement provides a value of  $S_C$ . Obviously, a constant-rate aquifer test would not provide a unique value unless a steady-state condition is reached. However, the change of  $S_C$  over time at a constant discharge rate is minor (Jacob 1947; Todd 1980). Step-drawdown tests typically include several steps of constant pumping rates that increase for subsequent steps. The method offers one  $S_C$  value for each step performed. However, the estimated values may differ greatly between the first and last steps. Values of  $S_C$  decreasing with increasing pumping rates reflect well losses that increase with higher pumping rates (see Chapter 3, Clark 1977; Todd 1980). The length of each step in Hawaii is generally 90 minutes and rarely exceeds 3 hours, which implies that steady state is not reached in most cases.

An example of a typical step-drawdown is shown in Figure 3.9. The quadratic relationship between steady-state drawdown in a well and discharge is given in Equation (3.1) when  $w = 2$  (Jacob 1947). Jalludin and Razack (2004) showed that correcting for well loss significantly reduces the uncertainty in the prediction by improving the

correlation between  $T$  and  $S_C$  and by narrowing the prediction interval that encompasses the estimated values with 95% confidence.

### *Aquifer-Parameter Analysis*

The same data from single-well constant-rate and variable-rate aquifer tests, which was used in Chapter 3, were analyzed to assess the relationship between aquifer parameters and  $S_C$ . Recovery tests were ignored, and different tests at the same well were treated as separate data pairs. Data utilized includes 78 constant-rate tests in 63 wells and 86 step-drawdown tests in 79 wells. The locations of wells, as indicated by type of test conducted, are shown in Figure 4.1.

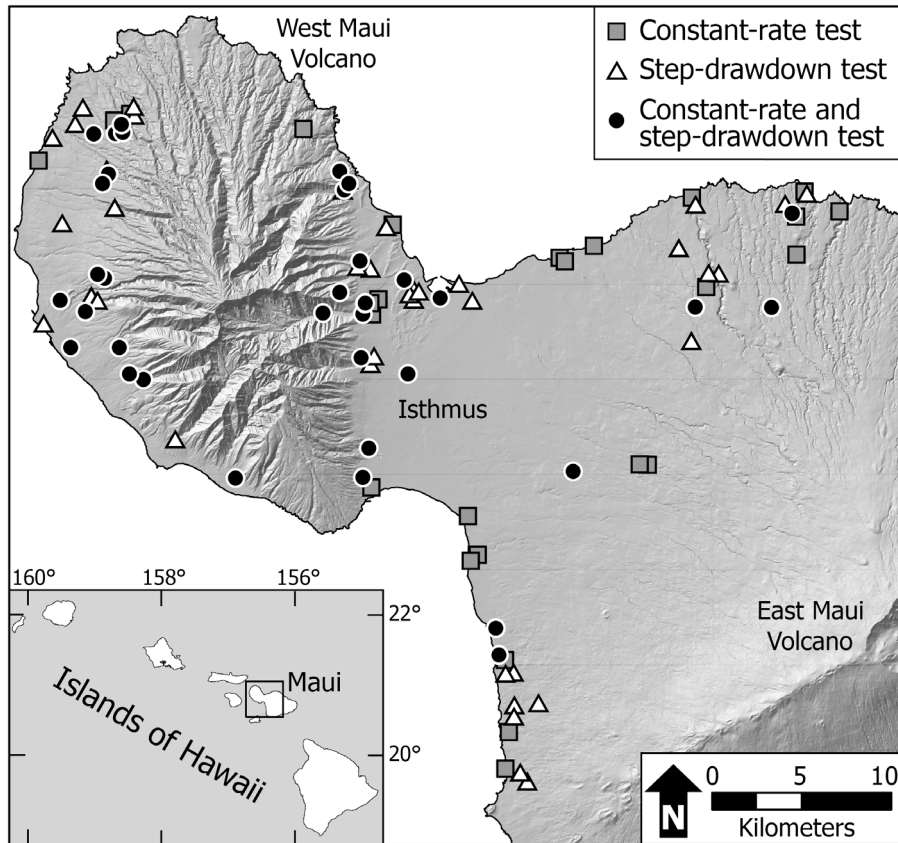


**Figure 4.1.** Location of wells on Maui, as indicated by type of aquifer tests conducted.

Constant-rate tests were analyzed using the methods of Theis (1935) and Cooper–Jacob (1946) to estimate  $T$ . These methods may be applied to single-well tests in unconfined aquifers if drawdown is insignificant when compared to aquifer thickness (Gingerich 1999a). No evidence of leakage or delayed yield was observed in constant-rate aquifer-test data used in this study (Chapter 3). Step-drawdown tests were analyzed using the methods of Zangar (1953) and Harr (1962)/Polubarinova–Kochina (1962) to estimate  $K$  (see Chapter 3). Estimates were converted from  $T$  to  $K$  and vice versa using Equation (3.11). As in the previous chapter, the aquifer thickness was defined as the distance from the well base to the water table (Gingerich 1999a) due to the lack of more accurate subsurface information. The arithmetic means of  $K$  and  $T$  based on the four methods mentioned above were used to evaluate the correlation with  $S_C$ . The use of average values is acceptable, considering that the standard deviation of different estimates for a given well was low (27% on the average).

The value of  $S_C$ , uncorrected for well loss, was determined either at the highest step in a step-drawdown test or when drawdown ceased during a constant-rate test. Both practices are used by CWRM to define specific capacity in its well database. The value of  $S_C$ , corrected for well loss, was estimated as the value  $1/B$  from step-drawdown tests based on least-squares fitting of Equation (3.1) with  $w = 2$ . The calculations yielded 114 and 86 data pairs ( $n$ ) for the uncorrected and corrected cases, respectively. In addition, to account for aquifer penetration,  $S_C$  values were divided by the uncased interval of the well ( $L$ ).

### ***Hydraulic-Conductivity Estimation***

To correlate either  $T$  or  $K$  with  $S_C$ , a linear regression of the log-transformed variables was applied. Correlation coefficients of the normal and the log-transformed values, the standard error, and 95% prediction intervals were determined. The prediction interval ( $P_{iv}$ ) is given by (e.g., Huntley et al. 1992)

$$P_{iv}(v) = \hat{v} \pm \sqrt{\frac{\sum_{i=1}^n (v_i - \hat{v})^2}{n-2}} t_{\alpha/2} \sqrt{1 + \frac{1}{n} + \frac{(\hat{z} - \bar{z})^2}{\sum_{i=1}^n (z_i - \bar{z})^2}}, \quad (4.3)$$

where  $v$  is the dependent variable ( $T$  or  $K$ ),  $\hat{v}$  is the predicted value of the dependent variable using the regression,  $n$  is the sample size;  $t_{\alpha/2}$  is the critical value of Student  $t$ -distribution for the significance level  $\alpha$  with  $n-2$  degrees of freedom,  $z$  is the independent variable ( $S_C$ ),  $\hat{z}$  is  $S_C$  for the prediction, and  $\bar{z}$  is the arithmetic mean of  $S_C$ .

The empirical relationship between  $K$  and  $S_C$  per unit aquifer penetration was assessed for all islands using data in the CWRM well database, which included 1,257  $S_C$  values. The data was not corrected for well losses. Data accuracy is not always assured, due to the lack of quality-control procedures in some cases. Compared to available aquifer-test data used in Chapter 3, 201  $S_C$  values are listed in the database for central and west Maui. The number of aquifer parameters estimated from  $S_C$  for this area is therefore 95% greater than from available aquifer-test data. To verify whether the relationship for Maui is applicable to the other islands, data pairs of  $K$  and  $S_C$  from single-well step-drawdown tests on Oahu (Soroos 1973) were compared with the data from Maui. Soroos (1973) estimated 89  $K$  values using the method of Zangar (1953).  $S_C$  values for the

uncorrected and the corrected case, as well as  $S_C$  per aquifer penetration, were determined with the methods described above.

### ***Geostatistical Analysis***

The large number of hydraulic parameters estimated from  $S_C$  enabled the application of geostatistical methods (e.g., Fabbri 1997; Razack and Lasm 2006). The geostatistical analyst, a toolbox in ESRI's ArcMap software package, was used to interpolate the point estimates to island-wide  $K$  maps for Oahu and Maui. Ordinary kriging was applied as in Chapter 3. Both the Maui and Oahu study areas encompass two volcanoes with flows propagating outward from the caldera in every direction. Thus, the experimental variograms were expected to be omni-directional. The equation of the spherical model to fit the variogram is given in Equation (3.12).

## **Results and Discussion**

### ***Empirical Relationships***

Table 4.2 shows detailed results from the regression analysis for the empirical relationships of  $S_C$  against both  $T$  and  $K$ . In general, the correlation coefficients for log-transformed values are greater than those for normal values, supporting a power-law relationship between the variables. The use of such a relationship (Equation 4.2) is consistent with its use in previous studies (Table 4.1). Trends in the residuals between observed and predicted values are not substantial. The absolute slope of regressions through the residuals does not exceed 0.05, and the correlation coefficients of observed and residual values are below 0.11.

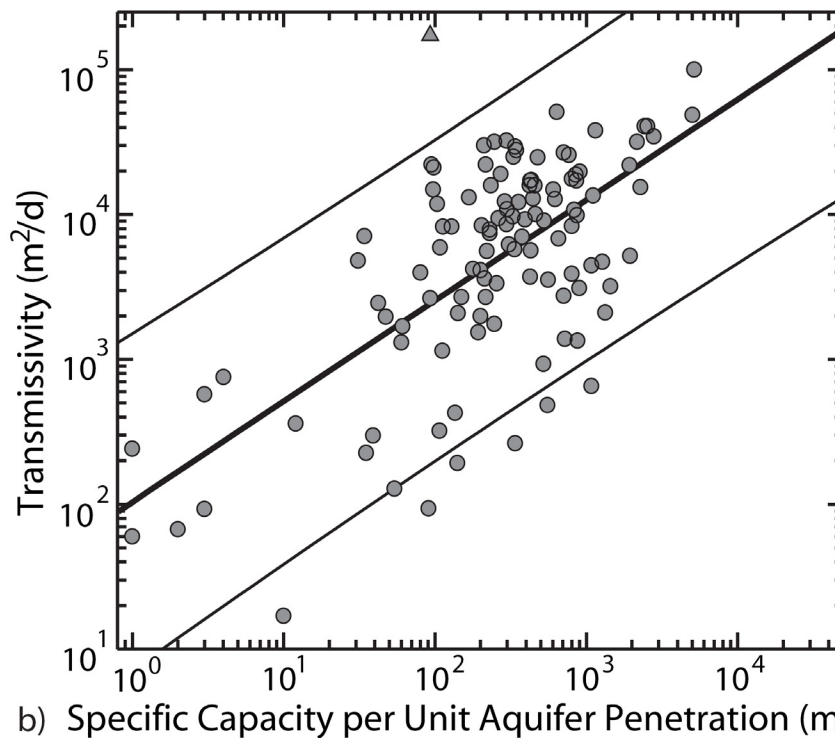
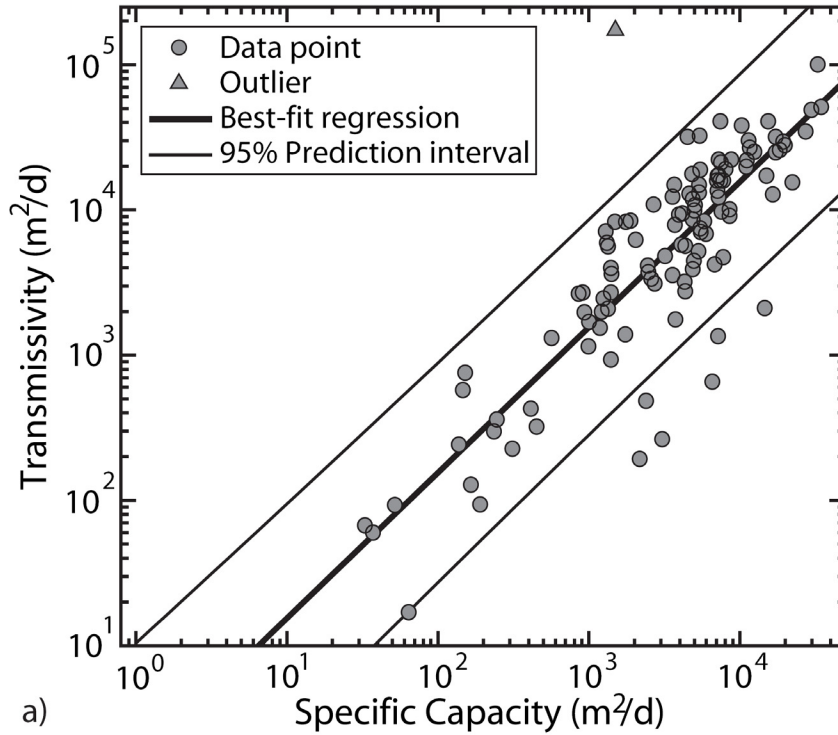
**Table 4.2.** Results from the regression analysis of transmissivity and hydraulic conductivity to specific-capacity ratios for Hawaii volcanic aquifers

Fig- ure	Aquifer parameters		<i>n</i>	Standard error (m <sup>2</sup> )	<i>R</i> Non- trans- formed	<i>R</i> Log- trans- formed	Regression coefficients <sup>b</sup>		Span (log cycles)	
	<i>y</i>	<i>S<sub>C</sub></i> <sup>a</sup>					<i>f</i> <sub>2</sub>	<i>c</i>	<i>y</i> -values	95% <i>P<sub>iv</sub></i>
4.2a	<i>T</i>	uncorrected	113	0.37	0.81	0.87	1.537	1.002	3.8	1.5
4.2b	<i>T</i>	uncorr. / <i>L</i>	113	0.56	0.68	0.67	103.883	0.695	3.8	2.2
4.3a	<i>K</i>	uncorrected	113	0.46	0.59	0.81	0.126	0.966	4.1	1.8
4.3b	<i>K</i>	uncorr. / <i>L</i>	113	0.42	0.88	0.84	1.917	0.914	4.1	1.7
4.4a	<i>K</i>	corrected	86	0.30	0.85	0.92	0.061	0.987	4.1	1.2
4.4b	<i>K</i>	corrected / <i>L</i>	84	0.13	0.98	0.99	1.211	0.920	4.1	0.5

<sup>a</sup>Uncorrected or corrected for well losses, *L* is the uncased interval of a well (m)

<sup>b</sup>Regression coefficients are for *S<sub>C</sub>* in m<sup>2</sup>/d or for the aquifer penetration case in m/d

A log-log plot of *T* against *S<sub>C</sub>*, uncorrected for well loss, is shown in Figure 4.2a. Moderate scatter of the data can be seen, and the 95% prediction interval spans 1.5 log cycles, which is large considering that predictions contain an uncertainty of ±0.7 order of magnitude. Still, a good correlation is evident by an *R*-value of 0.87. One outlier is excluded from the regression, whereas six values below the prediction interval are not because they did not influence the regression coefficients. However, excluding these points would shrink the prediction interval to 1.1 log cycles and increase the *R*-value to 0.93. As indicated before, the relationships between *S<sub>C</sub>* and *T* are site specific, as is confirmed here. The relationship derived in this study differs considerably from those for volcanic rock aquifers obtained by Choi (1999) and Hamm et al. (2005) (see Table 4.1). The regression parameter *f*<sub>2</sub>, given as 1.54, is slightly above Thomasson's (1960) theoretical upper limit of 1.52, considering that the slope *c* is equivalent in both cases.



**Figure 4.2.** (a) Plot of transmissivity from constant-rate and step-drawdown tests against specific capacity from constant-rate and step-drawdown tests, uncorrected for well loss. (b) Plot of transmissivity from constant-rate and step-drawdown tests against specific capacity per aquifer penetration from step-drawdown tests, uncorrected for well loss.

Comparing  $S_C$  per unit aquifer penetration against  $T$  reduces the correlation of the variables, as shown in Figure 4.2b. The  $R$ -value is lower (0.67), and the width of the 95% prediction interval spans more than 2 log cycles (Table 4.2). The wider prediction interval is associated with uncertainty of the aquifer thickness introduced with the conversion from  $K$  to  $T$ .

Analysis of step-drawdown tests for the Maui data set indicates that the mean difference of  $S_C$  between the first and last steps in the tests is 50%, with a standard deviation of 41% and a maximum difference of 184%. This large disparity shows that incorporating all  $S_C$  values from a step-drawdown test to define hydraulic parameters is unacceptable. The mean difference between corrected and uncorrected  $S_C$  is 52%, with a standard deviation of 21% and a maximum difference of 99%. The mean uncased interval of the Maui wells used in this analysis is 19 m, and the standard deviation is 22 m. Dividing  $S_C$  by  $L$  significantly reduces  $S_C$  (on average, one order of magnitude). The large variation of  $S_C$  associated with well-loss correction and consideration of aquifer penetration length emphasizes the necessity of using the appropriate relationship when estimating hydraulic parameters from  $S_C$ .

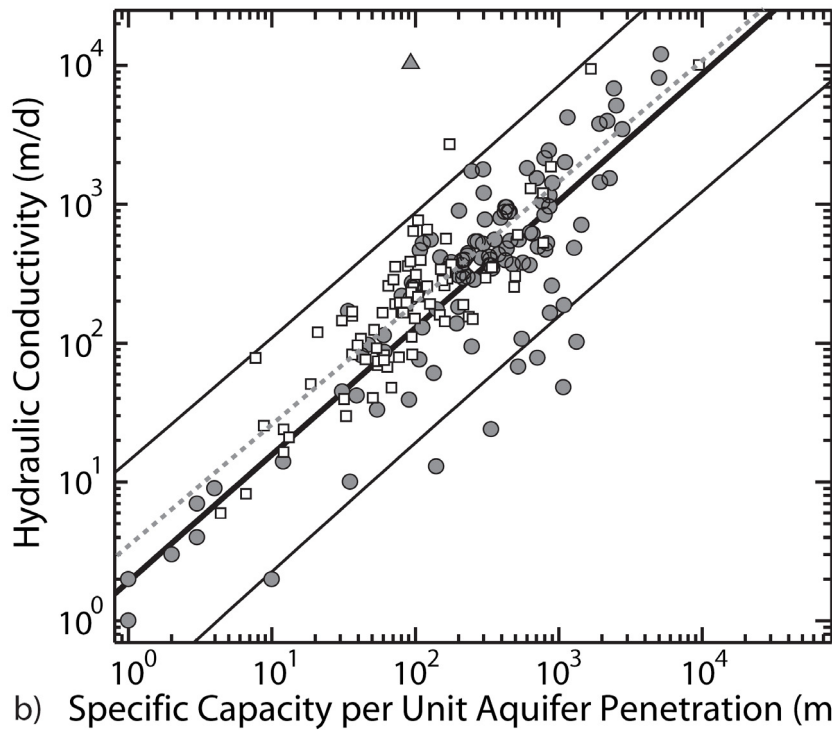
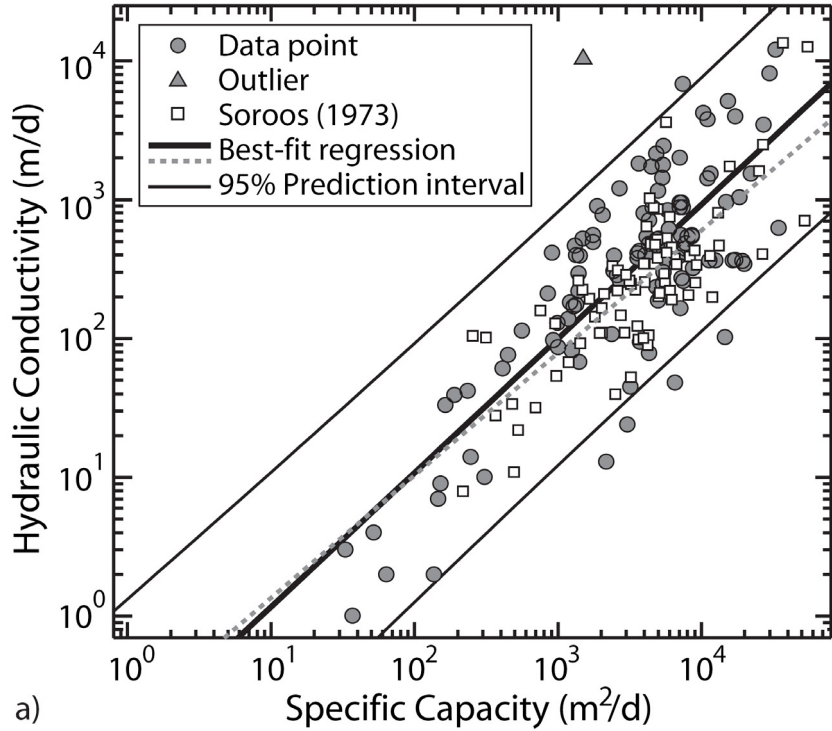


**Figure 4.3.** (a) Plot of hydraulic conductivity from constant-rate and step-drawdown tests against specific capacity from constant-rate and step-drawdown tests, uncorrected for well loss. (b) Plot of hydraulic conductivity from constant-rate and step-drawdown tests against specific capacity per aquifer penetration from step-drawdown tests, uncorrected for well loss.

The regression between  $\log S_C$ , uncorrected for turbulent head losses, and  $\log K$  is illustrated in Figure 4.3a. The data are more scattered than for the correlation with  $T$  (Figure 4.2a), and the 95% prediction interval spans 1.8 orders of magnitude. The standard error for the uncorrected relationship is higher ( $0.46 \text{ m}^2$ ) and the  $R$ -value lower (0.81) than the values for  $T$ . However, a prediction interval considerably larger than one log cycle is not uncommon in similar studies (e.g., Razack and Huntley 1991; Jalludin and Razack 2004). Considering aquifer-penetration length increases the correlation to 0.84, reduces the standard error to  $0.42 \text{ m}^2$ , and shrinks the prediction interval to 1.66 orders of magnitude (Figure 4.3b).

The relationship between  $K$  and  $S_C$ , corrected for well loss (Figure 4.4a), provides a more robust prediction of  $K$  with a better correlation ( $R = 0.92$ ) and a reduction of the prediction-interval width to 1.2 log cycles. The prediction improves further when the uncased interval is incorporated (Figure 4.4b). The relationship shows an excellent correlation of 0.99 with the lowest standard error ( $0.13 \text{ m}^2$ ) and the smallest prediction-interval width of 0.5 log cycle (Table 4.2). Except for well radius, the aquifer-loss coefficient ( $B$ ) and open interval ( $L$ ) are the main variables to estimate  $K$  by analytical solutions from step-drawdown test data (Table 3.1). The good match is thus not a surprise.

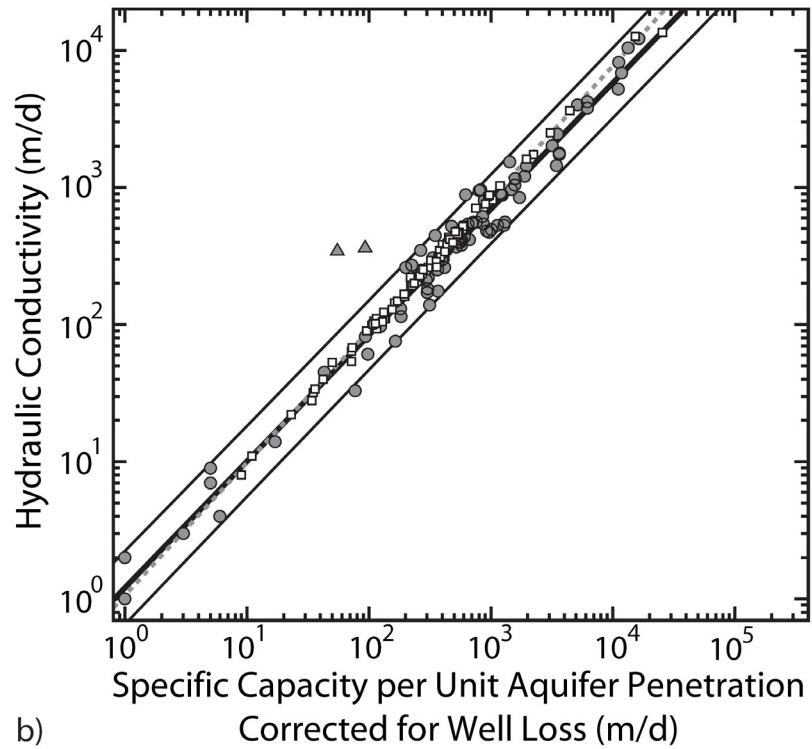
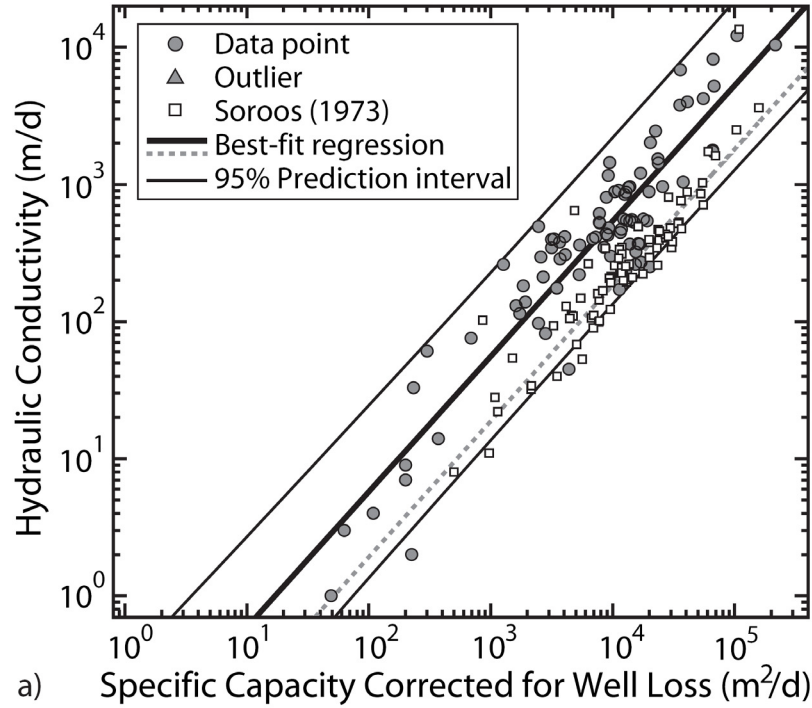


**Figure 4.4.** (a) Plot of hydraulic conductivity from constant-rate and step-drawdown tests against specific capacity from constant-rate and step-drawdown tests, corrected for well loss. (b) Plot of hydraulic conductivity from constant-rate and step-drawdown tests against specific capacity per aquifer penetration from step-drawdown tests, corrected for well loss.

Data from step-drawdown aquifer tests analyzed by Soroos (1973) were used to test the applicability of the Maui-based regression to the island of Oahu. Figure 4.3a plots data from both islands for the uncorrected case; it shows a good match, considering that the Oahu data fall within the 95% prediction interval. The regression line for the Oahu data is the gray dashed line. The regression lines are almost identical for the data sets of both islands. A similar match is shown in Figure 4.3b, with most of the Oahu data falling within the 95% prediction interval and with similar regression lines.

Plotting the data corrected for well loss shows a different match in Figure 4.4a, as compared to that shown in Figure 4.3. Although the Oahu data plots mostly within the 95% prediction interval of the Maui data and the regression line yields a similar slope, the Oahu  $y$ -intercept is lower than that for Maui by a factor of 0.36. A possible reason for the discrepancy is that the open interval of the wells used in the step-drawdown tests on Oahu is significantly greater. On average, the screened length of Oahu wells is 190% greater than that of Maui wells. A greater open interval produces a lower  $K$  value relative to the value of  $S_C$ , considering that the other variables used in the analytical solution of Zangar (1953) are in the same range for both islands. Adjusting the  $S_C$  values with the uncased interval resolves this discrepancy. In Figure 4.4b, the Oahu  $S_C$  data per aquifer penetration that are corrected for well losses plot very closely to the Maui regression line.

### ***Hydraulic-Conductivity Estimation***

Unfortunately, it was not possible to assess suitability of the regression for the other islands due to the absence of comprehensive aquifer-test data. However, the good match in Figures 4.3 and 4.4, the similarity of Hawaii volcanic rocks, and the comparable

hydrogeologic settings of the Hawaii islands suggest suitability of the proposed relationship for all islands. Considering the assumptions included, the estimates can be useful in the absence of more accurate values.

Although correcting  $S_C$  for well losses improves the prediction, the uncorrected relationship was used in the statewide  $K$  estimation because available  $S_C$  values in the state's well database are not adjusted for turbulent head losses. Open well length data are available, and thus the relationship  $1.92 S_C^{0.91}$  (Figure 4.3b) was used to estimate  $K$  for the state of Hawaii in the absence of step-drawdown tests. When step-drawdown tests exist,  $K$  can better be directly estimated (Eagon and Johe 1972; Soroos 1973; Clark 1977) without the need to adopt the simplified approach based on empirical  $S_C$  relationships. As mentioned in Chapter 3, the results match between the log-transformed hydraulic conductivity from constant rate tests and step-drawdown tests, with a correlation of 0.81.

Figure 4.5 shows  $K$  values estimated from  $S_C$  for the major islands of Hawaii. Most wells are drilled in volcanic rocks; however, a large number (21%) are situated within dike complexes, where their respective water levels are elevated high above the freshwater lens and the effective horizontal  $K$  is low. The outline of dike-zone complexes in Figure 4.5 was adapted from Macdonald et al. (1983). Several (16%) of the shallow coastal wells tap the overlaying sediment. Although the estimated  $K$  values change considerably over short distances in some places, regional differentiation exists between wells inside and outside the designated dike-zone complex, as reflected by low and high  $K$  values, respectively. This is most evident for the islands of Kauai, Oahu, and Lanai, where numerous wells are located in the dike-zone complex. The  $K$  estimates of wells in

the dike zone range from 0.1 to 1,500 m/d, with a geometric mean of 7 m/d and a median value of 8 m/d. The asymmetrical interval of the standard deviation varies between 0.8 and 61 m/d.

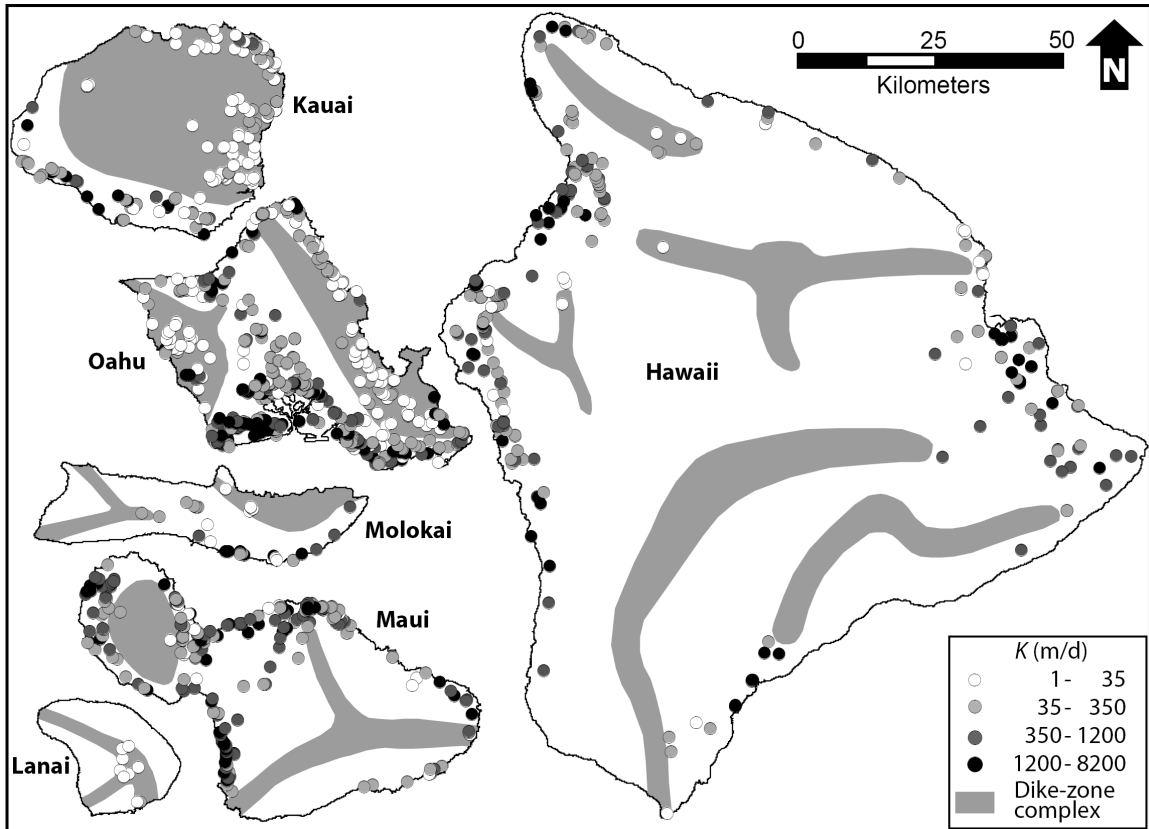


**Figure 4.5.** Hydraulic-conductivity estimates from specific capacity, and outline of dike-zone complexes (Stearns and Macdonald 1963) in the state of Hawaii.

This study emphasizes on dike-free volcanic rocks. Thus, wells that are situated in the dike-zone complex or near the complex with water levels above the freshwater lens (> 20 m amsl) were excluded from further analysis. Also excluded were wells situated in sediment or limestone.  $S_C$  values for 24 shafts, tunnels, and dug wells were ignored due to their large-diameter infiltration holes. The estimated  $K$  values for the remaining 768 wells in dike-free flank lavas on various islands were compared. A box-and-whisker plot shows

the distribution of the  $K$  values for five islands and for the entire state (Figure 4.6). The minimum and maximum values are shown as whiskers, while the 25% and 75% quartiles are the horizontally bounding sides of the boxes with a horizontal bar representing the median value in the center. The sample size is displayed in white within the boxes. Generally, the ranges of  $K$  estimates do not change considerably among islands. The notches in the boxes represent a robust estimate of the uncertainty about the medians. Since the notches for Kauai, Oahu, and Molokai overlap, the medians of those islands are indistinguishable at the 95% confidence level. The same is true for Maui and Hawaii, which are characterized by higher median values.

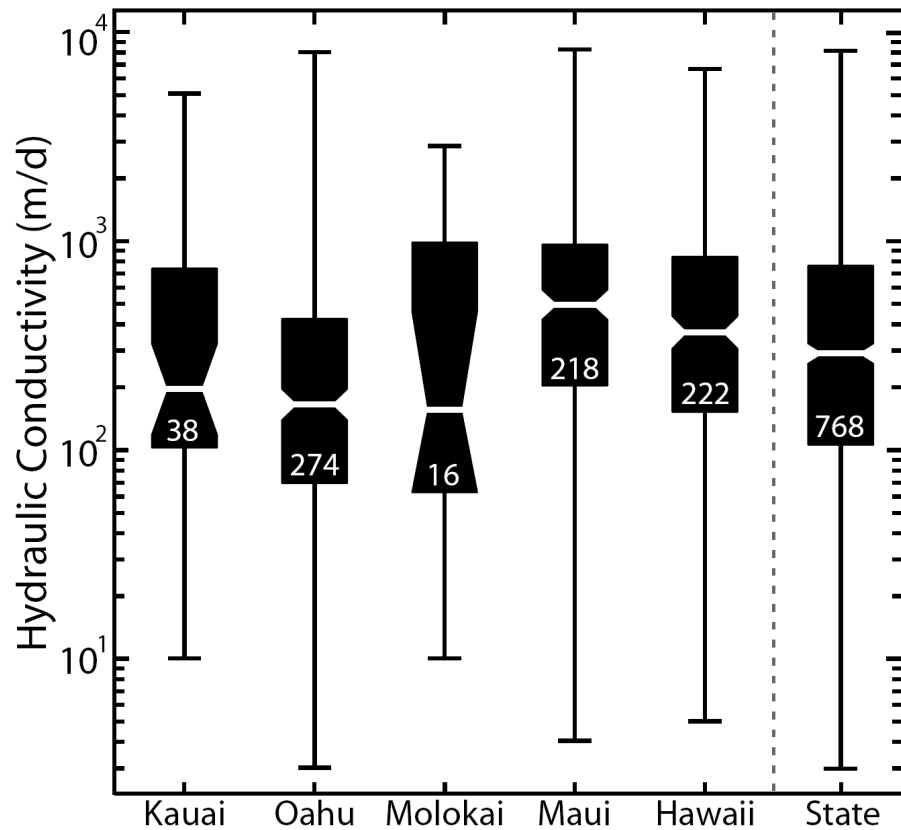


**Figure 4.6.** Box-and-whisker diagram for the hydraulic-conductivity estimates of dike-free volcanic rocks for five islands and for the state of Hawaii. The white number is the sample size.

Summary statistics of  $K$  values for dike-free basalts in the state of Hawaii are listed in Table 4.3. The  $K$  estimates for the entire state range from 3 to 8,200 m/d, with a geometric mean of 274 m/d and a median value of 292 m/d. The asymmetrical interval of the standard deviation ranges from 66 to 1,142 m/d. Half of the data covers less than one order of magnitude from 110 to 770 m/d. The median values of the individual islands are close to their respective geometric means. The  $K$  values estimated here from  $S_C$  not only fall in the range of  $K$  estimates for volcanic rocks documented by Hunt (1996) for Oahu but also are consistent with estimates in the same study area based on aquifer-test analyses (see Chapter 3).

**Table 4.3.** Summary statistics of hydraulic-conductivity estimates (m/d) from specific capacity for dike-free basalts in the state of Hawaii

	Hawaii Islands					State of Hawaii
	Kauai	Oahu	Molokai	Maui	Hawaii	
$n$	38	274	16	218	222	768
Geometric mean	242	171	203	423	336	274
Median	194	164	155	493	364	292
Mean - std. dev.	50	42	38	121	82	66
Mean + std. dev.	1,181	689	1,099	1,483	1,372	1,142

### ***Geostatistical Analysis***

Regional  $K$  predictions are of practical importance for ground-water management, especially for Oahu and Maui, where the aquifers are among the most stressed in the state. Defining aquifer  $K$  maps facilitates the development of a detailed numerical model for the area in the absence of detailed field assessments. The prediction of such maps requires spatial-variability analysis using experimental variograms. Figure 4.7 shows the

variogram for  $K$  estimates for Oahu and Maui. The parameters for the spherical model fit using Equation (3.12) are  $G_0 = 359,860$ ,  $G_1 = 207,597$ ,  $d = 6,973$ , and  $l = 500$  for Oahu and  $G_0 = 725,740$ ,  $G_1 = 467,480$ ,  $d = 5,956$ , and  $l = 500$  for Maui. A quasi-stationary plateau is reached at 7 km for Oahu and at 6 km for Maui, indicating that spatial correlations are significant over such distances. The spatial correlation is weak over large distances due to high  $K$  variances on a small scale.

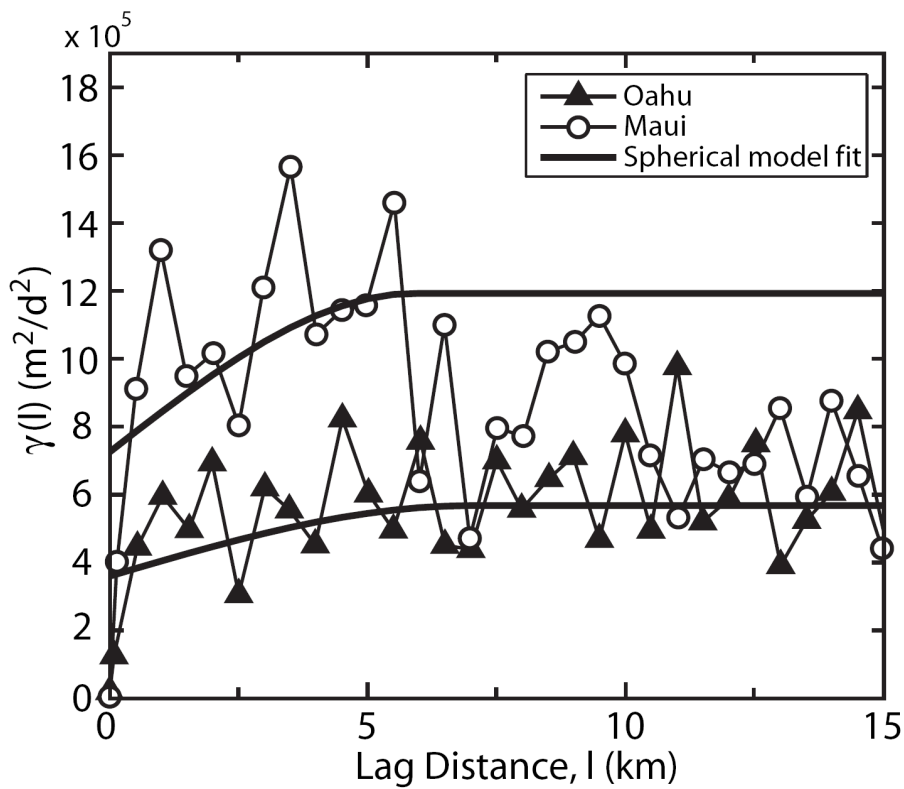


**Figure 4.7.** Experimental variogram of the spatial correlation of hydraulic conductivity for Oahu and Maui, and the spherical model fit.

The estimated  $K$  map for Oahu using ordinary kriging is shown in Figure 4.8a. The dike-zone complexes are masked to avoid misinterpretation of predicted  $K$  values in these areas. The  $K$  estimates in the map cover a smaller range than the point estimates

from 150 to 1,100 m/d due to the smoothing effect of the kriging interpolation. Lower values were predicted in the center and on the north tip. The center of Oahu is influenced by flow barriers that cause ground-water levels to rise to 85 m amsl. The wells on the northeast coast may be affected by proximity to the dike-zone complex. The extent of the marginal dike zone is not clearly defined, thus estimates in that area may be influenced by the presence of scattered dikes beyond the outlined dike zone. The standard error of the prediction for Oahu is shown in Figure 4.8b. Clearly, the prediction is more robust in places with a higher sample density. The root-mean-square error of the prediction for Oahu is 921 m/d, and the average standard error is 760 m/d. The weak spatial correlation of  $K$  values can cause these large errors. The large errors imply a  $K$  value that is equal to or less than zero, which is physically impossible. Thus, caution should be adopted in using the data and keeping in mind uncertainties in the estimates.

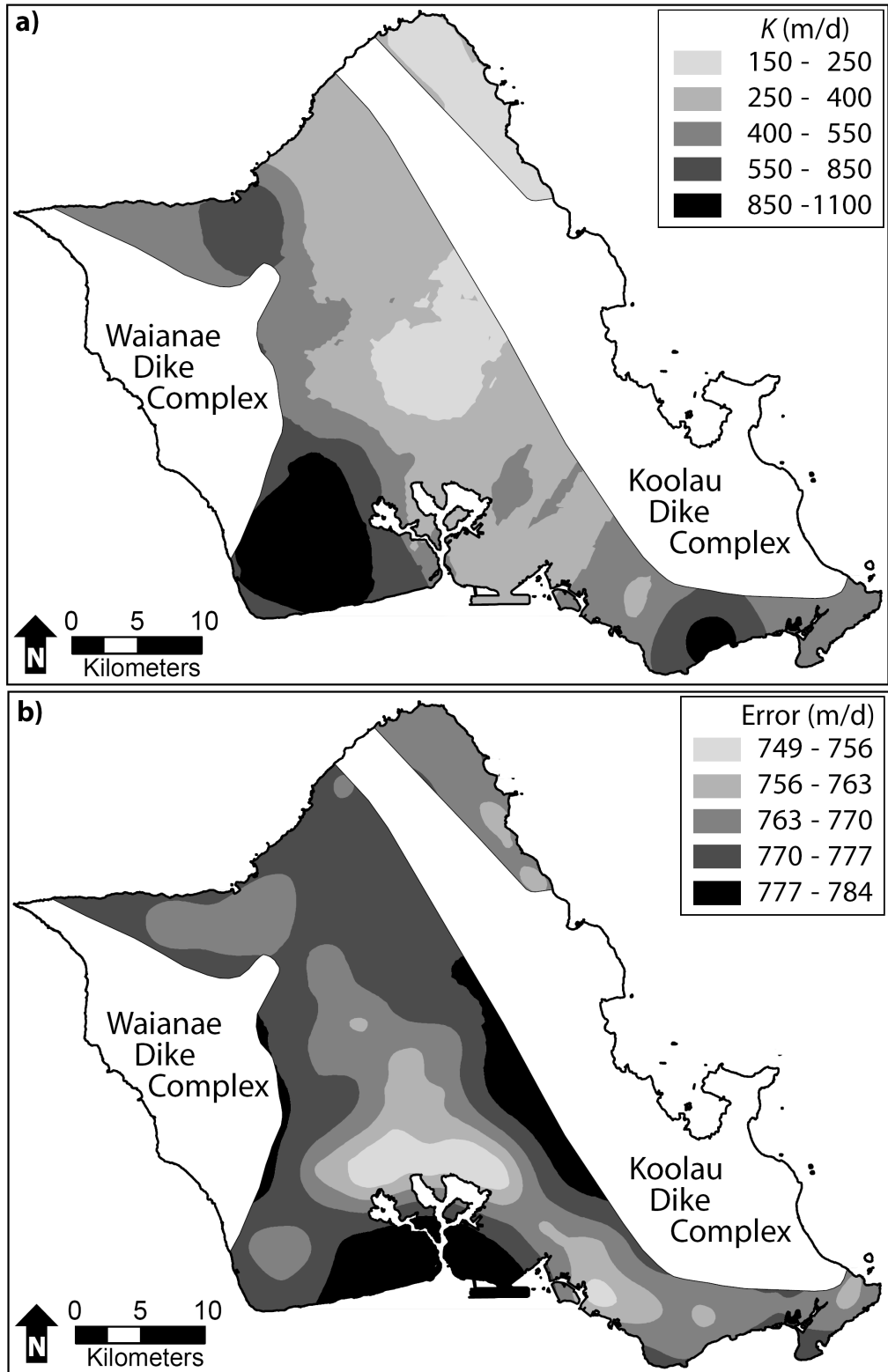


**Figure 4.8.** (a) Estimated hydraulic-conductivity map of dike-free volcanic rocks for the island of Oahu. (b) Predicted standard error map for Oahu.

The estimated  $K$  map for Maui is shown in Figure 4.9a.  $K$  estimates range from 250 to 1,300 m/d. Again, areas of lower estimates may be attributed to the influence of the dike zone. The standard error of the prediction for Maui is shown in Figure 4.9b. The southeast side of East Maui Volcano has only few sample points, which produce a less robust prediction of that area. The root-mean-square error of the prediction is 935 m/d, and the average standard error is 972 m/d. The error for Maui is larger than for Oahu. In Figure 4.7, the variance for Maui drops below the plateau after reaching the range, while that for Oahu stays around the plateau. Compared with the results from Chapter 3 (Figure 3.8), a different distribution emerges for the same study area. The highest contrast is found in north-central Maui, where a  $K$  range of 100 to 300 m/d was predicted. Using the map estimated from  $S_C$ , the values are 5 to 10 times higher with a contoured range of 1,000 to 1,300 m/d. The higher  $K$  prediction is attributed to seven wells that are not included in the aquifer-test dataset. The  $K$  estimates for those wells are above 1,000 m/d, while the highest estimate based on aquifer tests in this area is 900 m/d. The rest of the map in Figure 4.9a matches reasonably well with the  $K$  contour map based on aquifer-test results (Figure 3.8).

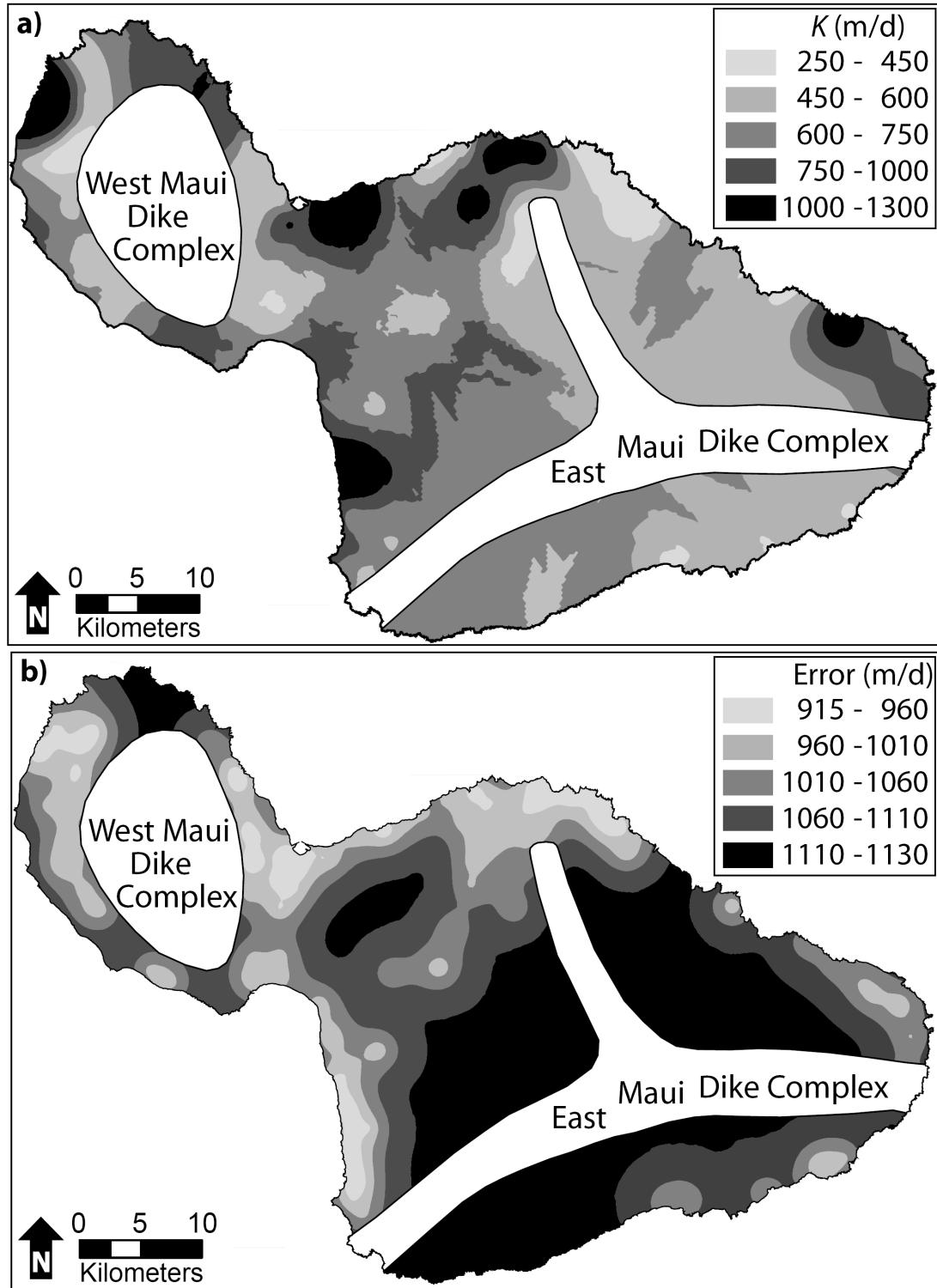


**Figure 4.9.** (a) Estimated hydraulic-conductivity map of dike-free volcanic rocks for the island of Maui. (b) Predicted standard error map for Maui.

## Chapter 4 Conclusions

A linear regression of log-transformed data from aquifer tests on Maui relates transmissivity and hydraulic conductivity to specific capacity. Correcting  $S_C$  for turbulent head loss using results from step-drawdown tests improves the correlation, narrows the width of the prediction interval for both  $T$  and  $K$ , and thus reduces uncertainty in the prediction. However, such a correction might not be necessary because aquifer parameters may be better estimated directly from step-drawdown data instead of using simplified approaches. Details about well construction were ignored in previous studies, so uncertainty was introduced in the predictions. The current analysis accounts for aquifer penetration length by dividing  $S_C$  values by the open interval of the well.

The derived relationship between  $T$  and  $S_C$  differs considerably from those published for volcanic rock aquifers, confirming that all relationships are essentially site specific. The empirical relationships extend over four orders of magnitude for the hydraulic parameters and provide a prediction of  $T$  and  $K$  with correlation coefficients between 0.81 and 0.99. Uncertainty in the  $K$  predictions is generally reduced by incorporating aquifer-penetration length and correcting for well losses. Still, the relationships can only provide an approximation of aquifer parameters in the absence of more accurate values.

$K$  was estimated from  $S_C$  per unit aquifer penetration documented in the Hawaii's well database using  $1.92 S_C^{0.91}$ . Data points from aquifer tests on Oahu (Soroos 1973) fit reasonably well to the Maui relationship, suggesting applicability of this relationship to other Hawaii islands. Statistical analysis shows that  $K$  estimates for dike-free volcanic

rocks cover similar ranges of values for various islands. For all islands, the values fall within previously established ranges for volcanic rocks: 3 to 8,200 m/d. The geometric-mean and median values are respectively 274 m/d and 292 m/d. The asymmetrical interval of the standard deviation ranges from 66 to 1,142 m/d. Half of the data spans less than one order of magnitude from 110 to 770 m/d.

The  $K$  point estimates were kriged to create an island-wide contour map for Oahu and Maui. Spatial correlation is weak over distances greater than 10 km. The predictions on Oahu range from 150 to 1,100 m/d. The predicted  $K$  surface shows areas of low values in the center and north tip, most likely due to the influence of the dike-zone complex.  $K$  predictions for Maui range from 250 to 1,300 m/d. These values match reasonably well with kriged  $K$  values based on aquifer tests on Maui. In general, and as should be expected, confidence in the prediction is greater in areas with higher sample density. The predicted standard errors are large and caution should be adopted in using the data. However, the kriged  $K$  maps can be of practical importance for ground-water management on Oahu and Maui in the absence of detailed field assessments because aquifers there are among the most stressed in the state of Hawaii.

## 5. Ocean Tides and Dual-Tide Influence

### Introduction

Ocean tides produce a natural forcing dominantly at the diurnal or semidiurnal frequency that affects ground-water levels in coastal aquifers. The amplitude of the harmonic signal attenuates exponentially and the phase lag increases linearly as it propagates through the aquifer at a rate that depends on the aquifer's properties and distance from shore (Jacob 1950). Early analytical solutions describing this phenomenon are one-dimensional and were derived for a homogeneous, isotropic, confined, and semi-infinite aquifer with a sharp boundary subject to oscillating head conditions (Jacob 1950; Ferris 1951). Similar solutions were developed for a homogeneous, isotropic, unconfined, and finite length aquifer (Werner and Norén 1951). However, the Jacob-Ferris method can be applied to unconfined aquifers if the tidal range is small compared to the saturated aquifer thickness (Erskine 1991).

Refinement of the simplified geometry at the boundary was achieved by several authors (e.g., Van der Kamp 1972; Li and Chen 1991; Li and Jiao 2001; Jeng et al. 2005; Chuang and Yeh 2006). Recently, Li et al. (2007) developed an analytical solution to include effects of a submarine aquifer with a sediment-covered outlet, which was expanded to multi-layered aquifers (Guo et al. 2007). The effect of leakage at the submarine outlet-capping was investigated by Xia et al. (2007). The consideration of sediment capping is particularly applicable to Hawaii aquifers, because low-permeability sediments overlie the basalt aquifer in some places along the coast. Other improvements

include addressing aquifer layering (e.g., Jiao and Tang 1999; Jeng et al. 2002; Li and Jiao 2002, 2003) and spatial heterogeneity in a composite aquifer (Trefry 1999). Some horizontal two-dimensional analytical solutions incorporate the effect of ocean tides in an aquifer with a L-shaped coastline (Li et al. 2002) and in a rectangular aquifer and estuary perpendicular to the coast (Sun 1997; Li et al. 2000).

The tidal response in a coastal aquifer commonly is used to characterize its hydraulic properties (e.g., Gregg 1966; Carr and Van der Kamp 1969; Dale 1974; Williams and Liu 1975; Erskine 1991; Serfes 1991; Oki 1997; Cruz and Silva 2001; Smith and Hick 2001; Merritt 2004; Trefry and Bekele 2004). The amplitude attenuation and phase lag observed in an aquifer can be used to estimate hydraulic diffusivity, which is defined as the ratio of transmissivity to storativity for confined aquifers and as the ratio of transmissivity to specific yield for unconfined aquifers. The use of tides to estimate aquifer parameters provides results covering greater areas than conventional aquifer tests. Additionally, lower costs and simpler logistics are associated with the naturally occurring tidal forcing. Still, a combination of the tidal method and other hydraulic parameter-estimation methods is desirable because estimates of diffusivity are more meaningful with independent estimates of transmissivity, hydraulic conductivity, and storage parameters.

Analytical solutions for the head in aquifers influenced by tides mostly focus on the one-sided attenuation of the tidal signal as it propagates inland perpendicular to the shoreline. However, island aquifers experience periodic forcing from the entire coast, which may result in overlapping effects in the center. The radially symmetric case is

applicable to circular islands (e.g., Dale 1974), but it assumes constant heads in the center (Townley 1995) and thus ignores potential superposition from opposing sides. Townley (1995) provided a solution for a finite length aquifer subject to dual loading by tides and periodic recharge. Trefry and Bekele (2004) applied this solution to synchronous and symmetric boundary conditions in a finite length dual-tide aquifer. Interaction of the tidal responses in the interior of an island is reflected by hyperbolic attenuations and non-linear phase lags. Dual-tide effects are particularly important in small highly permeable volcanic islands and atolls, where the tidal signal is measurable kilometers away from the coast. However, narrow, elongated islands with lower permeability may be similarly affected by dual-tide influences.

Current applications overlook the tidal lag around a coast. Ocean tides are non-uniform and asynchronous around the coastline of an island. The amplitude and phase of the tide may differ significantly on various locations on the same island. The tide circulates around amphidromic points, which have almost zero tidal range (Brown et al. 1989). The time lag depends mostly on the local bathymetry, although location and orientation of the island with respect to amphidromic points, as well as size and shape of the island may also influence the lag. For example, islands located in shallow seas favor a larger phase lag because the tidal waves slow down with decreasing water depth. Moreover, the high-tide lag from one point on the coastline to another can be different from the low-tide lag. The high-tide wave efficiently travels in deeper water and is therefore faster than the low-tide wave (Brown et al. 1989). The superposition of each tidal mode can locally result in an asymmetric behavior of the signal. The effect of dual-

tide influence with asynchronous and asymmetric boundary conditions on the head distribution has not been addressed.

The objectives of this chapter are to present an analytical one-dimensional solution for the head distribution in a finite-length, asynchronous dual-tide aquifer, to estimate hydraulic parameters for an unconfined volcanic island aquifer, and to examine the accuracy of the dual-tide analytical solution. The analytical solution allows consideration of a sediment-damping effect at the boundary. The amplitude reduction at the boundary was verified with a simple numerical model. The aquifers of central Maui were suitable for testing the applicability of the analytical dual-tide solution because the isthmus of central Maui has two opposing coastlines and because tidal peaks on the north coast occur almost two hours before the peaks on the south coast.

## **Analytical Solution**

### ***Dual-Tide Solution***

The configuration of an unconfined dual-tide aquifer is illustrated in Figure 5.1. The tidal forcing can differ on each side of the aquifer. Tidal influence from either side propagates into the interior of the aquifer and creates a mixed response of the water table. The aquifer is assumed homogeneous and isotropic with a vertical boundary between the land and ocean. The one-dimensional linear ground-water flow equation reads:

$$\frac{\partial h}{\partial t} = \frac{T}{S} \frac{\partial^2 h}{\partial x^2} \quad (5.1)$$

where  $h$  is the piezometric head (m),  $t$  is time (d),  $T$  is the transmissivity ( $\text{m}^2/\text{d}$ ),  $S$  is the specific yield for unconfined aquifers or storativity for confined aquifers (dimensionless), and  $x$  is the distance from the boundary (m).

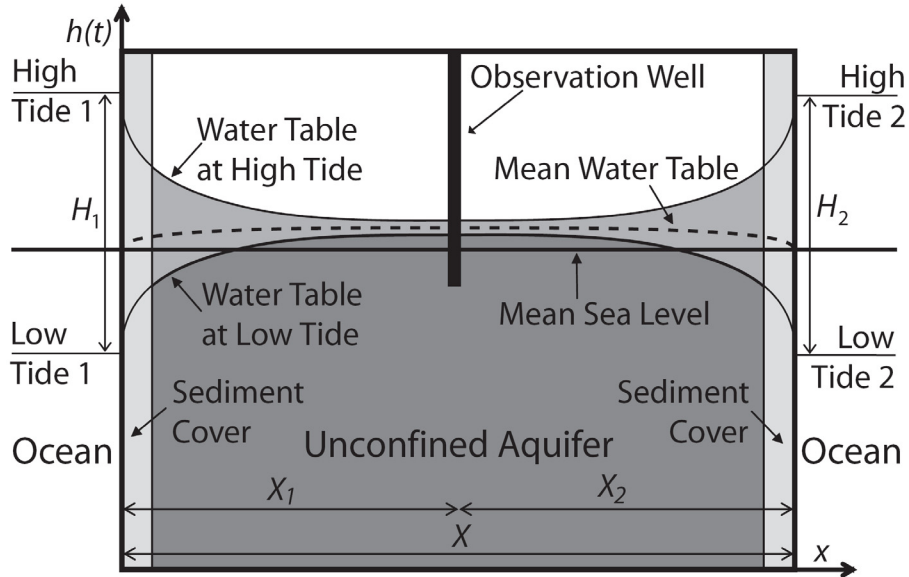


Figure 5.1. Schematic cross section of an unconfined dual-tide aquifer with sediment cover at the boundary.

The solution,  $h(x,t)$ , extends over a finite domain  $x \in [0, X]$ . The subscripts one and two, used for all symbols in this chapter, correspond to one and the opposite side of the domain, respectively. The Dirichlet boundary conditions for an asynchronous dual-tide aquifer are given by

$$h(0,t) = H_{1j} \cos(\omega_j t), \quad (5.2a)$$

$$h(X,t) = H_{2j} \cos(\omega_j t + \psi_j), \quad (5.2b)$$

where  $H_{1j}$  is the amplitude of the  $j^{\text{th}}$  tidal constituent of the harmonic oscillation on side one of the aquifer (m),  $\omega_j$  is the angular frequency of the  $j^{\text{th}}$  tidal constituent ( $\text{d}^{-1}$ ),  $X$  is the length of the aquifer (m),  $H_{2j}$  is the amplitude of the  $j^{\text{th}}$  tidal constituent on side two of the aquifer (m), and  $\psi_j$  is the tidal phase lag of the  $j^{\text{th}}$  constituent from one coast to the opposite coast (rad). Suppose that  $h(x,t)$  can be written as

$$h(x,t) = \text{Re}(\Lambda(x)e^{i\omega_j t}), \quad (5.3)$$

where  $\text{Re}$  denotes the real part of the complex expression,  $i = \sqrt{-1}$  and  $\Lambda(x)$  is an unknown complex function of  $x$ . Using the method of Li et al. (2007) one can derive the differential equation and boundary conditions satisfied by  $\Lambda(x)$ :

$$\frac{T}{S}\Lambda''(x) - i\omega_j\Lambda(x) = 0, \quad (5.4a)$$

$$\Lambda(0) = H_{1j}, \quad (5.4b)$$

$$\Lambda(X) = H_{2j}e^{i\psi_j}. \quad (5.4c)$$

The general solution of Equation (5.4a) is

$$\Lambda(x) = D_j e^{-ax(1+i)} + F_j e^{ax(1+i)}, \quad (5.5a)$$

$$a = \sqrt{\frac{\omega_j S}{2T}}, \quad (5.5b)$$

where  $a$  is the tidal propagation factor ( $m^{-1}$ ), and  $D$  and  $F$  are two complex constants, which may be determined using Equation (5.4b) and (5.4c) as

$$D = \frac{H_{1j} e^{aX(1+i)} - H_{2j} e^{i\psi_j}}{e^{aX(1+i)} - e^{-aX(1+i)}}, \quad (5.6a)$$

$$F = \frac{H_{2j} e^{i\psi_j} - H_{1j} e^{-aX(1+i)}}{e^{aX(1+i)} - e^{-aX(1+i)}}. \quad (5.6a)$$

Substituting Equation (5.5a), (5.6a), and (5.6b) in (5.3) gives

$$h(x, t) = \operatorname{Re} \left( \frac{H_{1j} e^{(aX-ax)(1+i)} - H_{1j} e^{(ax-aX)(1+i)} + H_{2j} e^{i\psi_j+ax(1+i)} - H_{2j} e^{i\psi_j-ax(1+i)}}{e^{aX(1+i)} - e^{-aX(1+i)}} \right), \quad (5.7)$$

which may be expressed as

$$\begin{aligned} h(x, t) = \sum_{j=1}^m \frac{1}{\Delta} \{ & [e^{2aX} \cos(2aX) - 1] H_{1j} e^{a(2X-x)} \cos(\omega_j t + a(2X-x)) \\ & - H_{1j} \sin(2aX) e^{a(4X-x)} \sin(\omega_j t + a(2X-x)) \\ & + [e^{2aL} \cos(2aX) - 1] H_{2j} e^{a(x+X)} \cos(\omega_j t + a(x+X) + \psi_j) \\ & - H_{2j} \sin(2aX) e^{a(3X+x)} \sin(\omega_j t + a(x+X) + \psi_j) \\ & - [e^{2aX} \cos(2aX) - 1] H_{2j} e^{a(X-x)} \cos(\omega_j t + a(X-x) + \psi_j) \\ & + H_{2j} \sin(2aX) e^{a(3X-x)} \sin(\omega_j t + a(X-x) + \psi_j) \\ & - [e^{2aX} \cos(2aX) - 1] H_{1j} e^{ax} \cos(\omega_j t + ax) \\ & + H_{1j} \sin(2aX) e^{a(2X+x)} \sin(\omega_j t + ax) \}, \end{aligned} \quad (5.8)$$

where  $\Delta = e^{4aX} + 1 - 2e^{2aX} \cos(2aX)$  (Hailong Li, Temple University, written commun.,

2007). Linearity of Equation (5.1) allows superimposing  $m$  tidal modes. The solution

given by Equation (5.8) assumes a homogeneous aquifer. However, it is common that the aquifer extends beyond the coastline with sediment covering the submarine interface. The hydraulic properties of the sediment can be different than those of the aquifer and cause a heterogeneous effect at the boundary (Li et al. 2007). If the sediment is less permeable than the rest of the aquifer, the amplitude of the tidal signal is reduced by a coefficient  $E$  and the phase is shifted by a value  $\phi$ . To determine both coefficients, the length of the submarine portion of the aquifer, the dimensions and hydraulic properties of the sediment are necessary (Li et al. 2007). To apply the damping effect, the coefficient  $E$  has to be multiplied by the ocean amplitude  $H$ , and the ocean phases must be modified to accommodate the additional phase shift  $\phi$ .

For large values of  $aX$ , Equation (5.8) reduces to the superposition of influences from both sides in the form of one-sided solutions. Values of  $aX$  are large when  $X$  is large or  $T/S$  is small. The factor  $aX$  is closely related to the non-dimensional aquifer response time,  $X^2S/T\tau$  (where  $\tau$  is the period of the oscillation), used by Townley (1995). The theoretical amplitude attenuations ( $A_{1j}$  and  $A_{2j}$ ) and phase differences ( $\Phi_{1j}$  and  $\Phi_{2j}$ ) for each harmonic component at a well at distance  $x$  (m) from one coast and at distance  $X-x$  (m) from the opposite coast are

$$A_{1j} = e^{-xa} \quad \text{and} \quad A_{2j} = e^{-(X-x)a}, \quad (5.9)$$

$$\Phi_{1j} = xa \quad \text{and} \quad \Phi_{2j} = (X-x)a. \quad (5.10)$$

For large values of  $aX$ , the last 4 terms on the right hand side of (5.8) approach zero and the first four terms may be approximated by

$$h(x,t) = \sum_{j=1}^m H_{1j} A_{1j} E_{1j} \cos(\omega_j t + \Phi_{1j} + \varphi_{1j}) + H_{2j} A_{2j} E_{2j} \cos(\omega_j t + \Phi_{2j} + \varphi_{2j} + \psi_j) \quad (5.11)$$

where  $E_1$  and  $E_2$  are the amplitude-damping coefficients and  $\varphi_1$  and  $\varphi_2$  are the phase shifts due to the sediment-covered boundary.

### ***Aquifer Parameters***

Equations (5.9) and (5.10) may be used to estimate hydraulic diffusivity ( $T/S$ , in  $\text{m}^2/\text{d}$ ) based on the one-sided Jacob-Ferris solution (Jacob 1950; Ferris 1951). As Trefry (1999) has noted, single- or multi-constituent forcings may result in complex waveforms throughout a dual-tide aquifer. The peaks may add up constructively or interfere destructively, depending on the phase of the oscillations. Therefore, it is not warranted to estimate hydraulic properties from points under dual influence. Those points were excluded from this analysis. It is, however, straightforward to solve for diffusivity, based on the one-sided attenuation for each harmonic component:

$$D_{\text{amp } j} = \frac{x^2 \omega_j}{2(\ln A_j)^2} \quad (5.12)$$

where  $D_{\text{amp}}$  is hydraulic diffusivity from amplitude attenuation of the  $j^{\text{th}}$  tidal constituent ( $\text{m}^2/\text{d}$ ) and  $A_j$  is the amplitude attenuation factor for the  $j^{\text{th}}$  tidal component (dimensionless), given by the ratio of the amplitude in the observation well and the amplitude in the ocean. In the same way, diffusivity from the phase lag for each harmonic component may be expressed as

$$D_{\text{pha } j} = \frac{x^2 \omega_j}{2\Phi_j^2} \quad (5.13)$$

where  $D_{\text{pha}}$  is hydraulic diffusivity from phase difference of the  $j^{\text{th}}$  tidal constituent ( $\text{m}^2/\text{d}$ ),  $\Phi_j$  is the difference between the aquifer phase and the ocean phase for the  $j^{\text{th}}$  tidal component (rad). A linear relationship is commonly established for each tidal mode between the amplitude attenuation factor and distance to shore on a semi-logarithmic scale plot. A similar relationship is displayed between the phase difference and distance to shore on a normal scale plot. Least-squares regression of the attenuation and lag was used to estimate a slope for each of the two lines. The attenuation slope may then be substituted in Equation (5.12) and the phase-lag slope in Equation (5.13) to estimate an effective aquifer diffusivity, rather than estimating diffusivity for each observation point.

## **Approaches**

### ***Data Collection***

Water-level data at four monitoring points in central Maui were collected for varying periods by the U.S. Geological Survey Pacific Islands Water Science Center (USGS) starting September 30, 2004. Vented pressure transducers, at an operating precision of  $\pm 0.15$  mm, recorded water levels every 5 minutes. Historic water levels exist for two other monitoring points from 1934 and 1983. The heads were continuously recorded by the USGS and documented in their unpublished well records. Monitoring-point locations are shown in Figure 5.2. Data regarding the type of monitoring point, the distances with respect to both coasts, and length of the records are listed in Table 5.1.

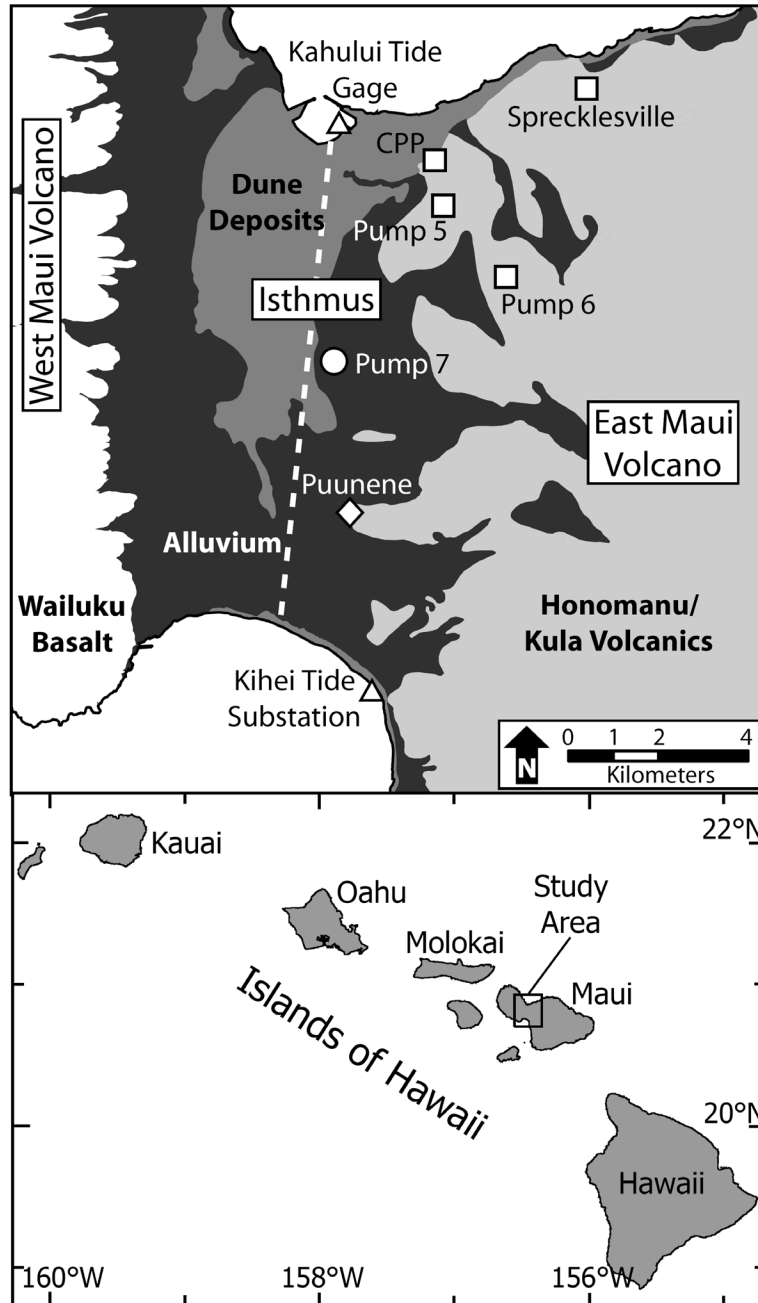


**Figure 5.2.** Location of the study area and central Maui surface-geology map (modified from Stearns and Macdonald 1942) with monitoring points and tide gages. The dashed white line traces the cross section of the numerical model.

All monitoring points are situated in Honomanu Basalt in an unconfined aquifer.

The historic water levels from 1934 and 1983 were manually digitized from chart

recorder plots, which affected accuracy of data reproduction. The resolution of the record for Sprecklesville (Table 5.1) was of good quality and allowed determination of water levels every two hours. The plot resolution of the record for Puunene was of poor quality, and only the high-tide and low-tide peaks were well defined. Both digitized time series were interpolated to 5-min intervals using a cubic-spline function. Each long-term record was divided into data subsets of 32-day periods to ensure that each data set included at least two spring- and neap-tide cycles. The subsets and the long-term records were used in the analysis to assess consistency of results.

**Table 5.1.** Information about ground-water monitoring points and time series

Monitoring point		Distance to coast		Time series		
Name	Type	North $X_1$ (km)	South $X_2$ (km)	Start	Length (d)	Subsets
Sprecklesville	Tunnel	0.73	13.80	01/13/1934	125.0	3
CPP	Well sump	1.05	10.98	09/30/2004	349.9	10
Pump 5	Shaft	2.08	10.08	09/30/2004	161.0	5
Pump 6	Shaft	4.08	9.24	09/30/2004	424.7	11
Pump 7	Shaft	4.87	6.02	09/30/2004	425.0	13
Puunene	Shaft	8.28	2.97	10/01/1983	382.6	11

Tides in Hawaii occur as a mixed type between a strictly diurnal and a strictly semidiurnal type with a mean tidal range of 0.5 m and spring-tide range of 0.7 m. The tidal wave arrives from the northeast and sweeps around each island. In particular, the time lag between the Kahului tide gage and the Kihei tide substation (Figure 5.2) is 1.3 hours between high-tide peaks and 1.9 hours between low-tide peaks. Thus, an asymmetric effect between high-tide and low-tide peaks exists. Water levels at the north coast of the isthmus were recorded by the National Oceanographic and Atmospheric

Administration (NOAA) (2005) at the Kahului tide gage since 1996. Ocean water levels, recorded in 6-min intervals, were interpolated to 5-min intervals for cross-correlation analyses with the ground-water monitoring points. For the south coast, observed ocean water levels do not exist. Hence, the ocean tide was calculated for the Kihei tide substation using the software package Xtide (Flater 1998). The tide for 1983 and 1934 was hindcast using T\_TIDE (Pawlowicz et al. 2002) with the time series from 2004. T\_TIDE is a MATLAB routine that performs classical harmonic analysis using 68 astronomical constituents to predict the tidal signal.

### ***Data Analysis***

The observed water levels were detrended in order to eliminate any non-tidal influence. Low-frequency fluctuations, such as aperiodic atmospheric pressure fluctuations, recharge, and long-period sea-level oscillations, were removed by subtracting the daily moving average. The filtering degraded the amplitudes of the diurnal frequency on average by 0.41%, which was considered acceptable for the analysis. Pumping effects in the records of two shafts were removed from the measured water levels by eliminating the drawdown during times of withdrawal. The first two 32-day data subsets from Pump 6 were disregarded because of severe pumping influence, which could not be successfully removed.

The tidal signal may be decomposed into five major constituents that contribute about 95% of the signal (Brown et al. 1989). The diurnal harmonic components and their frequencies (in  $d^{-1}$ ) are  $O_1$  (0.9295) and  $K_1$  (1.0027), while the semidiurnal components are  $N_2$  (1.8960),  $M_2$  (1.9323), and  $S_2$  (2.0000). The solar components ( $K_1$  and  $S_2$ ) are

influenced by ocean tides and periodic atmospheric-pressure fluctuations (Oki 1997; Merritt 2004). Constraining the aquifer-parameter estimation to purely tide-induced oscillations resulted in consideration of the lunar diurnal ( $O_1$ ) and the lunar semidiurnal ( $M_2$ ) harmonic components. The lunar elliptic constituent ( $N_2$ ) has smaller amplitudes and larger standard deviations compared with the  $O_1$  and  $M_2$  estimates and was therefore disregarded in the parameter estimation. Dale (1974) concluded that earth tides are insignificant in Hawaii. Hence, they were ignored in the current study.

Two approaches are generally used for the analysis of amplitude and phase of harmonic components in measured water levels: least-squares fitting of the major tidal frequencies (e.g., Oki 1997; Merritt 2004) and spectral analysis using discrete Fourier transformation (e.g., Smith and Hick 2001; Trefry and Bekele 2004). Since the frequencies of the tidal constituents are well known, the least-squares regression technique was preferred in this study over spectral analysis. The regression using the five tidal modes was applied to the entire record and to the 32-day data subsets. The time lag may be evaluated either for each tidal harmonic or for the entire signal. The time lag of the whole time series was determined by cross-correlating water levels from the ocean and the aquifer.

The agreement of diffusivity estimates from attenuation and lag is a valuable quality measure of the one-dimensional tidal propagation models. The dimensionless slope factor  $SF$  (Trefry and Bekele 2004) from the effective amplitude and phase diffusivity is determined by

$$SF = \sqrt{\frac{D_{\text{amp}}}{D_{\text{pha}}}}. \quad (5.14)$$

A slope factor of unity resembles perfect Jacob-Ferris representation, but significant deviation from unity is common in practical analysis. For nine tidal applications, (see Trefry and Bekele 2004) estimates of the slope factor ranged from 0.3 to 3.8. The average of slope factors above unity was 2.1 (2 values), and the average of slope factors below unity was 0.52 (7 values). Aquifer heterogeneity and layering may cause a deviation from unity.

### ***Numerical Model***

The damping effect at the boundary was verified with a simple one-dimensional numerical simulation using MODFLOW-2000 (Harbaugh et al. 2000). The simulated cross-section of an aquifer was 10.9 km long and extended vertically from 1.8 km below sea level to 10 m above sea level. The size of the model grid was taken as 10 meters around the observation wells and at the boundaries, and gradually increased to 200 meters. A trace of the modeled cross section is shown in Figure 5.2. The model simulated an unconfined homogeneous aquifer with the adjacent cell to the boundary representing a low-conductivity zone (i.e., caprock and Kula Basalt). Transient-head conditions that match the ocean tide signal at Kahului and Kihei were applied at the respective boundaries. A no-flow condition was set at the bottom and top boundaries and the initial head was taken as 0.14 m. The model simulated ten days starting November 16, 2004 with 1-hour time steps. The hydraulic properties for the basalt are based on the results of the aquifer-parameter estimation via the tidal method. The automated parameter-

estimation routine PEST (Doherty 2004) was applied to estimate hydraulic properties of the low-conductivity zone on both sides based on observed water-level responses in the aquifer.

## **Results and Discussion**

Results of the aquifer-parameter estimation for central Maui and the numerical experiment are presented first. Then, the analytical solution for dual-tide effects is tested using the estimated hydraulic parameters and compared against observed tidal response near the center of the aquifer.

### ***Aquifer Parameters***

The amplitude spectra of Fourier transformations for the Kahului tide gage and Pump 7, which is located roughly 4.8 km and 6.0 km away from the north and south coast, respectively, are shown in Figure 5.3. Clearly, the major tidal modes are identified at Pump 7, although the respective diurnal and the semidiurnal amplitudes are only 2.7% and 1.7% of the amplitude at the coast. Semidiurnal frequencies are attenuated more easily than diurnal frequencies due to higher internal friction losses, which is consistent with observations from other studies (e.g., Dale 1974; Oki 1997).

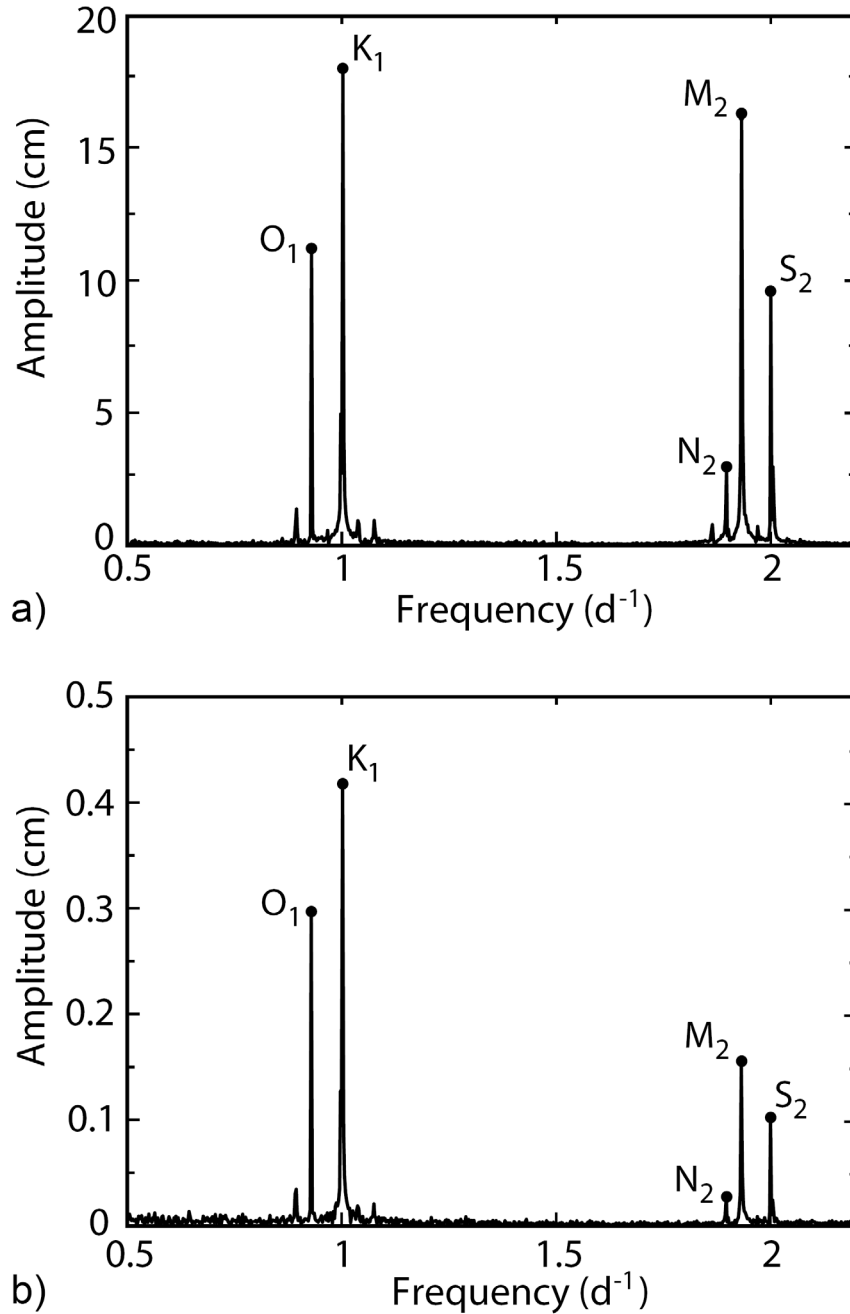


**Figure 5.3.** Amplitude spectra at a 5-min sampling interval (a) for a 425-day ocean-tide time series from Kahului Harbor and (b) for a 425-day observed-head time series in Pump 7.

The amplitude attenuation factor and phase difference estimated from different 32-day data subsets show insignificant variations for the O<sub>1</sub> and M<sub>2</sub> modes. Pump 7 is analyzed with respect to Kahului and Kihei tides. The mean normalized standard

deviation (standard deviation/mean) for the amplitude attenuation factor is 0.09 and 0.03 for the  $O_1$  and  $M_2$  mode, respectively (Table 5.2). The mean normalized standard deviation for the phase difference is 0.05 and 0.11 for the  $O_1$  and  $M_2$  modes, respectively. Puunene has the largest deviations due to poor quality of the chard recorder plot, especially for the phase difference of the  $M_2$  mode (0.45).

**Table 5.2.** Standard deviation and normalized standard deviation of the estimated tidal responses based on 32-day subsets

Monitoring point	with respect to	Standard deviation				Normalized standard deviation <sup>a</sup>			
		Attenuation factor		Phase difference		Attenuation factor		Phase difference	
		$O_1$	$M_2$	$O_1$	$M_2$	$O_1$	$M_2$	$O_1$	$M_2$
Sprecklesville	to Kahului	0.0139	0.0050	0.043	0.102	0.06	0.03	0.08	0.15
CPP		0.0032	0.0014	0.025	0.014	0.02	0.01	0.04	0.02
Pump 5		0.0018	0.0005	0.028	0.014	0.02	0.01	0.03	0.01
Pump 6		0.0073	0.0005	0.137	0.185	0.15	0.02	0.08	0.09
Pump 7		0.0009	0.0003	0.034	0.037	0.04	0.03	0.02	0.01
Pump 7	to Kihei	0.0020	0.0004	0.089	0.056	0.08	0.05	0.04	0.03
Puunene		0.0070	0.0018	0.180	1.448	0.23	0.10	0.10	0.45

<sup>a</sup>standard deviation / arithmetic mean (Table 5.4)

The arithmetic means of amplitudes and phases of the 32-day data subsets compared to those of the entire time series also show very little disparities (Table 5.3). The largest differences exist at Sprecklesville (<10%) and Puunene (<4%). Differences for the other observation points do not exceed 1.6% and 0.8% for the estimated amplitude attenuation and phase difference, respectively. Regardless of whether the data are analyzed by subgroups or in their entity, the resulting amplitudes and phases are

essentially identical. For simplicity, only the arithmetic mean of the 32-day subsets is reported hereafter.

**Table 5.3.** Difference between estimated tidal response from the entire dataset and the arithmetic mean of 32-day subsets

Monitoring point	with respect to	% Difference			
		Attenuation factor		Phase difference	
		O <sub>1</sub>	M <sub>2</sub>	O <sub>1</sub>	M <sub>2</sub>
Sprecklesville		1.00	0.80	9.15	6.26
CPP		1.63	0.47	0.36	0.42
Pump 5	to Kahului	1.24	0.15	0.78	0.34
Pump 6		1.46	0.76	0.15	0.60
Pump 7		1.46	0.62	0.27	0.04
Pump 7	to Kihei	1.48	1.13	0.21	0.04
Puunene		3.75	2.35	3.31	3.13

The time lag from the cross-correlation, the estimated attenuation factor, and the phase difference for the O<sub>1</sub> and M<sub>2</sub> modes for all monitoring points are presented in Table 5.4. The time lags of time series from monitoring points on the north side of central Maui were used to examine the dual-tide problem. Figure 5.4 illustrates the time lag against the distance from the coast, and the line fitted to the four points closest to the north boundary. The same symbols for monitoring points in Figure 5.2 are used in this figure. The plot shows that the time lag is not zero at the boundary, most likely due to the damping influence of the caprock and Kula Basalt. This damping effect will be investigated with a numerical experiment (see below).

**Table 5.4.** Estimated tidal responses based on the arithmetic mean of 32-day time series

Monitoring point	with respect to	Time lag (d)	Attenuation factor $A$ (-)		Phase difference $\Phi$ (rad)	
			$O_1$	$M_2$	$O_1$	$M_2$
Sprecklesville	Kahului	0.065	0.227	0.191	0.568	0.680
CPP		0.072	0.155	0.128	0.670	0.704
Pump 5		0.106	0.089	0.065	0.961	1.021
Pump 6		0.204	0.046	0.024	1.728	2.043
Pump 7		0.292	0.024	0.010	2.178	2.769
Pump 7	Kihei	0.223	0.027	0.009	2.031	1.941
Puunene		0.277	0.030	0.019	1.884	3.194

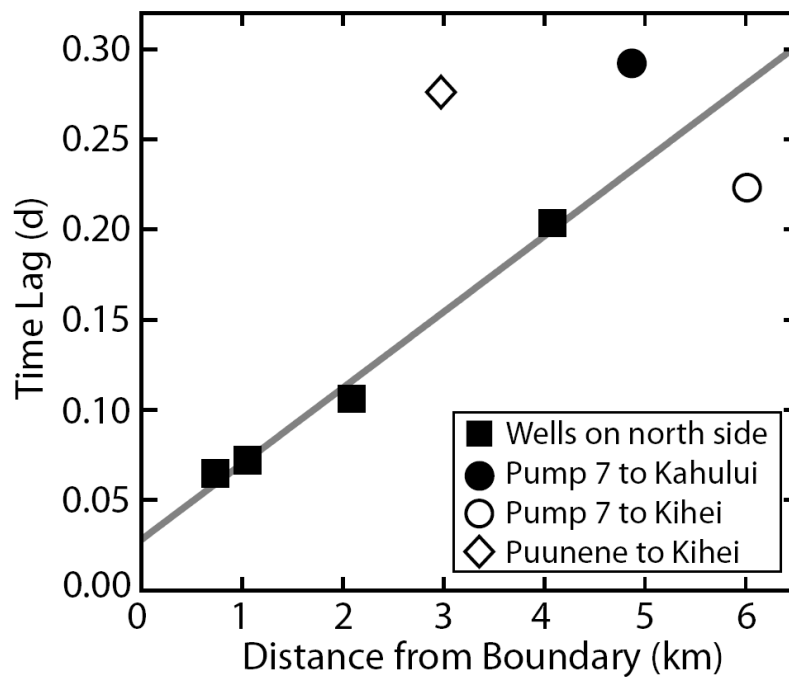


**Figure 5.4.** Time lag for the monitoring points calculated from cross correlation. The black and the white symbols represent the correlation to Kahului and to Kihei, respectively.

The time lag near the center of the aquifer (Pump 7) may be estimated by using tide information from either Kahului or Kihei. Figure 5.4 clearly shows that neither

estimated time lag at this point coincides with the predicted time lag from the regression line, which assumes homogeneity throughout the entire isthmus. The discrepancy thus could reflect heterogeneity of the volcanic portion of the aquifer. However, this factor seems unlikely, considering that the four other points show excellent correlation with a correlation coefficient of 0.99. In addition, the time lags of Puunene and Pump 7 with respect to the south boundary do not fit well on a potential regression line for the south side. It is thus possible that Pump 7 is affected by tidal influences from both sides of the aquifer.

A number of factors influence applicability of one-dimensional solutions. Horizontal two-dimensional effects are not included: neither is the coastline straight, nor are the observation points located on a straight line, perpendicular to the coast. The horizontal variation in thickness of coastal sediments and lava flows is therefore disregarded. Additionally, the phase shift of the ocean tide from the coast at Sprecklesville to Kahului tide gage is overlooked. The tidal lag is considered insignificant, because the distance along the coast (6 km) is relatively short compared to the distance from Kahului to Kihei (140 km clockwise and 70 km counter-clockwise around the island), which shows a time lag of 1.6 hours. The tidal lag between the coast at Sprecklesville and Kahului tide gage is estimated to range between 5 and 10 minutes, assuming a linear behavior of the time lag with distance. Assuming a sharp boundary in the one-dimensional analytical solution is reasonable considering that the horizontal distance from the water line at low tide to high tide is small compared to the length of tidal influence in the aquifer. Using beach slopes derived from profiles in central Maui

(Gibbs et al. 2001) and a spring-tide range of 0.7 m, the width of the inertial zone is 4-8 m on the north shore and 5-10 m on the south shore. However, the offshore tidal loading on the island aquifer is neglected because of the sharp interface assumption.

Results from the estimated tidal propagation in the aquifer are shown in Figure 5.5. The left and right sides of the ordinate in both figures represent Kahului and Kihei, respectively. In agreement with the theory, the amplitude attenuation decreases exponentially while the phase difference increases linearly with increasing distance away from the boundary. The diurnal component ( $O_1$  mode) has higher amplitude ratios and smaller phase lags than the semidiurnal component ( $M_2$  mode) because higher frequencies are preferentially damped by the aquifer. The solid black lines are fitted lines corresponding to the one-sided propagation on the north side. Due to the dual-tide influence stated above, data from Pump 7 is excluded from the regression analysis. In theory, the amplitude attenuation factor at the tide gage is one and the phase lag is zero. However, the aquifer is heterogeneous due to the presence of sediments and less-permeable Kula Basalt at the boundary, which is indicated by the  $y$ -intercept considerably less than one in Figure 5.5a and greater than zero in Figure 5.5b (Table 5.5).

**Table 5.5.** Estimated  $y$ -intercepts and numerically estimated sediment-damping factors of one-sided tidal-propagation scenarios

Side		$y$ -intercept			Damping factor
		$O_1$	$M_2$	Mean of $O_1$ & $M_2$	Numerically (PEST)
North & South Sc1	amplitude	0.27	0.26	0.26	$E_1 = 0.25$
	phase	0.29	0.28	0.29	$\varphi_1 = 0.37$
South Sc2	amplitude	0.11	0.11	0.11	$E_2 = 0.10$
	phase	0.85	1.95	1.40	$\varphi_2 = 0.92$

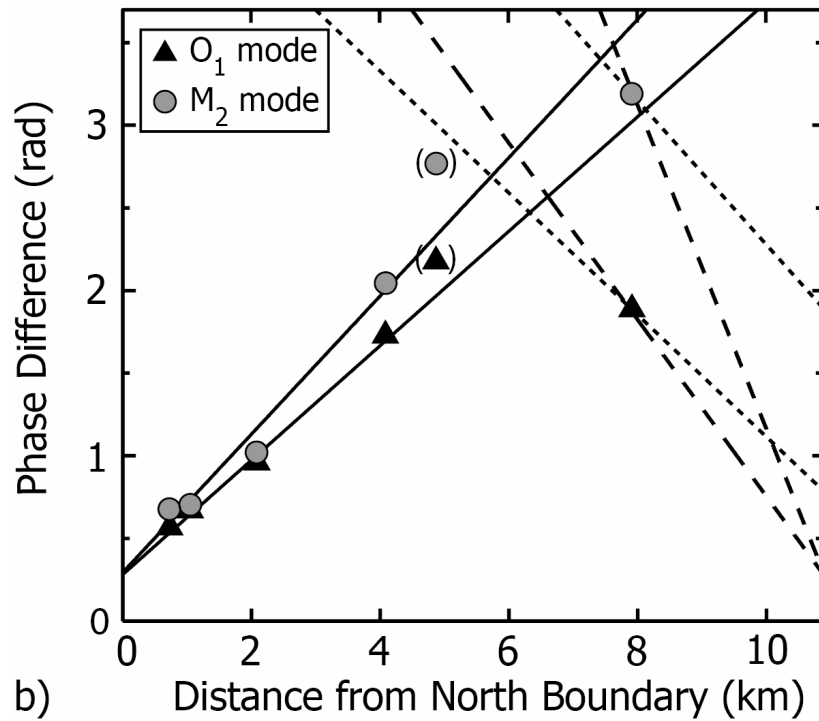
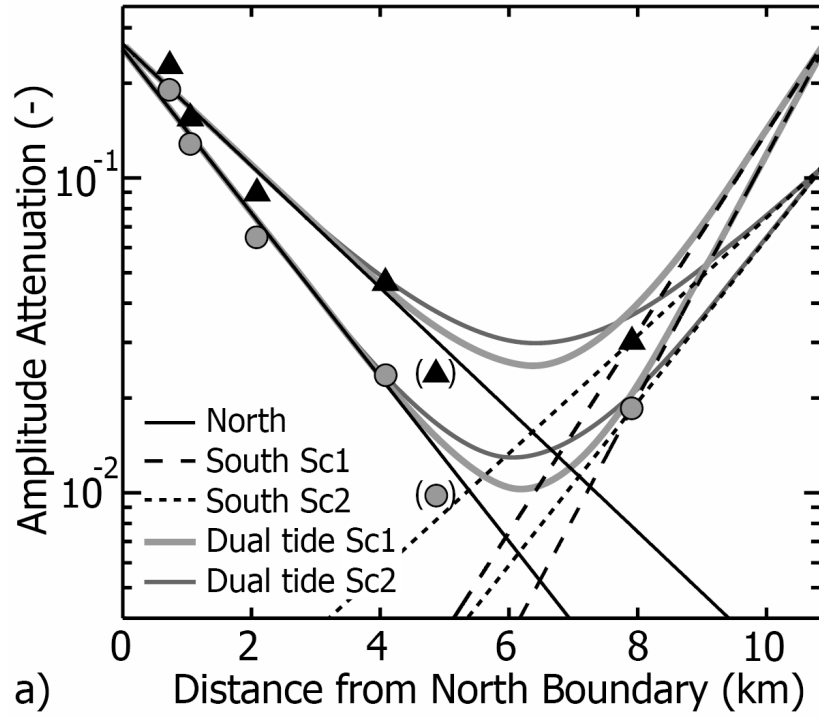


**Figure 5.5.** (a) Estimated modal attenuation and (b) phase difference against distance from Kahului. The black solid lines are the north side regression, from which Pump 7 (in parenthesis) is excluded. The dashed lines are the scenarios for the south side and the gray lines are the dual-tide solutions.

Only one monitoring point, Puunene, is located in the southern half of the isthmus (Figure 5.2). It is not meaningful to fit a line through one point. Hence, two scenarios were tested (Table 5.6). Scenario 1, denoted Sc1, uses the same  $y$ -intercept from the north side (Table 5.5), assuming similar boundary damping effects. This case seems reasonable considering that the seabed slope and the coastal caprock thickness on either side (25 m) are comparable. This scenario yields a different diffusivity on the north and south side of the central Maui aquifer (Table 5.7). Scenario 2, denoted Sc2, assumes the same diffusivity throughout the Honomanu Basalt reflected by equal slopes, which in turn produces different  $y$ -intercepts (Table 5.5). This can be explained with different damping effects at the south boundary. Although the sediment thickness is the same on both sides, the type of sediment is different. The consolidated alluvium on the south side is less permeable compared to the well-sorted dune deposits on the north side. Moreover, the portion of the less-permeable Kula Basalt that is below sea level is potentially thicker on the south side of the isthmus (Stephen Gingerich, USGS, written commun., 2007). Both factors could result in a larger damping effect on the south side. All monitoring points are situated in the same formation, which suggests the effective aquifer parameters should be similar. Therefore, Sc2 is more reasonable based on available geologic evidence. However, more monitoring points on the south side would facilitate the hydrogeologic understanding.

**Table 5.6.** Summary of one-sided tidal-propagation scenarios

Scenario	Sediment-damping effect	Basalt hydraulic diffusivity	Geological reasonable?
Sc1	same on both sides	lower on south side	less
Sc2	larger on south side	same on both sides	more

**Table 5.7.** Estimated hydraulic diffusivities ( $\text{m}^2/\text{d}$ ) and slope factors (-) of one-sided tidal-propagation scenarios

Side		$O_1$	$M_2$	Mean of $O_1$ & $M_2$	$D^*$
North & South Sc2	$D_{\text{amp}}$	$1.5 \times 10^7$	$1.7 \times 10^7$	$1.6 \times 10^7$	$2.3 \times 10^7$
	$D_{\text{pha}}$	$2.4 \times 10^7$	$3.5 \times 10^7$	$2.9 \times 10^7$	
	$SF$	0.78	0.70	0.73	
South Sc1	$D_{\text{amp}}$	$5.5 \times 10^6$	$7.8 \times 10^6$	$6.6 \times 10^6$	$7.5 \times 10^6$
	$D_{\text{pha}}$	$1.0 \times 10^7$	$6.3 \times 10^6$	$8.3 \times 10^6$	
	$SF$	0.73	1.11	0.89	

$D^*$  = arithmetic mean of  $D_{\text{amp}}$  and  $D_{\text{pha}}$

Aquifer-diffusivity values and slope factors for the aquifers of central Maui are summarized in Table 5.7. The mean diffusivity,  $D^*$ , estimated from attenuation and phase lag for the  $O_1$  and  $M_2$  modes is  $2.3 \times 10^7 \text{ m}^2/\text{d}$  from Sc2. Oki (1997) used the tidal response in aquifers of northern Oahu and estimated hydraulic diffusivity to be about  $2 \times 10^7 \text{ m}^2/\text{d}$ , which is consistent with this result. The mean slope factor is 0.73 for Sc2. The deviation from unity supports the hypothesis that the aquifer system cannot be fully characterized by the analytical solution developed under simplified conditions. Although the manual digitization of the paper chart for Puunene was performed in a meticulous and diligent way, the semidiurnal peaks were often unrecognizable. It is expected thus that the confidence in the estimated amplitude attenuation is higher than that in the phase differences, especially for the  $M_2$  mode.

Hydraulic-diffusivity curves for plausible ranges of aquifer thickness, hydraulic conductivity, and specific-yield values are presented in Figure 5.6. The effective hydraulic diffusivity,  $D^*$  from Sc2, was used to generate the curves. Specific-yield

values, between 2% and 10%, are within the expected ranges (Oki 1997; Rotzoll and El-Kadi 2007); aquifer thickness is likely not to exceed 1.8 km (Souza and Voss 1987); and hydraulic conductivity for dike-free basaltic rocks on Maui ranges between 1 and 2,500 m/d (Chapter 3). All of the hypothetical diffusivity curves fall within the expected ranges for unconfined aquifers. Assuming that the tidal signal propagates through the entire aquifer thickness of 1.8 km and the specific yield is 0.04, the resulting hydraulic conductivity would then be 500 m/d. The one-sided analytical solution thus provides meaningful diffusivity estimates for central Maui.

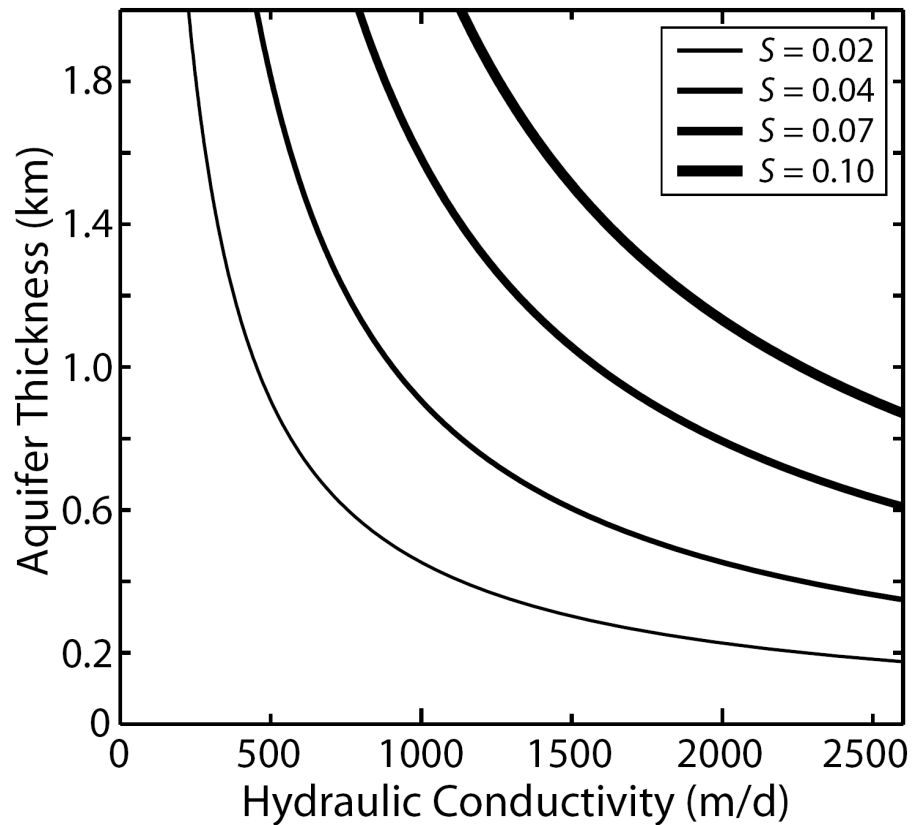


**Figure 5.6.** Hydraulic-diffusivity curves of  $2.3 \times 10^7 \text{ m}^2/\text{d}$  for plausible ranges of aquifer thickness, hydraulic conductivity, and specific-yield values.

### *Numerical Model*

The heterogeneity effect at the boundary in the Sc2 scenario was tested with a numerical experiment. The hydraulic conductivity and specific yield of the basalt were taken as 500 m/d and 0.04, respectively. A specific-yield value of 0.1 was used for the low-conductivity unit (Oki 2005). The PEST routine (Doherty 2004) estimated hydraulic conductivity of this unit to be 0.97 and 0.35 m/d on the north side and south side, respectively, which fall within range of values for capping units (Oki 2005). However, such values are meaningless unless accurate dimensions and geometry of the sediment layer and the Kula Basalt are incorporated. Nevertheless, simplified geometry and approximate dimensions were used here to address the great significance of the low-conductivity zone and validity of the assumptions adopted in the absence of appropriate data on the south side.

Figure 5.7 illustrates simulated and observed water levels for a 2-day period, which is a typical subset of the simulation. The model shows immediate responses to the head change at the boundary. Figure 5.7a shows water levels in the ocean and in the cell adjacent to the low-permeability unit, which reveals a large amplitude damping and phase shift. The tidal amplitudes in the ocean are reduced by 75% and 90% on the Kahului and Kihei side, respectively. The phase lag introduced by the heterogeneous boundary is 0.37 and 0.92 rad on the north and south side, respectively. The amplitude-damping coefficients are within 10% and the phase lags of the  $O_1$  component are within 20% of the  $y$ -intercepts from the regression analysis listed in Table 5.5. As mentioned earlier, the confidence in the phase lag of the  $M_2$  component on the south side is low. The  $y$ -

intercepts of the modal attenuation and phase differences estimated by the regression can therefore approximate the sediment-damping factors.

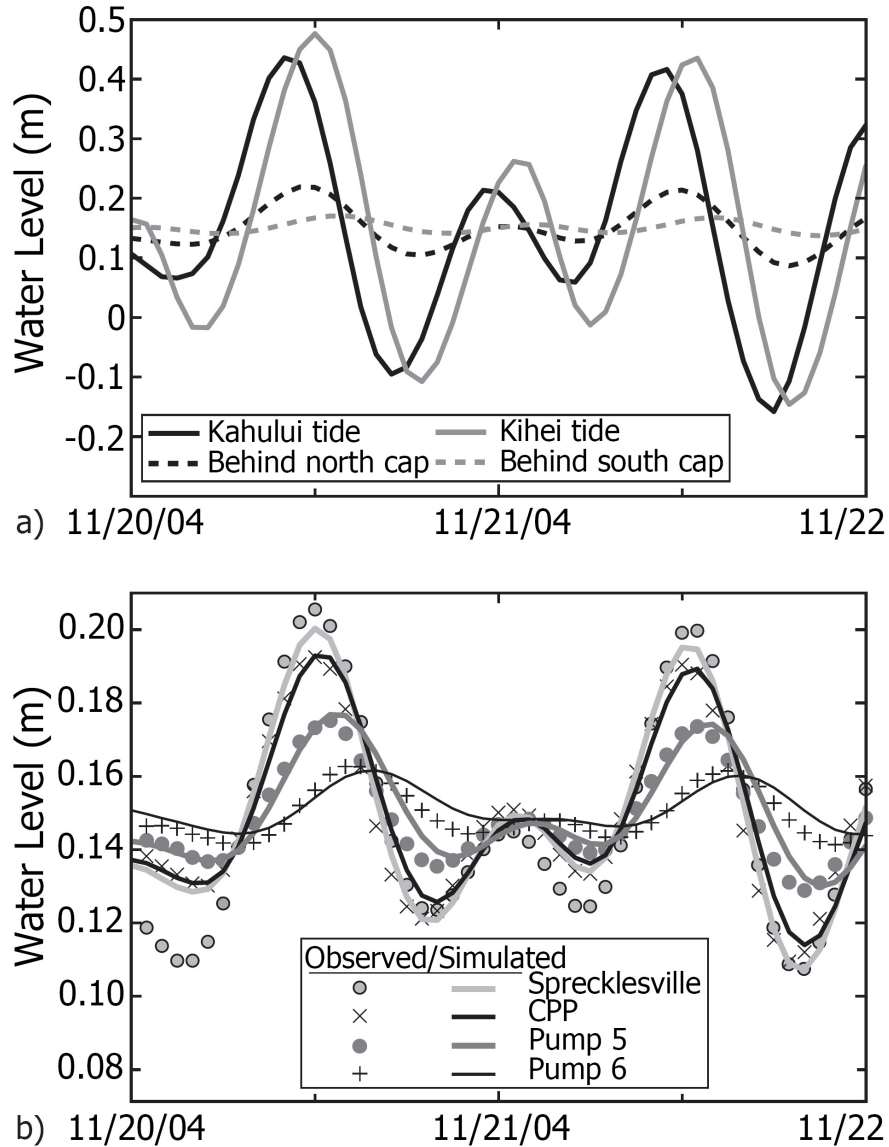


**Figure 5.7.** Numerical simulation of the capping boundary effect. Plot (a) showing calculated water levels in the ocean and the cell adjacent to the capping unit at each boundary. Plot (b) showing observed and calculated water levels on the north side of the isthmus.

Figure 5.7b shows the simulated and observed water levels in the aquifer. The calculated water levels match the observed ones using one hydraulic-diffusivity value for

the basalt aquifer, except for the semi-diurnal low-tide peaks for Specklesville. The overall good match suggests that the assumptions of a different damping effect at the boundaries and of a homogeneous aquifer are acceptable. The existence of lower-conductive units at the boundary justifies the use of certain values for the damping coefficients needed for the analytical dual-solution.

### ***Dual Tide***

The amplitude attenuation for the dual-tide analytical solution is plotted as gray lines in Figure 5.5a. The dual-tide relationship shown in Figure 5.5a only applies to cases in which the tidal signal from one side is in phase with the signal from the other side at a given location (constructive interference). For cases in which the signal from one side is out of phase with that from the other side (destructive interference), the superimposed dual-tide signal amplitude is smaller than the values given by the gray lines. This phenomenon is more obvious when comparing theoretical tidal responses near the center of the aquifer to observed head fluctuations at the Pump 7.

The applicability of the dual-tide solution is examined by various combinations. Six estimates for head responses to tidal influences are compared based on the one-sided Jacob-Ferris solution from the north side, the one-sided Jacob-Ferris solution from the south side (for both Scenarios: Sc1 and Sc2), the simplified dual-tide solution proposed in this study (Sc1 and Sc2), and the exact dual-tide solution (Sc2). The  $y$ -intercepts, reflecting the damping effect (Table 5.5) and the estimated effective hydraulic diffusivities,  $D^*$  (Table 5.7) for Sc2, were used to generate harmonic fluctuations for Pump 7 using Equations (5.8) and (5.11) with five tidal modes. Head values were

calculated for the entire duration of the observed time series (425 days) and a representative shorter period of 6 days, which is shown in Figure 5.8. The observed time series was detrended and smoothed using a 2-hour moving average to facilitate the comparison. Table 5.8 lists error statistics. The results are consistent for the short and long periods. The one-sided tidal propagation from the north side fits reasonably well the observed data, but overestimates the amplitude. Such an overestimation is evident in Figure 5.5a, which shows that the estimated amplitude attenuation of Pump 7 is significantly lower than the prediction determined by the regression line at this location. Not only does the south-side tidal propagation have the highest error and the lowest correlation coefficient, but also it is completely out of phase with the observed head (Figure 5.8), which is indicated by a negative correlation coefficient (Table 5.8). The amplitude is underestimated because of the significant lower hydraulic-diffusivity value (Sc1) or the greater damping effect (Sc2) and the larger distance to the boundary.

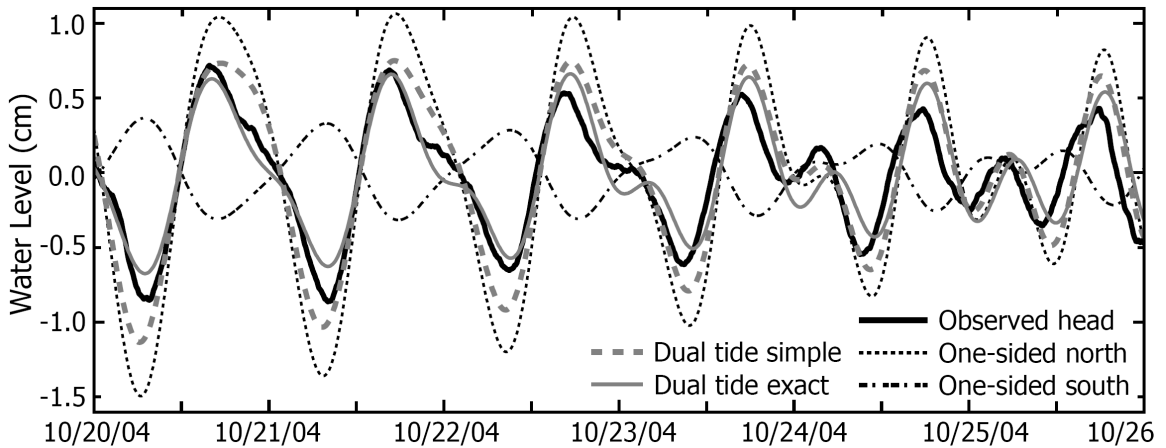


**Figure 5.8.** Analytical solutions for tide-induced head fluctuations for Sc2 at Pump 7 against observed head. The observed time series was detrended and smoothed with a 2-h moving average.

**Table 5.8.** Error summary of the different analytical solutions for the entire time series observed in Pump 7 and for the subset shown in Figure 5.8

Analytical solution	Time series (d)	Sum of absolute error (m)	Sum of squared error (m <sup>2</sup> )	Standard deviation of error (m)	<i>R</i> (-)
One-sided north	425	389	1.86	0.0039	0.89
One-sided south Sc1		463	2.52	0.0045	-0.58
One-sided south Sc2		577	3.91	0.0057	-0.85
Dual tide simple Sc1		345	1.47	0.0035	0.89
Dual tide simple Sc2		258	0.81	0.0026	0.89
Dual tide exact Sc2		206	0.56	0.0021	0.85
One-sided north	6	5.36	0.0231	0.0037	0.93
One-sided south Sc1		6.15	0.0330	0.0044	-0.72
One-sided south Sc2		7.57	0.0508	0.0054	-0.85
Dual tide simple Sc1		4.69	0.0177	0.0032	0.93
Dual tide simple Sc2		2.81	0.0068	0.0020	0.95
Dual tide exact Sc2		2.23	0.0043	0.0016	0.91

In general, the one-sided north and the dual-tide solutions exhibit large *R*-values above 0.85. The simplified dual-tide solutions provide a better fit to the observed values for both scenarios than the one-sided approaches. Due to the phase-shifted response from the south side, the dual-tide signal matches the observed head better in amplitude and phase. Sc2 fits the observed data better than Sc1 and improves the correlation coefficient to 0.95 for the data subset, supporting the use of Sc2. For central Maui, the values of  $aX$  are large enough to warrant the use of the simplified dual-tide solution. The values of  $aX$  are 3.9 and 5.7 for the  $O_1$  and  $M_2$  mode, respectively. The exact dual-tide solution has the best fit of any solution to the observed data for both datasets in Table 5.8, as indicated by the lowest error.

The results show that the monitoring point near the center of the aquifer is influenced by tides from both sides and that the common one-sided Jacob-Ferris solution may not be sufficient to describe tide-induced head fluctuations in a coastal aquifer with two boundaries. Equation (5.11) provides a suitable solution to characterize the head distribution in such an aquifer. However, a better fit is achieved with the exact solution provided by Equation (5.8). Similar results were obtained for Puunene and Pump 6. However, because the tidal amplitude decays exponentially with distance, the influence from the side that is farther away becomes insignificant at some point. For example, the theoretical  $O_1$  amplitude at Pump 6 is 4.4% compared to the ocean tide from the north side and 0.03% from the south side using Sc2.

## **Chapter 5 Conclusions**

Tidal responses in the unconfined central Maui aquifer were analyzed. The monitoring point near the center of the aquifer is influenced by asymmetric and asynchronous tides from opposite sides. The analytical dual-tide solution is confirmed by comparing theoretical tidal responses near the center of the aquifer to observed head fluctuations. The one-sided Jacob-Ferris solutions do not adequately reproduce observed water levels. The simplified dual-tide solution (Equation 5.11) provides a better fit and the exact dual-tide solution (Equation 5.8) offers the best fit for the head responses in the center of the aquifer.

As expected, the tidal response shows exponentially decreasing amplitudes and linearly increasing phase lags with increasing distance away from the coast. The effective hydraulic diffusivity estimate based on the Jacob-Ferris model is  $2.3 \times 10^7 \text{ m}^2/\text{d}$  for the

volcanic aquifer, which agrees with previously published values based on tides on Oahu. Assuming that the tidal signal propagates through the entire aquifer thickness of 1.8 km and the specific yield is 0.04, the resulting hydraulic-conductivity is about 500 m/d. The tidal analysis yields reasonable hydraulic-diffusivity estimates for central Maui.

A one-dimensional numerical simulation was applied to test a damping effect at the boundary caused by overlying low-permeability units. The calculated and observed water levels in the aquifer match using one effective hydraulic-diffusivity value for the basalt aquifer. The low-permeability cap results in a significant amplitude damping and phase shift, which is comparable with the  $y$ -intercepts of the modal attenuation and phase differences estimated by the regression. The  $y$ -intercepts may therefore approximate the sediment-damping factors.

## 6. Wave Setup

### Introduction

Various ocean processes including tides, wave runup, and wave setup can influence coastal ground-water tables. Wave setup is the wave-driven ocean level change at the shoreline. The elevated mean water level occurs due to momentum transfer of breaking waves to the water column (Figure 6.1). The cross-shore gradient of the momentum flux is balanced by a sloping water level, causing setdown outside the breaker zone and setup inside the surf zone and at the coast (Longuet-Higgins and Stewart 1962, 1963). Appreciable setup at the shoreline can last for several days, depending on the duration of energetic swell events. Studies relating wave setup and ground-water table variations are limited to beaches (e.g., Nielsen 1989; Gourlay 1992; Turner et al. 1997; Massel 2001). Observations of ground-water responses to setup farther than 150 m from the coast are nonexistent.

Wave setup is significantly different from wave runup, with the latter occurring on a time scale of seconds. The interaction between wave runup and the ground-water table in the littoral zone is well known (e.g., Hegge and Masselink 1991; Turner 1998). Runup on a sloping beach is characterized by instantaneous swash infiltration, resulting in ground-water responses in the beach zone (Li and Barry 2000). The wave swash drives a circulation, where water infiltrates at the upper part of the beach and exfiltrates at the lower, submerged part of the beach. Swashes that extend beyond the mean ground-water level cause the ground-water table to rise, directly proportional to the amplitude of the

wave run-up (Hegge and Masselink 1991). The amplitude becomes increasingly damped inland (Li et al. 1997) and is hardly detectable further than a few tens of meters away from the shoreline (Cartwright et al. 2006).

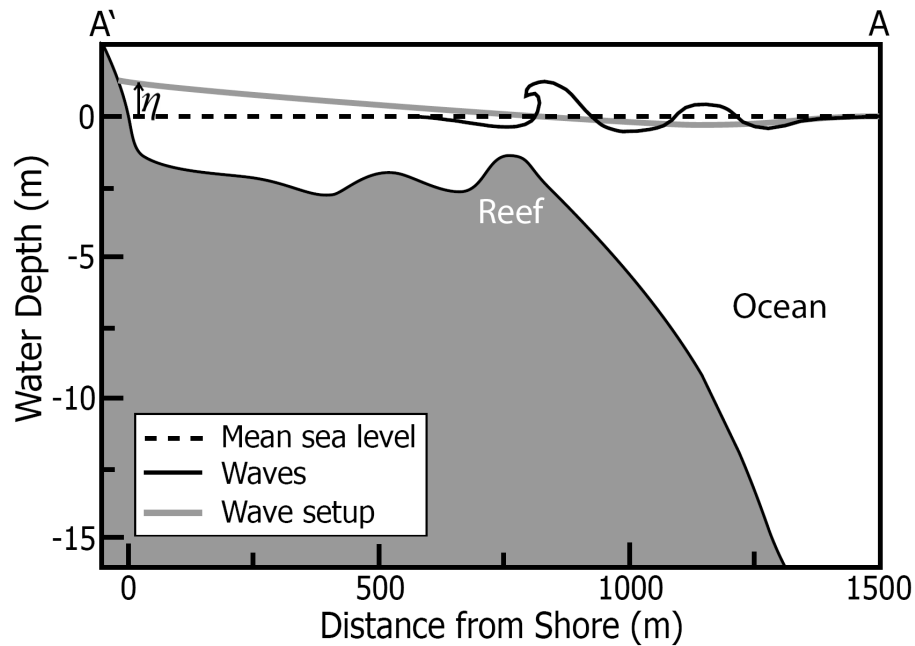


**Figure 6.1.** Cross-shore profile A-A' illustrating the effect of wave breaking, with wave setdown occurring outside the breaker zone, and wave setup ( $\eta$ ) occurring inside the surf zone and at the coast.

Ocean tides are commonly used to estimate aquifer parameters (e.g., Merritt 2004; Trefry and Bekele 2004). The harmonic signal decays as it propagates inland as a function of the aquifers hydraulic properties and distance to shore (Jacob 1950; Ferris 1951). However, wave setup has not been used in aquifer-parameter estimation. Utilization of tides or setup to estimate aquifer parameters has an added advantage over aquifer tests by covering greater areas. In addition, the use is appealing due to the low costs and simple logistics involved. Wave buoy data are readily available, and reliable swell forecasts exist for seven days in advance through the NOAA WAVEWATCH-III

model (Chao et al. 2003). The advantage of setup over tides is the deeper penetration into the aquifer associated with longer period oscillations.

This chapter investigates the influence of wave setup on water-table elevations in central Maui and uses setup to estimate hydraulic parameters. A simple numerical ground-water flow model is used to evaluate the accuracy of the estimated hydraulic parameters.

### **Study Site**

The coastal regions on the north side of central Maui are situated in the center of a V-shaped embayment (Figure 6.2). The wave heights on north-facing shorelines in Hawaii are characterized by a quasi-normal distribution with a maximum in January and a minimum in July. From December to February the large swells experience a shift toward more west-northwesterly directions, due to the southerly migration of the north Pacific storm track (Caldwell 2005). The coastal bathymetry includes a 1- to 2-km wide shelf with a deeper channel at the harbor entrance. A shallow reef, where waves break, is followed by a steeper forereef. The slopes at the forereef range between 0.014 and 0.032, with an average of 0.02 rad (derived from several profiles of high-resolution bathymetry data). A typical cross-shore profile is shown in Figure 6.1.

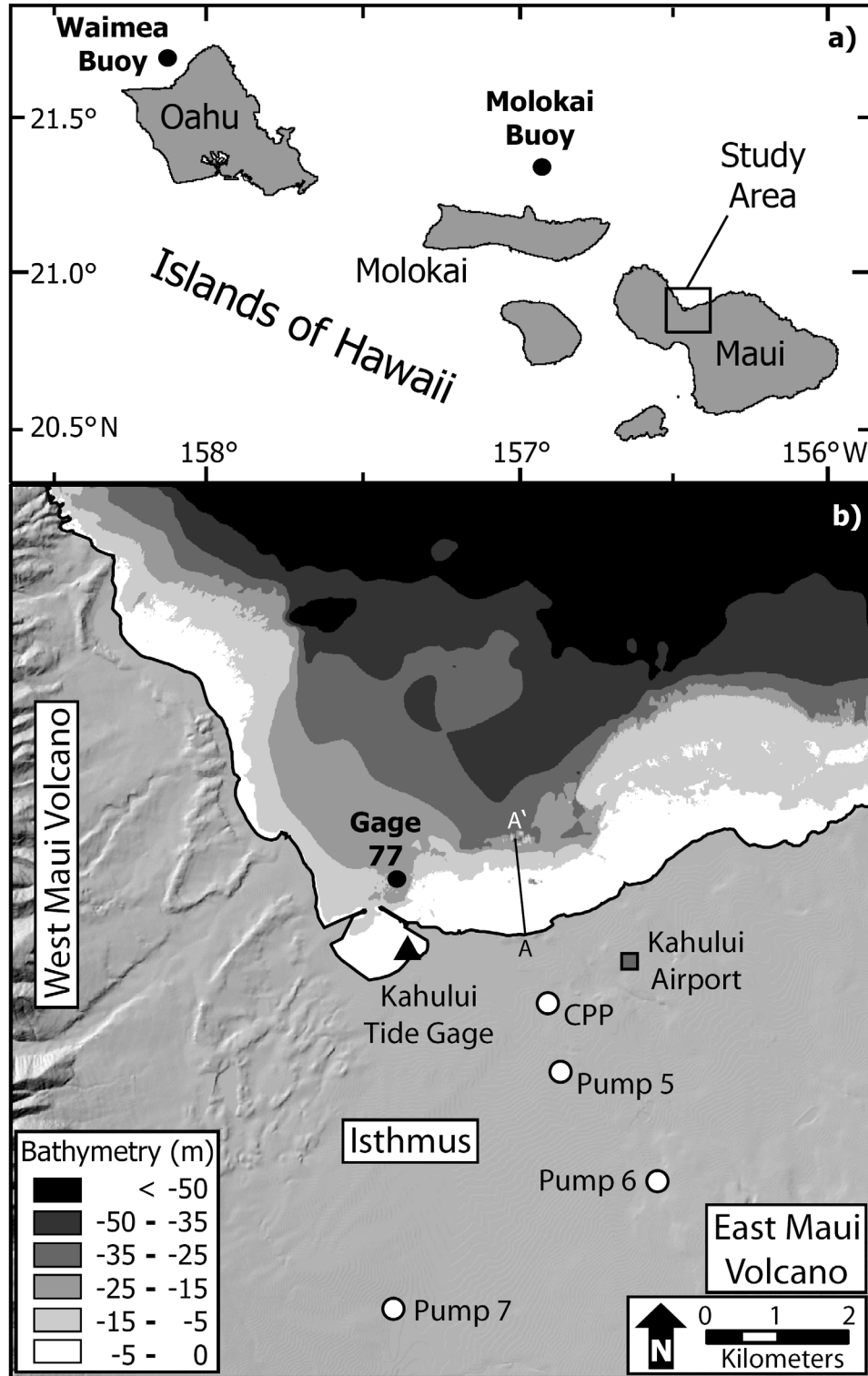


**Figure 6.2.** (a) Map showing the study area and offshore wave buoys. (b) Observation points in the study area, bathymetry of the coastal region, and trace of cross-shore profile A-A' shown in Figure 6.1.

## **Approaches**

### ***Data Collection***

Table 5.1 lists information about the monitoring points where the setup analysis was carried out and the location of such points is shown in Figure 6.2. A 3-month period, starting on December 11, 2004, was chosen due to the occurrence of high-energy swells during the winter. Ocean water levels were recorded at 6-minute intervals by NOAA (2005) at the tide gage inside Kahului Harbor. Hourly recorded barometric pressure data were taken at Kahului airport from the National Climatic Data Center (2005).

The Waimea wave buoy recorded significant wave height, dominant wave period and dominant wave direction every 30 minutes (Coastal Data Information Program 2005). Since the Waimea buoy is 190 km away from the study area (Figure 6.2), a time shift between the arrival of the waves at the Waimea buoy and the arrival in the Kahului area was required for the analysis. For group waves traveling in deep water with a wave period of 17 seconds, the time lag is approximately 4 hours (Brown et al. 1989). The study area is sheltered from westerly swells by the local coastline and by other islands farther to the west (Thompson and Demirbilek 2002). To account for the swell-shadowing effect, a directional correction was applied. Mark Merrifield (University of Hawaii, written commun., 2007) compared significant wave heights and wave direction from Molokai buoy (NDBC buoy 51026), with bottom pressure measurements taken outside Kahului Harbor (CDIP gage 77). He analyzed 314 days during the wintertime from 1993 to 1995.

The corrected wave height for Kahului ( $H_{sK}$ ) is given by the regression equation:

$$H_{sK} = H_{sO} \left( -3.63 \times 10^{-5} \theta^2 + 7.95 \times 10^{-4} \theta + 0.423 \right) \quad (6.1)$$

where  $H_{sO}$  is the significant wave height offshore (m) and  $\theta$  is the wave direction (deg TN). In the absence of data, the same wave-height correction is assumed applicable to Waimea buoy wave heights. Such an assumption is reasonable due to a similar deepwater wave climate (Thompson and Demirbilek 2002) and a comparable exposure to westerly swells, considering that Kauai blocks the west swell for the Waimea buoy as Oahu does for the Molokai buoy (Caldwell 2005).

### ***Data Filtering***

A low-pass filter was applied to the observed head, the tide-gage records, and the barometric pressure time series to eliminate tidal and semidiurnal atmospheric pressure fluctuations. The daily-moving-average filter was applied twice. The time series were detrended to remove linear drift during the study period. Barometric pressure was detrended with a second-order polynomial (Figure 6.3a). All data that were sampled at intervals longer than 5 minutes were linearly interpolated to 5-minute time steps to allow for a direct comparison with data at the monitoring points.

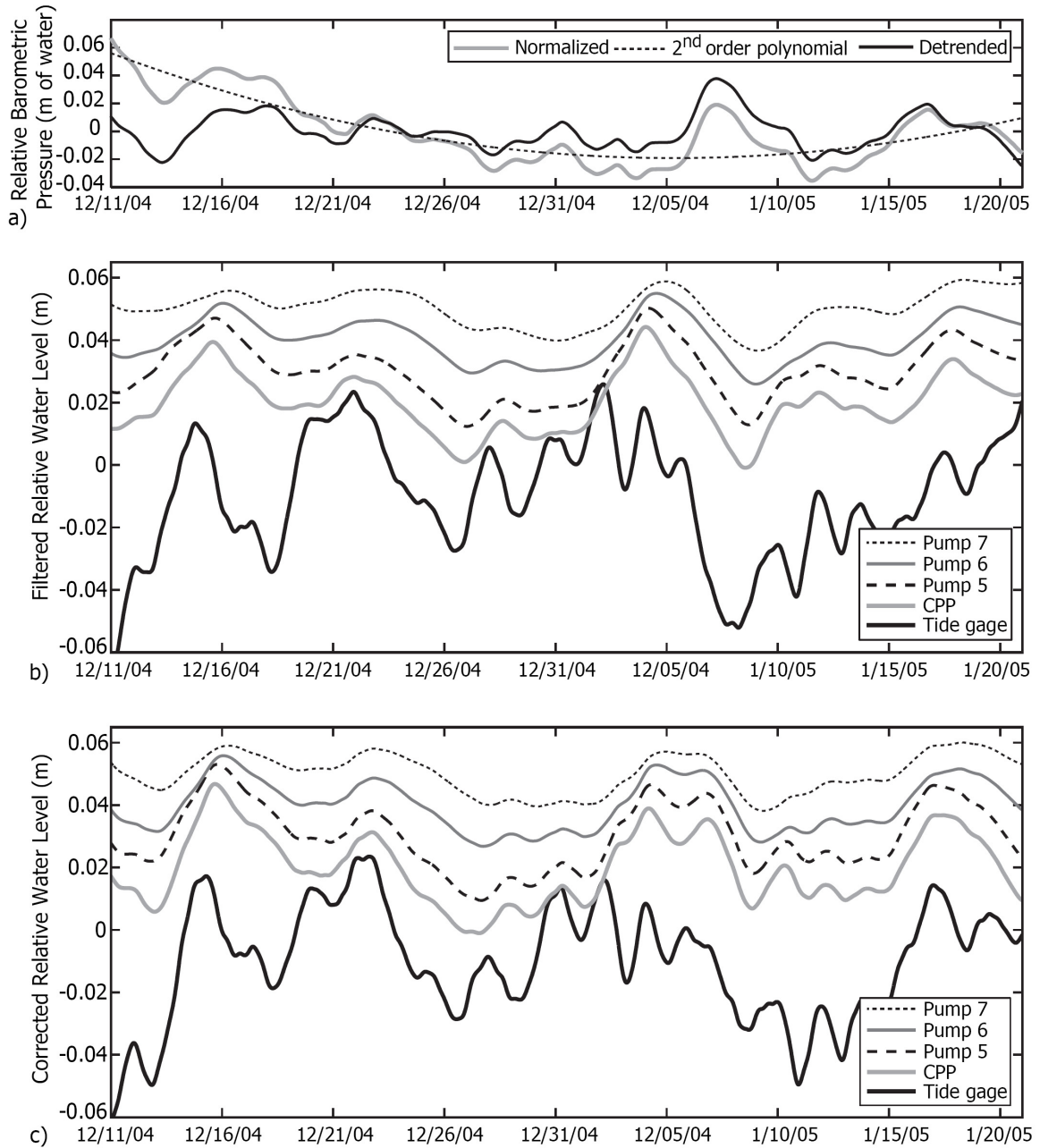


**Figure 6.3.** (a) Barometric pressure, (b) filtered and detrended water levels, and (c) water levels corrected for barometric fluctuations for the SWELL subset. Water levels are offset to facilitate the comparison.

For some parts of the analysis, it was also necessary to remove aperiodic barometric pressure oscillations. Changes in atmospheric pressure are inversely

correlated to ground-water head (Jacob 1940). A constant barometric efficiency factor,  $B_e$ , was estimated for each observation well by least-squares regression of the filtered barometric pressure (converted to meters of water) and filtered observed head fluctuations. Clark (1967) proposed that incremental changes in water level plotted against incremental changes in barometric pressure yields a slope of the regression line equaling  $B_e$ . The coefficients from both methods are listed in Table 6.1. The values do not differ significantly, although some discrepancy exists for CPP and Pump 5. Merrit (2004) found that the method of Clark is not entirely robust, hence the values from the least-squares regression were used for the aperiodic barometric-pressure removal. A transient evaluation of the barometric well response may improve the removal in unconfined aquifers (Oki 1997; Spane 2002), because it accounts for airflow in the unsaturated zone (Weeks 1979). However, the use of a constant barometric efficiency factor was considered satisfactory, considering that semidiurnal fluctuations already have been removed. The scaled inverted barometric pressure was subtracted from the observed head. The filtered and barometrically corrected water levels are illustrated in Figures 6.3b and 6.3c, respectively.

Table 6.1. Barometric loading efficiencies for monitoring points

Monitoring Point	Barometric efficiency, $B_e$ (-)	
	Regression	Clark's method
Tide gage	-0.878	-0.836
CPP	-0.536	-0.408
Pump 5	-0.418	-0.344
Pump 6	-0.261	-0.288
Pump 7	-0.210	-0.247

### ***Wave Setup***

Wave setup that potentially affects ground-water levels in the study area occurs in Kahului Harbor and along the 5-km stretch to the east of the harbor. The water-table rise at the coast is correlated with the significant wave height outside the breaker zone (Guza and Thornton 1981). Numerous studies have defined empirical scaling factors for beaches (e.g., Guza and Thornton 1981; Holman and Sallenger 1985; Raubenheimer et al. 2001; Stockdon et al. 2006), while others have investigated wave transformation over coral reefs (e.g., Tait 1972; Gourlay 1994; Hardy and Young 1996; Lugo-Fernandez et al. 1998; Vetter 2007). The approaches proposed by Vetter (2007) and Stockdon et al. (2006) were applied in this study. Based on observed setup on the north shore of Oahu, Vetter defined the relationship:

$$\eta_V = 0.11H_s \quad (6.2)$$

where  $\eta_V$  is the setup (m) and  $H_s$  is the significant wave height measured at Waimea buoy (m). The similarity of reef platform and forereef slopes suggests applicability to the Kahului area. Stockdon et al. (2006) evaluated 10 field experiments, including wave length and foreshore beach slope  $\beta$  (rad), and proposed the relationship:

$$\eta_S = 0.35\beta\sqrt{H_s \frac{gP^2}{2\pi}} \quad (6.3)$$

where  $\eta_S$  is the setup (m),  $g$  is the acceleration due to gravity ( $\text{m/s}^2$ ), and  $P$  is the wave period (sec). Although developed for beach environments, the formulation is appealing for reef settings due to the consideration of wave energy and bottom slope. Instead of

using the foreshore beach slope, we applied the forereef slope reflecting the location where wave breaking occurs. Tidal dependence of setup was ignored in this study due to the lack of field data. Nevertheless, the assumption is supported by Vetter (2007), who concluded that tidal modulation of  $H_s$  is secondary to strong wave dissipation.

Setup is site-specific and uncertainty is likely to occur due to the use of empirical relationships, in particular for a three-dimensional domain. Yet, the objective of the study was to provide a useful setup approximation for aquifer-parameter estimation in the absence of detailed field data. Setup was estimated with the corrected offshore wave height,  $H_{sK}$ , using Equations (2) and (3), with a  $\beta$  value of 0.02. The time series were filtered with a daily-moving average.

### ***Cross-Correlation and Regression Analysis***

The observation period was split into two sections, termed SWELL and BARO, to investigate the effects of setup and barometric pressure on ground-water levels. Observation of SWELL started on Dec. 12, 2004 and lasted for 41 days, and that of BARO started on Jan. 30, 2005 and lasted for 35 days. The SWELL subset contains four major swell events and is characterized by modest barometric fluctuations. In contrast, the BARO subset shows more significant atmospheric pressure variations while setup is relatively uniform (Figures 6.4d and 6.4e). Although the setup is smaller during summertime due to the lack of large swells, low-frequency barometric changes are also of smaller magnitude, due to the more stable trade-wind pattern. The time lag of the SWELL subset was evaluated by cross-correlating setup and observed head, corrected for barometric changes.

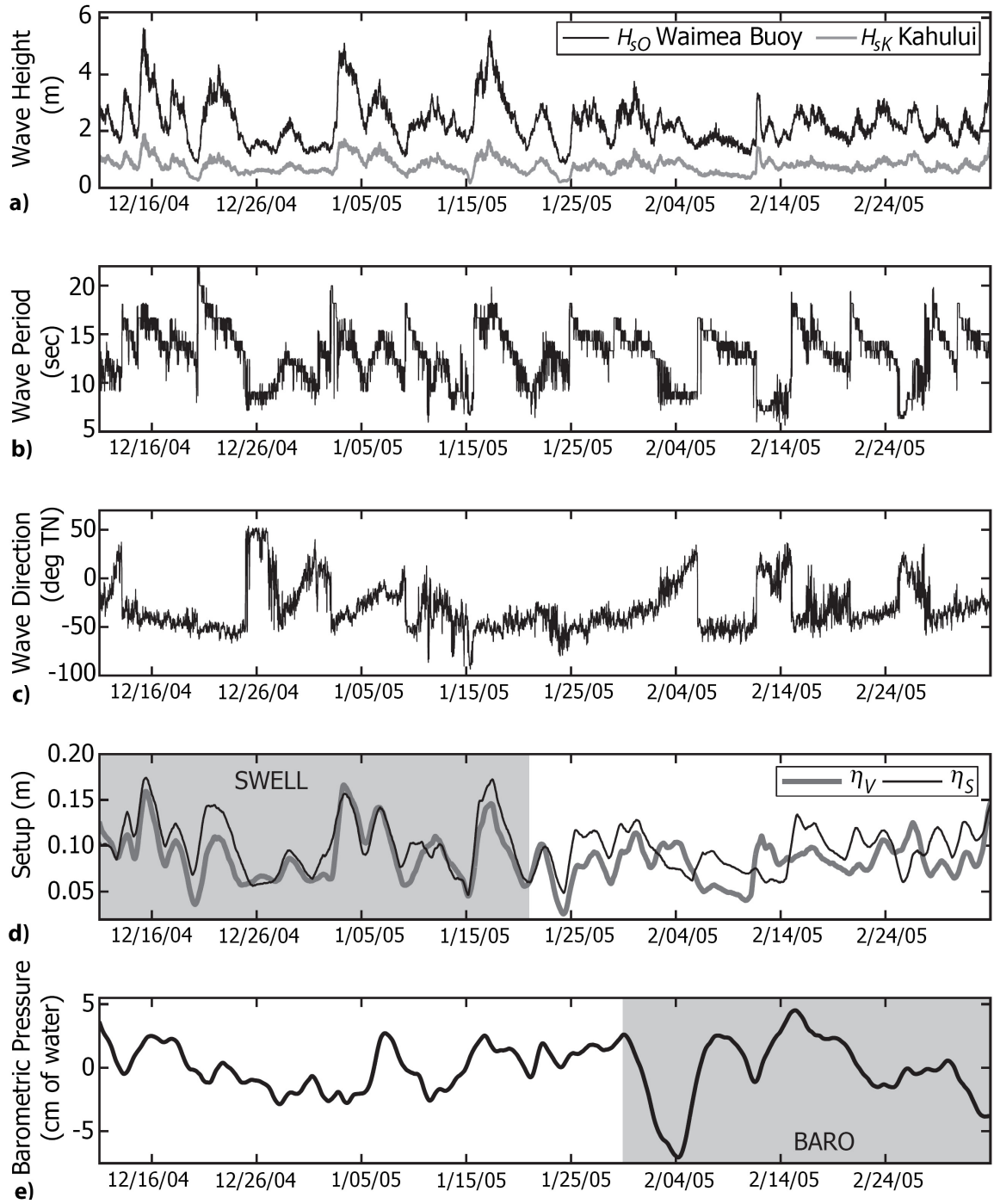


**Figure 6.4.** (a) Significant wave height at Waimea Buoy and estimated wave height at Kahului, (b) dominant wave period at Waimea Buoy, (c) dominant wave direction at Waimea Buoy, (d) estimated wave setups, and (e) filtered and detrended barometric pressure for the observation period.

The effects of setup and low-frequency barometric pressure changes on head fluctuations were investigated using a single-variable regression model. Setup and barometric pressure, were fitted to the observed head, uncorrected for barometric variations, for the SWELL and BARO subsets. In addition, both variables were fitted by multi-variable regression, because ocean- and ground-water levels are most likely affected by the combined effects of barometric and ocean-level changes. The setup time lag at each observation point, specified in Table 6.2, was included in the regression analysis.

### ***Aquifer Parameters***

The Jacob-Ferris solution (Jacob 1950; Ferris 1951) for tides was used to estimate hydraulic parameters from setup propagation. The one-dimensional ground-water flow equation with a harmonic oscillating boundary condition assumes aquifer homogeneity and a vertical boundary between land and ocean. Sediment cover at the boundary can cause an additional damping effect (Li et al. 2007). The amplitude of the signal is reduced by a coefficient,  $E$ , and the phase is shifted by a value,  $\phi$ . The equation for diffusivity from attenuation,  $D_{\text{amp}}$  (m<sup>2</sup>/d), in an unconfined aquifer is

$$D_{\text{amp}} = \frac{T}{S} = \frac{x^2 \pi}{(\ln A)^2 \tau} \quad (6.4)$$

where  $T$  is transmissivity (m<sup>2</sup>/d),  $S$  is specific yield (dimensionless),  $x$  is distance to the coast (m),  $A$  is the amplitude attenuation factor (dimensionless), and  $\tau$  is the period of the oscillation (d).  $A$  is given by the ratio of the amplitude of the oscillation in the

observation well to the amplitude in the ocean, which was estimated in two ways. The first involved the use of least-squares regression of observed head, corrected for barometric changes, and setup applied to the SWELL subset. The second is a more sophisticated approach involving the use of spectral analysis to find matching peak frequencies in the setup signal and observed-head responses. Discrete Fourier transforms were applied to setup and ground-water head data, corrected for barometric pressure. The identified frequencies are, however, only representative of the analyzed record.

Diffusivity from the phase lag,  $D_{\text{pha}}$  ( $\text{m}^2/\text{d}$ ), may be expressed as

$$D_{\text{pha}} = \frac{T}{S} = \frac{x^2 \pi}{\Phi^2 \tau} \quad (6.5)$$

where  $\Phi$  is the difference between the phase of the oscillation in the observation well and that in the ocean (rad). The time lag from the cross correlation and the phase difference between matching frequencies in the aquifer and ocean were evaluated. A relationship between  $A$  and  $x$  on a semi-logarithmic scale and  $\Phi$  and  $x$  on a normal scale allows linear regression to fit the data. The attenuation slope was substituted in Equation (6.4) and the phase-lag slope in Equation (6.5) to estimate effective aquifer diffusivities. The  $y$ -intercepts may approximate the damping coefficients  $E$  and  $\varphi$  (see chapter 5).

### ***Numerical Model***

A one-dimensional ground-water flow model was developed to assess the accuracy of the estimated aquifer parameters using MODFLOW 2000 (Harbaugh et al. 2000). The simulated aquifer cross section was 11 km long and extended vertically from

1.8 km below sea level to 10 m above sea level. The minimum cell size of 10 m was around the observation points and at the ocean boundary. Cell size increased gradually to 200 m away from these places. The model simulated an unconfined homogeneous aquifer with the cell adjacent to the ocean boundary representing less-conductive sediment cover or Kula Basalt. In chapter 5, this approach successfully accounts for a thin low-conductivity zone at the boundary in the tidal simulation of the same study area. The same estimated properties for the capping unit were used in the setup analysis. The specific-yield value was set to 0.1 and the hydraulic conductivity value to 0.97 m/d. A transient-head condition that matches the estimated setup at Kahului was applied at the ocean boundary. The landward boundary was a constant-head boundary. The model simulated the SWELL period in 4-hour time steps. The hydraulic properties for the basalt aquifer were estimated by matching observed and calculated head responses using the automated parameter-estimation algorithm PEST (Doherty 2004).

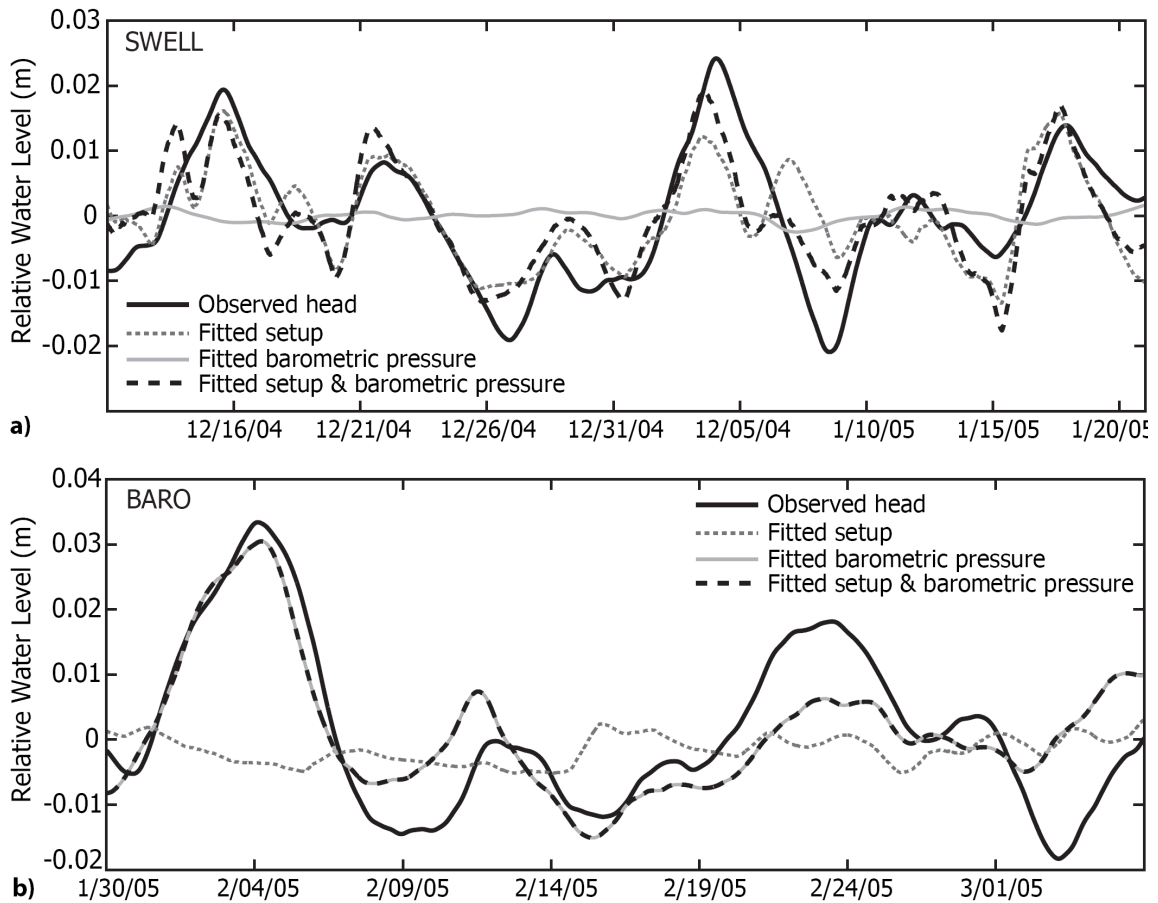
## **Results and Discussion**

Figure 6.4a illustrates the corrected wave height for Kahului ( $H_{sK}$ ), as estimated using Equation 6.1. Significant wave heights in the Kahului area are approximately one-third of wave heights at the Waimea buoy. Most of the large swells during the observation period came from westerly directions ( $-60^\circ$  to  $-20^\circ$  TN), which indicates the importance of the directional correction (Figure 6.4c). Figure 6.4d shows estimated setups based on the two approaches represented by Equations (6.2) and (6.3). The two estimates are close, with maximum values below 0.2 m. When compared,  $\eta_S$  is characterized by longer setup events than  $\eta_V$ . The elongated peaks are associated with

consideration of the wave period in the relationship, which leads to an earlier increase in setup (Figures 6.4a and 6.4b). Differences between the two approaches are minimal in the SWELL subset. On the other hand, larger deviations are observed in the BARO subset, which is also due to the influence of wave period on  $\eta_S$ . Both setup estimates are assumed acceptable for the analysis, considering that the objective of this study was to estimate aquifer parameters using setup propagation. However, confidence in the analysis would significantly improve with setup measurements in the Kahului area.

### ***Regression Analysis***

Influences of wave setup and inverted barometric pressure on water-table changes were investigated by regression analysis. Fitted and observed water levels of CPP for the SWELL subset are shown in Figure 6.5a. The correlation coefficient ( $R$ ) between ground-water head and  $\eta_S$  during this period is 0.72, whereas barometric pressure shows a weak correlation with an  $R$ -value of 0.08. Including barometric pressure in the regression improves the fit over using setup alone, with a change in correlation from 0.72 to 0.81. Figure 6.5b shows fitted and observed water levels at CPP for the BARO subset. A negative correlation of 0.16 exists between  $\eta_S$  and ground-water table fluctuations. Barometric pressure changes are mainly responsible for low-frequency ground-water variations with a correlation of 0.80. As should be expected, no improvement in correlation occurs by combining the effects of barometric pressure and setup, due to the negative correlation with  $\eta_S$ .



**Figure 6.5.** Single- and multi-variable regression of filtered water levels at CPP to setup  $\eta_S$  and barometric records (a) for the SWELL subset and (b) for the BARO subset.

The two examples shown in Figure 6.5 are typical of the ground-water responses for three other locations in central Maui, which also were correlated with setup and barometric records. A summary of correlation coefficients for the SWELL and BARO subsets for each observation point with either  $\eta_V$  or  $\eta_S$  is shown in Figure 6.6. The results are consistent for both setup estimates. The regression with  $\eta_S$  shows slightly higher  $R$ -values for the SWELL subset (Figure 6.6b) and negative ones for the BARO subset (Figure 6.6d). The dominating effect of setup in the SWELL subset and the governing influence of barometric pressure in the BARO subset are similar for all ground-water

observation points. The correlation in the SWELL subset improves when both variables are included, but this is not the case with the BARO subset. This difference is due to the omnipresence of barometric fluctuations in both subsets and the weak presence of setup pulses in the BARO subset. The correlation with setup decreases slightly with increasing distance from the coast (e.g., from CPP to Pump 7). This is expected due to the decaying character of the propagating signal. However, setup influences still can be detected as far as 5 kilometers away from the coast, with amplitudes of approximately 0.014 m. The regression analysis thus shows that setup could affect and dominate ground-water fluctuations in a permeable volcanic aquifer in times of energetic swell events.

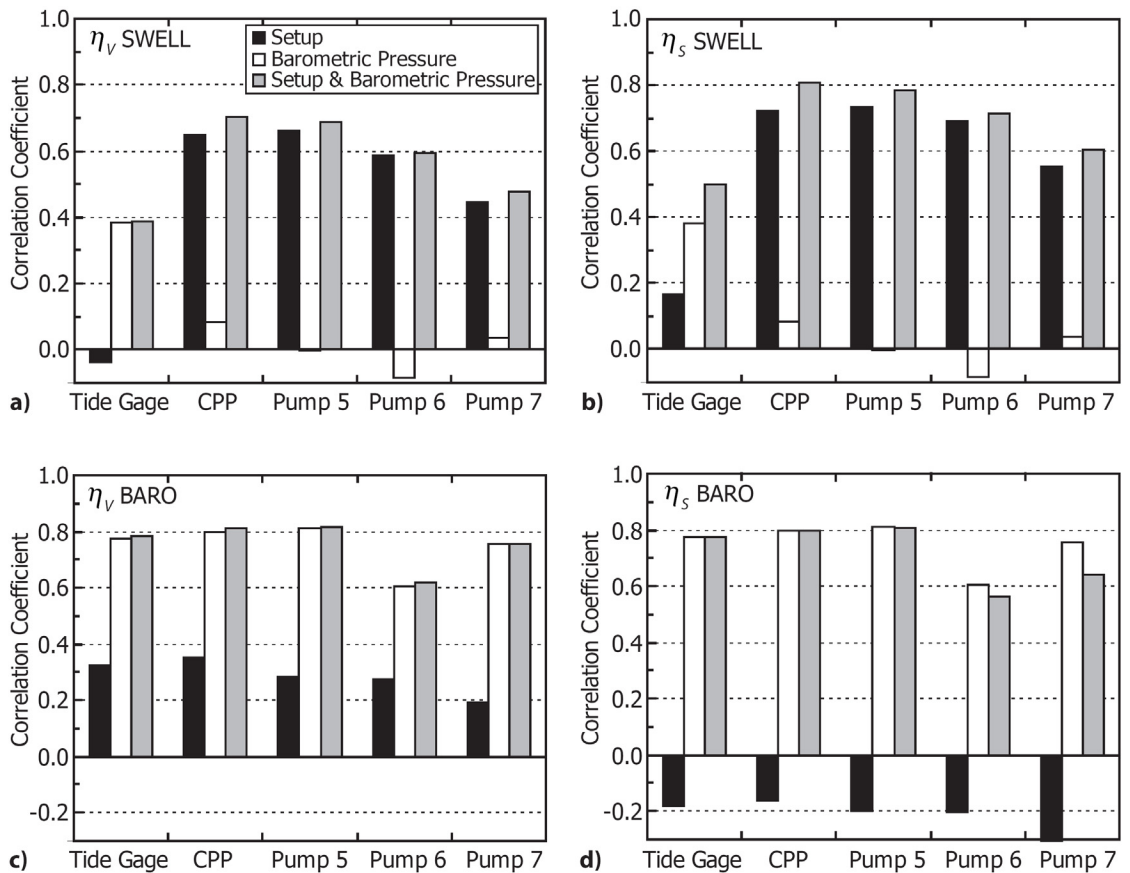


**Figure 6.6.** Correlation coefficients of the regression analysis (a) for the SWELL subset with  $\eta_V$ , and (b) with  $\eta_S$ , (c) for the BARO subset with  $\eta_V$ , and (d) with  $\eta_S$ .

Figures 6.6a and 6.6b show a weak correlation of setup and the ocean-water level at the tide gage (-0.04 for  $\eta_V$  and 0.17 for  $\eta_S$ ). The gage seems to experience a different response to wave setup than the ground-water observation points. Setup is a local phenomenon that is greatly influenced by the bathymetry of the near-shore area (Gourlay 1992). The geometry of the harbor, including the deep channel at the entrance and the protecting breakwaters can account for a different wave climate inside the harbor compared to that along the rest of the coast.

A detailed study of wave responses in Kahului Harbor showed that wave heights at Gage 77, outside the harbor, have an amplification factor of 0.25 at the west side of the pier, where the tide gage is installed, and a factor of 0.1 on the east side of the pier (Thompson et al. 1996). Assuming a wave setup of 0.17 m, the setup would be 0.042 and 0.019 m on the west and east sides of the pier, respectively. In fact, setup amplitudes during swell events at the tide gage do not exceed 0.05 m, uncorrected (Figure 6.3b) or corrected for barometric influences (Figure 6.3c). Regressing  $\eta_S$  on the filtered and detrended tide data, corrected for barometric changes, yields an amplitude coefficient of 0.23, which supports the observation of reduced wave energy in the southeast corner of the harbor. Additionally, the matching amplitude reduction in the harbor strengthens the confidence in the magnitude of the setup estimations outside the harbor. Although small waves break in the northwest corner (Thompson et al. 1996), it can be concluded that significantly less energy is transferred to the water column in the harbor. Hence, the water level at the tide gage is not representative of setup along the coast.

### *Aquifer Parameters*

Hydraulic parameter estimation requires quantification of time lag and amplitude attenuation of the propagating setup pulse. The tide gage data are not included in the estimation for the reasons stated above. The time lag of ground-water head to setup is identical for  $\eta_V$  and  $\eta_S$ . The average duration, including rise and fall of the ocean water level to complete a quasi-sinusoidal oscillation, of four major swell events in the SWELL subset, is 6.4 days for  $\eta_V$  and 6.9 days for  $\eta_S$ . As noted earlier,  $\eta_S$  is characterized by longer setup events. The average periods were used to convert the time lag to phase differences. The lags and amplitude attenuation of the entire signal of the SWELL subset are listed in Table 6.2.

**Table 6.2.** Estimated setup responses for  $\eta_V$  and  $\eta_S$  at observation points in the aquifer analyzing the entire signal

Monitoring point	Distance to coast (km)	Time lag (d)	Attenuation factor $A$ (-)		Phase difference $\Phi$ (rad)	
					$\tau = 6.4$	$\tau = 6.9$
			$\eta_V$	$\eta_S$	$\eta_V$	$\eta_S$
CPP	0.73	0.134	0.281	0.309	0.136	0.147
Pump 5	1.05	0.230	0.260	0.285	0.234	0.253
Pump 6	2.08	0.503	0.176	0.202	0.513	0.553
Pump 7	4.08	0.611	0.117	0.140	0.622	0.671

Amplitude spectra of setup and head time series show peak frequencies in the low-frequency bandwidth from  $3 \times 10^{-7}$  to  $1 \times 10^{-5}$  Hz, which correspond to periods of 38.6 and 1.1 d, respectively (Figure 6.7). Peak frequencies that occur in the setup signals and in observed-head responses were  $1.7 \times 10^{-6}$  Hz,  $3.1 \times 10^{-6}$  Hz,  $3.7 \times 10^{-6}$  Hz, and  $6.2 \times 10^{-6}$  Hz. The matching frequencies in both signals are not as distinct as the tidal

signature. However, the objective is to estimate the attenuation of oscillations. The two most dominant frequencies in all time series were  $1.7 \times 10^{-6}$  Hz and  $3.7 \times 10^{-6}$  Hz, which correspond to periods of 6.83 and 3.15 d, respectively. Although the  $6.2 \times 10^{-6}$  Hz frequency is also considerable, the oscillation is too short (1.7 d) compared to the observed length of setup events ( $> 5$  d) and is therefore not evaluated. Estimated setup attenuations of the decomposed signal of  $\eta_V$  and  $\eta_S$  at the observation points are listed in Table 6.3 and Table 6.4, respectively.

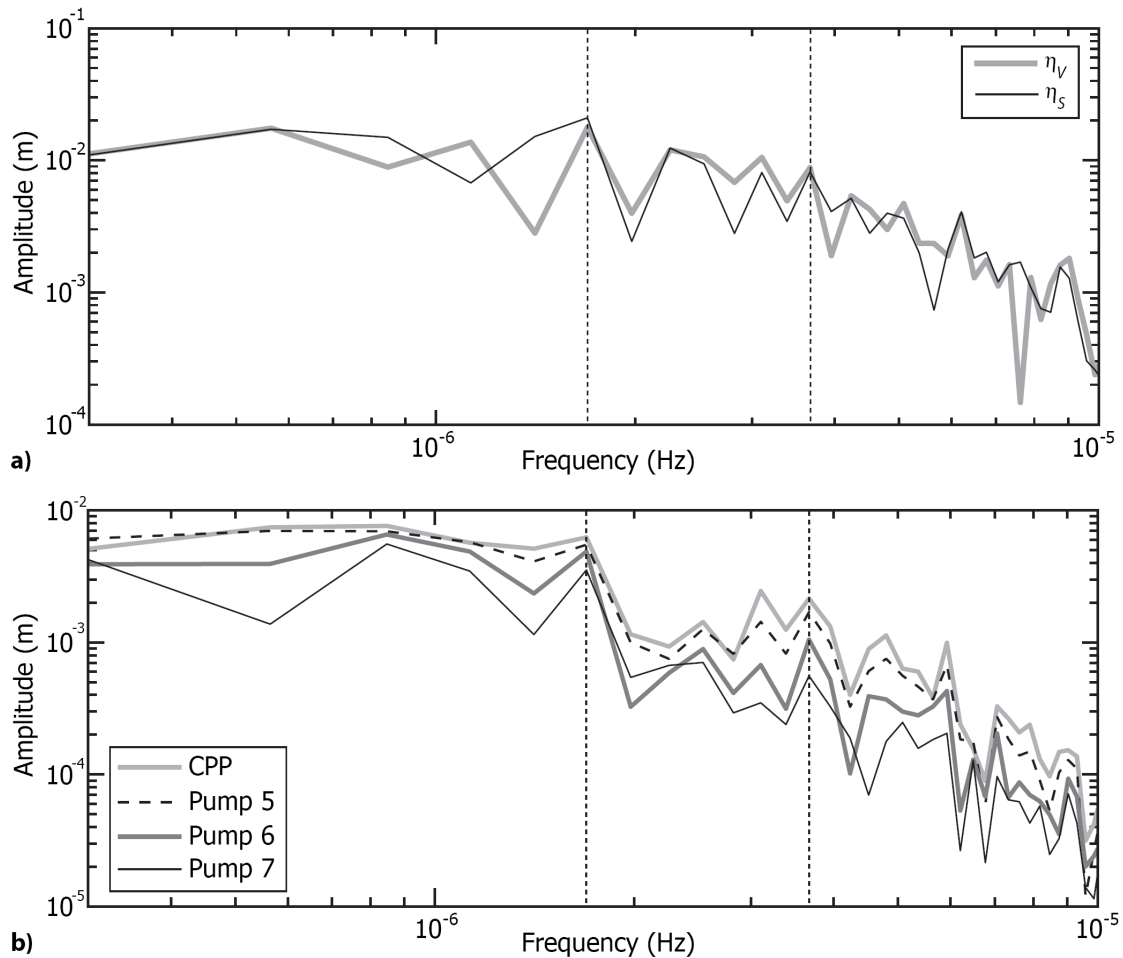


**Figure 6.7.** Amplitude spectra of the SWELL subset for (a) setup  $\eta_V$  and  $\eta_S$ , and (b) observed head, corrected for barometric-pressure effects. The matching peak frequencies in both plots are  $1.69 \times 10^{-6}$  Hz and  $3.67 \times 10^{-6}$  Hz.

**Table 6.3.** Estimated wave setup responses for  $\eta_V$  at observation points in the aquifer analyzing the decomposed signal

Monitoring point	Attenuation factor $A$ (-)		Phase difference $\Phi$ (rad)	
	$\tau = 6.8$	$\tau = 3.2$	$\tau = 6.8$	$\tau = 3.2$
CPP	0.352	0.244	0.396	0.123
Pump 5	0.309	0.193	0.416	0.370
Pump 6	0.274	0.119	0.752	0.663
Pump 7	0.199	0.063	0.897	0.833

**Table 6.4.** Estimated wave setup responses for  $\eta_S$  at observation points in the aquifer analyzing the decomposed signal

Monitoring point	Attenuation factor $A$ (-)		Phase difference $\Phi$ (rad)	
	$\tau = 6.8$	$\tau = 3.2$	$\tau = 6.8$	$\tau = 3.2$
CPP	0.298	0.263	0.684	0.219
Pump 5	0.262	0.208	0.703	0.466
Pump 6	0.232	0.129	1.039	0.759
Pump 7	0.168	0.068	1.184	0.929

The amplitude attenuation for both setup estimates is shown in Figures 6.8a and 6.8b. Attenuation factors with respect to  $\eta_V$  and  $\eta_S$  are comparable due to similarity in magnitude of the estimated setups. The phase differences between aquifer and both setup estimates are shown in Figures 6.8c and 6.8d. Results from tidal propagation at the same observation points (Chapter 5) are shown for comparison in all plots. Similar to transmitted tidal fluctuations, the amplitude of setup propagation decays exponentially and the phase lag increases linearly with increasing distance from the coast. This indicates that the setup signal propagation also occurs as a diffusive process and implies that there is potential to use setup in hydraulic parameter estimation by applying the same analytical solutions derived for tides.

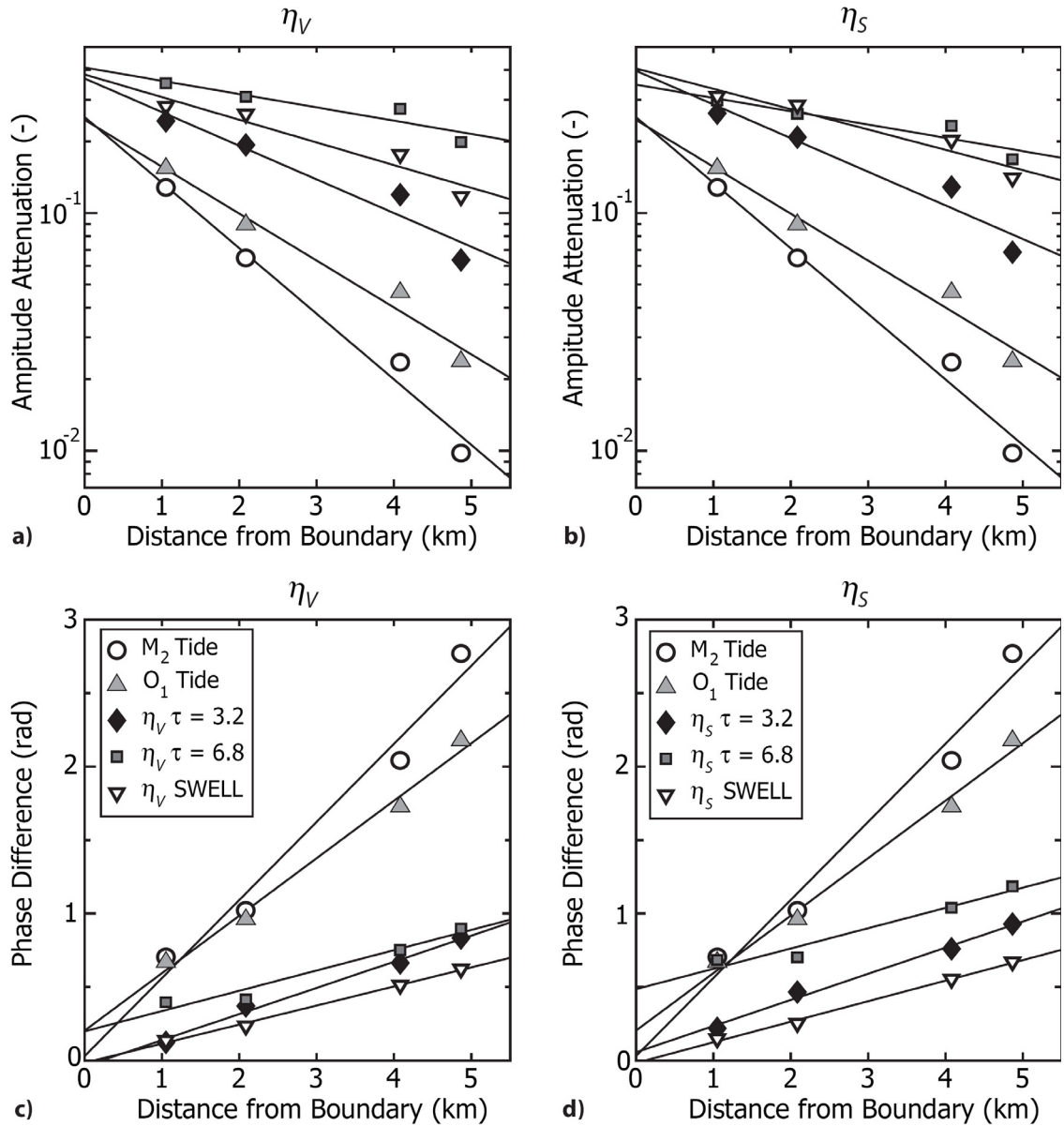


**Figure 6.8.** Amplitude attenuation for setup propagation of (a)  $\eta_V$  and (b)  $\eta_S$ , and phase difference for setup propagation of (c)  $\eta_V$  and (d)  $\eta_S$  in the aquifer.

Figures 6.8a and 6.8b show that setup attenuation has milder slopes than tidal attenuation and that the setup oscillation with the longer period of 6.8 days has milder slopes than the fluctuation occurring every 3.2 days for both setup estimates. The slopes of phase difference behave in the same way, showing a gentler gradient for the longer

period oscillations (Figures 6.8c and 6.8d). The aquifer responses of the entire setup signal agree with those from the decomposed signal. The milder setup slopes are consistent with observations from other tidal studies (e.g., Oki 1997; Merritt 2004) and heat-diffusion literature (e.g., Turcotte and Schubert 2002), which indicate that oscillations with longer periods penetrate deeper into the aquifer. The characteristic length scale  $(\tau T/S)^{0.5}$  describes the distance of diffusive wave propagation (e.g., Turcotte and Schubert 2002). For the central Maui hydraulic diffusivity, the penetration length for semidiurnal and diurnal tides, as well as for the 3.2-day and 6.8-day setup oscillation is 3.4 km, 4.9 km, 8.5 km, and 12.5 km, respectively. Thus, setup signal propagation has the advantage over tides by providing information over larger length scales.

In theory, the value of the amplitude attenuation factor at the coastline is one and the phase lag is zero, but the regression lines intercept the  $y$ -axis at considerably smaller values than one in Figures 6.8a and 6.8b and larger values than zero in Figures 6.8c and 6.8d. This probably reflects, at least in part, aquifer heterogeneity, especially due to the presence of less-permeable sediments and Kula Basalt at the boundary. The regression intercept depends on dimension and hydraulic properties of the capping unit (Chapter 5). The magnitude of the estimated setup is uncertain and therefore plays an additional role affecting the  $y$ -intercept in this case. With slightly greater estimated setup amplitudes, the intercept would match the one from tidal propagation. However, regardless of the value of the intercept, the aquifer-parameter estimation of the basalt only depends on the slope of the regression line.

Aquifer parameters were estimated with Equations (6.4) and (6.5) using the corresponding periods for the SWELL subset and those identified in the spectral analysis. The results are listed in Table 6.5 and compared with results for the same study area using ocean tides. Hydraulic diffusivity estimated from the decomposed setup signal yields identical results for  $\eta_S$  and  $\eta_V$ , with an effective diffusivity of  $2.3 \times 10^7 \text{ m}^2/\text{d}$ . The attenuation of the entire signal gives similar results as the decomposed signal.

**Table 6.5.** Hydraulic diffusivity and conductivity estimated analytically and numerically from setup using discrete frequencies, the complete time series, and ocean tides

Setup	Estimation method	$D_{\text{amp}}$ ( $\text{m}^2/\text{d}$ )	$K^a$ ( $\text{m}/\text{d}$ )	$D_{\text{pha}}$ ( $\text{m}^2/\text{d}$ )	$K^a$ ( $\text{m}/\text{d}$ )	$D^*$ ( $\text{m}^2/\text{d}$ )	$K^{*a}$ ( $\text{m}/\text{d}$ )
Setup	Mean of Fourier transform	$1.9 \times 10^7$	415	$2.8 \times 10^7$	620	$2.3 \times 10^7$	520
$\tau = 6.83$	Fourier transform	$2.8 \times 10^7$	620	$2.4 \times 10^7$	540	$2.6 \times 10^7$	580
$\tau = 3.15$	Fourier transform	$9.4 \times 10^6$	210	$3.2 \times 10^7$	700	$2.0 \times 10^7$	460
$\eta_V \tau = 6.4$	regression/cross correlation	$1.0 \times 10^7$	230	$2.9 \times 10^7$	650	$2.0 \times 10^7$	440
$\eta_S \tau = 6.9$	regression/cross correlation	$1.2 \times 10^7$	260	$2.3 \times 10^7$	520	$1.8 \times 10^7$	390
$\eta_V$	MODFLOW/PEST					$2.9 \times 10^7$	650
$\eta_S$	MODFLOW/PEST					$2.1 \times 10^7$	460
Ocean tide	Chapter 5	$1.6 \times 10^7$	350	$2.9 \times 10^7$	655	$2.3 \times 10^7$	500

<sup>a</sup>estimated from diffusivity using  $S$  of 0.04 and  $b$  of 1.8 km

\*arithmetic mean of  $D_{\text{amp}}$  and  $D_{\text{pha}}$

Diffusivity can be converted to hydraulic conductivity ( $K$ ), by assuming typical values for aquifer depth ( $b$ ) and specific yield through the relationship  $K = DS/b$ . The effective diffusivity from the analytical method translates into a hydraulic conductivity of 520 m/d assuming  $S$  of 0.04 and  $b$  of 1.8 km. In general,  $D_{\text{pha}}$  is greater than  $D_{\text{amp}}$ , which may reflect heterogeneity within the basalt aquifer. A larger  $D_{\text{pha}}$  is common in tidal

propagation studies, resulting in a slope factor (Equation 5.14) below unity of 0.82 (see Trefry and Bekele 2004). The effective diffusivities,  $D^*$ , estimated from setup are identical with the ones estimated from ocean tides in the same study area. Therefore, setup propagation is suitable to estimate hydraulic parameters.

### ***Numerical Model***

A numerical ground-water flow model was used to evaluate the accuracy of the estimated hydraulic parameters. In two simulations, the estimated setups  $\eta_V$  and  $\eta_S$  were set at the boundary and the model was calibrated with the observed heads, corrected for barometric pressure fluctuations. The model provided the best results with a specific yield value of 0.04 and a hydraulic conductivity value of 650 m/d for the basalt using  $\eta_V$  and 460 m/d using  $\eta_S$  (Table 6.5). Both numerically estimated conductivities are close to  $K^*$  based on the analytical solution. Moreover, the matching hydraulic parameters indicate that the amplitudes of the estimated setup signal at the coast were reasonable.

Figure 6.9 shows observed and calculated water levels for the SWELL subset. The water levels are shifted along the  $y$ -axis for visual clarity. The amplitudes of the calculated heads match at all observation points (Table 6.6), although local differences exist. The largest deviation is for CPP with 14% overestimation of the calculated response. The amplitudes at other monitoring points do not exceed 6% difference. Local differences that appear in all observation points (12/31/04 and 1/15/05) may be attributed to inaccuracies of the estimated setup signal as a source. The time lag of the setup pulses in the aquifer is adequately calculated and does not differ more than 2.7 hours. The correlation coefficient between observed and calculated water levels ranges from 0.75 for

Pump 7 to 0.89 for CPP, with an average correlation of 0.84. The higher correlation compared to the regression analysis is attributed to the removal of barometric effects.

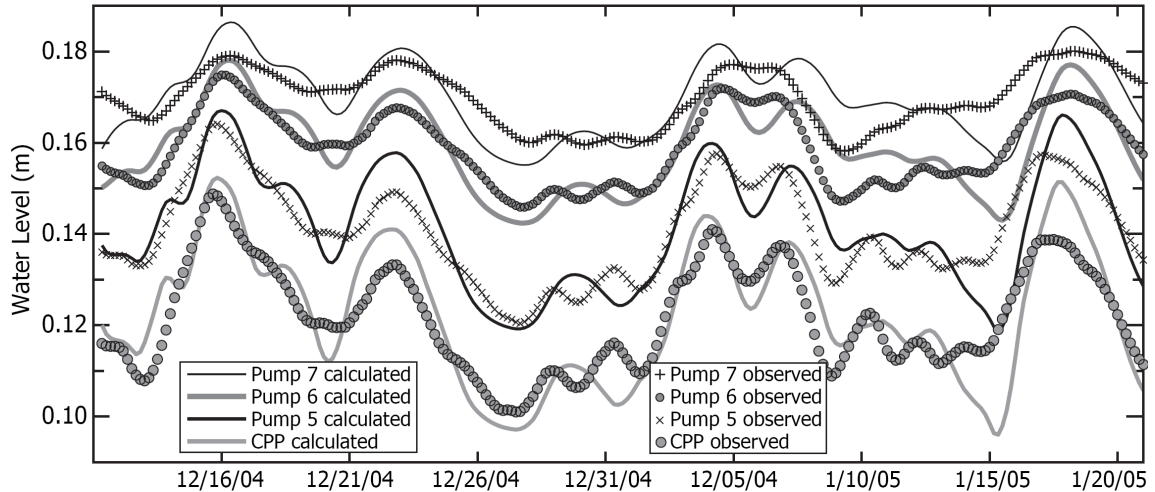


**Figure 6.9.** Observed (symbols) and calculated (lines) water levels using 1-D MODFLOW modeling to simulate wave-setup attenuation in the aquifer.

**Table 6.6.** Error summary of observed against calculated setup responses

Monitoring point	$R$ (-)	Sum of squared error ( $m^2$ )	Root mean square error ( $m^2$ )	Difference between calculated and observed	
				Amplitude (%)	Time lag (d)
CPP	0.89	0.0119	0.0070	14.4	0.01
Pump 5	0.88	0.0092	0.0061	5.7	0.11
Pump 6	0.85	0.0061	0.0050	0.9	0.11
Pump 7	0.75	0.0076	0.0056	-1.8	-0.09

The use of setup as a source for transient heads at the boundary, a low-permeability unit at the boundary (estimated in Chapter 5), and an effective diffusivity for the basalt aquifer that is consistent with the analytically estimated value, results in calculated setup responses that match the observed water-table fluctuations. This supports that setup propagation can be successfully used in hydraulic parameter estimation.

## Chapter 6 Conclusions

The influence of wave setup on coastal ground-water elevations and the possibility of using the propagating setup signal in aquifer parameter estimation were investigated. In the absence of field observations, two approaches were used to estimate setup in the Kahului area, proposed by Vetter (2007) and Stockdon et al. (2006). Water-level changes at the Kahului tide gage are not representative of the rest of the coastal area, because severe wave amplitude damping occurs inside Kahului Harbor.

The regression analysis shows that the setup signal is detectable at observation points as far away as 5 km from the coast. Correlation coefficients between setup and ground-water fluctuations are as high as 0.66, based on the approach of Vetter (2007), or 0.73 based on the approach of Stockdon et al. (2006). Barometric influence is insignificant ( $<0.1$ ) in the SWELL subset. However, the correlation coefficient improves using setup and barometric changes. In contrast, in the BARO subset, correlations with setup are weak and the influence of barometric pressure variations is strong, reaching correlations up to 0.81. Therefore, setup can significantly affect ground-water elevations in coastal aquifers and can overshadow barometric influence in times of large ocean swells. At other times, the barometric loading dominates.

Setup propagation through the aquifer is similar to that for tides with exponentially decreasing amplitudes and linearly increasing time lags between setup and observed ground-water responses. The average duration of swell events in the SWELL subset is approximately 6 days, and spectral analysis shows matching peak periods at 6.8 and 3.2 days in setup and ground-water observations. The longer periods explain the

milder amplitude attenuation and milder phase-lag gradients of setup compared to tidal propagation. This can be very useful, because setup signals propagate deeper into the aquifer (~10 km in central Maui) than diurnal tides (5 km) and can therefore provide information on greater length scales.

Aquifer parameters were estimated from setup attenuation using the analytical solutions of tidal propagation. The results are consistent with parameters estimated from tides. Mean hydraulic diffusivity from setup attenuation is identical for the Vetter (2007) and Stockdon et al. (2006) approaches and is estimated as  $2.3 \times 10^7 \text{ m}^2/\text{d}$ . Assuming that the setup signal travels through the entire aquifer thickness of 1.8 km and the specific yield is 0.04, the hydraulic conductivity is 520 m/d.

A one-dimensional numerical model reproduced the results of the analytical solution. The best fit was achieved with a hydraulic-conductivity value of 650 or 460 m/d, based on the Vetter (2007) and Stockdon et al. (2006) approaches, respectively. The model simulated groundwater responses that match the head at observation points reflecting the amplitude attenuation and the time lag of setup pulses. The mean correlation coefficient is 0.84 for all observation points. The setup propagation was successfully used to estimate hydraulic parameters. The technique is expected to be beneficial to many high-permeability coastal environments, such as volcanic islands and atolls, and will provide a practical approach for aquifer parameter estimation as an important step toward managing valuable ground-water resources.

## **7. Summary and Conclusions**

In recent years, the ground-water demand of the population of the island of Maui, Hawaii, has significantly increased. To ensure prudent management of the ground-water resources for Maui and the other islands of Hawaii, an improved understanding of the ground-water flow systems is needed. At present, large-scale estimations of aquifer properties, such as hydraulic conductivity and storage parameters, are lacking for Maui. Four different methods that analytically estimate such properties were evaluated in this study. Unconventional step-drawdown tests were compared with traditional constant-rate aquifer tests; an empirical relationship between specific capacity and hydraulic conductivity was developed and applied; and ocean tides and wave setup were used to estimate formation properties based on the propagating signal through the aquifer.

### **Aquifer Tests**

Seven analytical methods using constant-rate and variable-rate withdrawals for single wells provide an estimate of hydraulic conductivity and transmissivity for 103 wells in central Maui. Unconventional methods, such as the Harr method and infrequently used step-drawdown tests, offer estimates consistent with those of constant-rate tests. Both methods provide useful tools for aquifer-parameter estimations if abundant data is available. A numerical model supports the suitability of analytical solutions for step-drawdown tests and additionally provides an estimate of storage parameters. The results indicate that hydraulic conductivity in Maui is log-normally distributed and that for dike-free volcanic rocks it ranges over several orders of

magnitude from 1 to 2,500 m/d. The geometric-mean and median value of hydraulic conductivity are respectively 276 and 370 m/d for dike-free basalt. The corresponding values for sediment are 46 and 30 m/d. A geostatistical approach using ordinary kriging yields a prediction of hydraulic conductivity on a larger scale than the point estimates based on aquifer-test results. The hydraulic-conductivity contour map can be very useful for regional hydrogeologic assessments.

### **Relationship between Hydraulic Conductivity and Specific Capacity**

Site-specific relationships between specific capacity and hydraulic parameters (transmissivity and hydraulic conductivity) were investigated for volcanic rocks in Maui, Hawaii. Details about well construction were ignored in previous studies. To improve on such efforts, specific-capacity values were divided by the open interval of the well. Correcting specific capacity for turbulent head losses using step-drawdown tests and consideration of aquifer penetration length improved the correlation between specific capacity and hydraulic conductivity and reduced uncertainty in the prediction of hydraulic parameters. The relationships provide estimates of aquifer parameters with correlation coefficients between 0.81 and 0.99. The relationships for Maui can probably be extended to other Hawaii islands, given the similarity of aquifer formations and a reasonable fit to step-drawdown data from Oahu. Hydraulic conductivity was estimated from 1,257 specific-capacity values in the Hawaii's well database. Hydraulic-conductivity estimates for dike-free volcanic rocks are consistent on different islands. The differences among the mean values from different islands are small, considering the variation within a single island. For all islands, the estimates range from 3 to 8,200 m/d,

with a geometric-mean and median value of 272 m/d and 291 m/d, respectively. A geostatistical approach was applied to Maui and Oahu to generate island-wide hydraulic-conductivity maps to facilitate ground-water management efforts. The map for Maui generally matches the one obtained from aquifer tests, except a cluster of high hydraulic conductivity on the north side of central Maui.

### **Ocean Tides and Dual-Tide Influence**

Most published solutions for aquifer responses to ocean tides focus on the one-sided attenuation of the signal as it propagates inland. However, island aquifers experience periodic forcing from the entire coast, which can lead to integrated effects of different tidal signals, especially on highly permeable volcanic islands. In general, studies disregard a potential time lag as the tidal wave sweeps around the island. A one-dimensional analytical solution to the ground-water flow equation subject to asynchronous and asymmetric oscillating head conditions on opposite boundaries was presented and tested on data from Maui. The solution considers sediment-damping effects at the coastline. The responses of central Maui aquifers indicate that water-table elevations near the center of the aquifer are influenced by a combination of tides from opposite coasts. A better match between the observed ground-water head and the theoretical response can be obtained with the proposed dual-tide analytical solution than with single-sided solutions. Hydraulic diffusivity was estimated to be  $2.3 \times 10^7 \text{ m}^2/\text{d}$ . This translates into a hydraulic conductivity of 500 m/d, assuming a specific yield of 0.04 and an aquifer thickness of 1.8 km. A numerical experiment confirmed the hydraulic-diffusivity value and showed that the  $y$ -intercepts of the modal attenuation and phase

differences estimated by the regression can approximate damping factors caused by low-permeability units at the boundary.

### **Wave Setup**

Wave setup is the elevated mean water table at the coast associated with wave breaking occurring generally over several days. Ground-water responses to wave setup were observed as far as 5 km inland in the central Maui aquifer. The analysis showed that at times of energetic swell events setup pulses dominate low-frequency ground-water fluctuations associated with barometric pressure effects. Matching peak frequencies at  $1.7 \times 10^{-6}$  Hz and  $3.7 \times 10^{-6}$  Hz were identified in setup and observed head using spectral decomposition. Similar to tides, the setup propagation through the aquifer shows exponentially decreasing amplitudes and linearly increasing time lags. Due to the longer periods of setup oscillations, the signal propagates deeper into the aquifer (~10 km in central Maui) than diurnal tides (5 km) and can therefore provide information on greater length scales. Hydraulic diffusivity was estimated based on the setup propagation. An effective diffusivity of  $2.3 \times 10^7$  m<sup>2</sup>/d is consistent with aquifer parameters based on aquifer tests and tides. A one-dimensional numerical model supports the results of the analytical solution and strengthens the suitability to estimate hydraulic parameters from setup propagation. The new approach is expected to be beneficial to high-permeability coastal environments, such as on volcanic islands and atolls.

**Table 7.1.** Hydraulic diffusivity and conductivity estimated from various analytical methods for dike-free basalts in Maui, Hawaii

Method	Estimated through	Diffusivity (m <sup>2</sup> /d)	<i>K</i> (m/d)	<i>K</i> * <sup>b</sup> (m/d)
Aquifer test	Theis	—	220	280
	Cooper–Jacob	—	240	
	Harr $t = 10^4$	—	180	
	Harr $t = 10^6$	—	140	
	Recovery	—	240	
	Zangar	—	300	
	Polubarinova	—	330	
	Thomasson	—	360	
Specific capacity	$S_C$ vs. $K$ for Maui	—	420	350
	$S_C$ vs. $K$ for state of Hawaii	—	270	
Ocean tide	$O_1$ attenuation	$1.5 \times 10^7$	330 <sup>a</sup>	500
	$M_2$ attenuation	$1.7 \times 10^7$	370 <sup>a</sup>	
	$O_1$ phase lag	$2.4 \times 10^7$	580 <sup>a</sup>	
	$M_2$ phase lag	$3.5 \times 10^7$	770 <sup>a</sup>	
Wave setup	$\tau = 6.8$ attenuation	$2.8 \times 10^7$	620 <sup>a</sup>	520
	$\tau = 3.2$ attenuation	$9.4 \times 10^6$	210 <sup>a</sup>	
	$\tau = 6.8$ phase lag	$2.4 \times 10^7$	540 <sup>a</sup>	
	$\tau = 3.2$ phase lag	$3.2 \times 10^7$	700 <sup>a</sup>	
Arithmetic mean		$2.3 \times 10^7$	380	410
Standard deviation		$8.1 \times 10^6$	190	120
Standard error of the mean		$2.9 \times 10^6$	45	60

<sup>a</sup>estimated from diffusivity using  $S$  of 0.04 and  $b$  of 1.8 km

<sup>b</sup>arithmetic mean of individual method

### Comparison of Hydraulic-Parameter Estimation Methods

Table 7.1 lists the geometric means of  $K$  from different aquifer-test methods and the specific-capacity relationship, as well as hydraulic diffusivity and conductivity estimated from tide and setup propagation. The arithmetic mean of the results,  $K^*$ , provides one  $K$  estimate per method. The mean from individual estimation techniques,  $K$ ,

and the mean of all four methods,  $K^*$ , provide one arithmetic-mean value and standard deviation for all methods combined. The results are consistent, with aquifer-test values comparable to the specific-capacity method and tides very similar to setup estimates. The estimated hydraulic conductivity of the four methods ranges between 300 and 500 m/d for basalts in Maui, with an overall mean value of 410 m/d, a standard deviation of 120 m/d and a standard error of the mean of 60 m/d (Table 7.1). Finally, the results are consistent with values previously published for other Hawaii islands.

Stephen Gingerich (USGS, Honolulu, Hawaii) is currently developing a three-dimensional numerical ground-water flow model for central and west Maui. The model has been calibrated using a transversal horizontal hydraulic conductivity of 335 m/d for flank lava (Stephen Gingerich, USGS, written commun., 2007). Transversal refers to the direction normal to lava flows and is along the north-south direction in central Maui. The transversal flow direction coincides with the tidal and setup signal propagation through the aquifer. The  $K$  values for Maui, estimated in this study (Table 7.1), correspond closely to the 335 m/d value used in the latest USGS model. In conclusion, the four methods including single-well aquifer-test analysis, specific-capacity relationship, tidal-, and setup-signal propagation can be applied to volcanic aquifers and yield consistent aquifer-parameter estimates.

## **Future Research**

Aquifer tests with multiple observation wells are scarce in Hawaii (Williams and Soroos 1973; Rotzoll and El-Kadi 2007). The understanding of hydrogeology, particularly in areas intruded by dikes or divided by low-permeability valley fills, may be improved with multiple monitoring wells. Such tests would help understand unsaturated-zone effects and yield estimates of storage properties derived from analytical solutions. Impermeable boundaries, such as dikes, could be located with a triangulation approach of two or more monitoring wells. The effect of low-permeability valley fills on ground-water flow was initiated by Oki (2005) and extended by Rotzoll and El-Kadi (2007). These initial approaches need to be expanded to deepen the understanding of local flow patterns.

The unknown aquifer thickness in Hawaii poses a problem to various analytical aquifer-test solutions and every time a transmissivity value is converted to hydraulic conductivity. A better approach to define the actual thickness of contributing basalt layers is necessary to improve the use of analytical solutions by satisfying the underlying assumptions.

Knowledge of dual-tide effects in the central Maui aquifer may be significantly enhanced with more observations from the center and south side of the isthmus, especially with regard to the asynchronous dual-tide influence and sediment-damping effects on the south side. The understanding of the sediment-damping influence at the boundary may also be enhanced applying three-dimensional numerical models by addressing the geometry of sediment capping units and lower-permeable Kula basalt.

The analysis of wave setup would significantly improve with setup measurements in conjunction with ground-water observations in the same area, preferably on a transect perpendicular to the coast. The approach can easily be expanded to the other islands of Hawaii and other coastal areas with appreciable setup. Overlooked in this analysis is the effect of offshore loading of the elevated ocean-water level on the aquifer to avoid over complication. A numerical model can provide information how significant this simplification is on the propagation.

Strong onshore winds generate elevated mean ocean water levels by pushing water masses on the coast and should produce effects like those due to wave setup. The supra-elevation is termed wind setup. In central Maui, onshore-directed NE-trade winds are characterized by a daily cycle with maximum wind speeds from noon to 4 p.m., while at night, the winds are generally calm or their direction is reversed. However, due to the diurnal influence, it can be difficult to separate wind setup from diurnal tide effects. The effect of wind setup occurring over longer periods (several days) was briefly investigated but not reported in this study. The strongest trade winds occur during the summer months. However, no correlation could be found between daily-averaged onshore wind speeds and ground-water fluctuations from April to August 2005, mainly because strong wind speeds do not occur in isolated events that are detectable in the ground-water response. Again, measurements of ocean-water levels can identify magnitudes of wind setup and should reveal the significance of this factor.

Aquifer-parameter estimation techniques may also prove beneficial with regard to characterization and quantification of perturbations associated with sea-level change on

island-aquifer systems. Island aquifers, like Hawaii, are dependent on the freshwater-lens supply, and are thus vulnerable. High risks are associated with uncertainty of local, regional, and far-field effects of global warming. The major consequence of a sea-level rise to ground-water dynamics would be the rising freshwater/saltwater interface. However, a hypothetical sea-level rise of one meter in the next 100 years and a resulting elevated transition zone is secondary to the rise induced by pumping, which is currently at a rate of 2 meters per year in Maui (Stephen Gingerich, USGS, oral commun., 2007). Shallow coastal wells and shafts may become unsuitable for drinking-water withdrawals due to the rise of the interface. For coastal wells, a greater effect is probably seawater inundation from above than intrusion from below. In addition, those wells are typically not used for drinking water or irrigation. Assuming similar recharge conditions, the rise of the basal lens may also result in higher discharge through springs, which in turn may lead to an irreversible reduction of the basal lens. Numerical modeling of this scenario would be very effective and the results may provide future advice for aquifer management. Aquifer-parameter estimation techniques will be integral in assessing how such changes may be manifested.

## 8. Appendix A. Results of Aquifer-Test Analysis

**Table A.1.** Hydraulic conductivity estimates (m/d) of individual wells

Formation	Well No.	$r$	$b$	$L$	Theis	Cooper-Jacob	Harr $t = 10^4$	Harr $t = 10^6$	Recovery	Zangar	Polubarinova	Thomasson	$K^*$	$\sigma$
Wailuku Basalt	4830-01	0.20	9.1	11.2	20	30	90	40					40	30
	4831-01	0.20	15.8	17.4		170	80	70		700	760	960	460	400
	4834-01	0.15	2.9	2.9					700				700	
	4835-04	0.15	3.1	3.9	20	10	20	10	20	50	50	70	30	20
	4930-01	0.15	6.1	11.1	50	50	70	50	60	220	240	210	120	90
	4936-01	0.25	8.8	8.8						120	140	220	160	50
	5130-01	0.20	57.3	66.4						1	1	1	1	0
	5130-02	0.51	152	158.0					5	2	2	2	2	2
	5131-01	0.46	32.0	37.9	410	550	140	130	250	210	230	270	270	140
	5137-01	0.30	9.4	12.0	90	100	90	60	90	240	270	360	160	110
	5138-01	0.41	13.7	14.8	220	160	90	70		880	970	1,500	550	550
	5238-01	0.36	16.5	16.5	660	700	230	200	320	340	380	580	430	190
	5330-03	0.05	15.4	15.4	9	20	6	3					9	10
	5330-07	0.05	38.0	11.0	320	460		1,900					890	880
	5330-09	0.46	57.6	81.5	730	550	560	440	470	70	70	60	370	260
	5330-10	0.46	54.3	81.8	420	580	320	260	300				370	130
	5330-11	0.46	76.2	81.4	200	460	40	40	340	200	210	240	220	140
	5339-01	0.20	18.2	18.2	380	450	190	160					290	140
	5339-02	0.30	17.4	17.8	900	620	620	430		1,200	1,300	1,800	980	490
	5339-03	0.30	16.2	16.6					490				490	
	5339-04	0.30	29.9	29.9						80	90	110	90	20
	5341-02	0.15	3.0	7.0						60	70	50	60	10
	5430-01	0.36	103	108.0						40	50	50	50	3
	5431-02	0.51	55.2	59.6	150	200	90	80	30	310	340	410	200	140
	5431-03	0.51	47.2	50.8					280	220	240	310	260	40
	5439-01	0.41	19.8	20.4	90	110	40	30	120	90	100	150	90	40
	5439-02	0.36	20.1	22.0	550	550	250	210	330	540	590	790	470	200
	5540-01	0.41	9.0	9.0						1,100	1,300	2,300	1,600	640
	5631-02	0.41	29.6	35.5					340	520	560	660	520	130
	5631-03	0.41	26.5	36.6	300	320	1,100	520		400	440	480	510	270
5638-03	0.36	16.2	18.6						410	450	600	480	100	
5731-02	0.41	16.5	17.9						840	930	1,300	1,000	270	

**Table A.1. (Continued)** Hydraulic conductivity estimates (m/d) of individual wells

Formation	Well No.	$r$	$b$	$L$	Theis	Cooper-Jacob	Harr $t = 10^4$	Harr $t = 10^6$	Recovery	Zangar	Polubarinova	Thomasson	$K^*$	$\sigma$
Wailuku Basalt	5731-03	0.41	16.5	17.5	1,700	2,300	550	500	1,800	1,000	1,100	1,600	1,300	650
	5731-04	0.41	16.8	18.0	1,100	1,500	320	290	420	530	580	850	700	430
	5731-05	0.05	18.5	18.5					980				980	
	5738-01	0.41	12.2	12.7	240	310	90	80	10	630	700	1100	400	390
	5739-01	0.41	17.4	18.2	230	190	70	60		220	240	360	190	100
	5739-02	0.41	14.6	16.1						410	460	670	520	140
	5741-01	0.15	6.1	8.3	520	430	600	400					490	90
	5832-03	0.20	8.2	8.2	130	200	200	130					170	40
	5838-01	0.30	10.1	11.5	870	1,100	310	270	1,200	590	650	940	740	350
	5838-02	0.30	10.1	11.7	340	280	260	190	2,300	430	480	680	620	680
	5838-03	0.36	9.4	11.5	110	100	60	40	230	120	130	180	120	60
	5838-04	0.36	6.1	8.2	1,600	2,400	500	460					1,200	920
	5839-02	0.20	23.8	24.9	240	230	200	150		350	380	470	290	120
	5840-01	0.20	3.0	6.0					120				120	
	5840-04	0.15	6.0	6.0					1,100				1,100	
	5938-02	0.36	18.5	18.5						520	570	860	650	180
5938-03	0.36	12.2	14.5						380	420	580	460	110	
5938-04	0.38	23.2	23.2	390	440	260	200	730				400	200	
5939-02	0.15	3.0	12.0					150	240	280	130	200	70	
Honomanu/Kula Basalt	3925-01	0.20	9.3	9.3						860	950	1,500	1,100	320
	3926-11	0.15	3.0	4.5	790	630	700	490	420				610	150
	4026-13	0.15	2.7	3.6	810	760	920	770		2,000	2,200		1,200	670
	4125-02	0.25	6.4	9.4					140	360	400	480	350	140
	4126-03	0.30	6.4	6.7						1,900	2,100		2,000	170
	4226-13	0.30	6.1	6.5						390	440	760	530	200
	4226-15	0.15	6.1	9.7	520	460	780	510	1,300				720	370
	4226-17	0.15	2.4	2.8	450	340	380	240	2,200	560	630	1100	730	640
	4326-09	0.15	7.3	9.9	360	380	410	300	950	1,200	1,400	1,500	820	520
	4327-07	0.15	7.7	7.7	2,300	2,300	890	740					1,500	850
	4727-08	0.20	6.7	8.0	690	860	210	160					480	350
	4821-01	0.15	15.2	18.6	90	100	150	100					110	30
	4822-01	0.15	16.5	19.5	90	90	50	40	60				60	20
4824-01	0.30	13.1	15.6	240	180	80	60	2,200	810	890	1,200	700	740	

**Table A.1. (Continued)** Hydraulic conductivity estimates (m/d) of individual wells

Formation	Well No.	$r$	$b$	$L$	Theis	Cooper-Jacob	Harr $t = 10^4$	Harr $t = 10^6$	Recovery	Zangar	Polubarinova	Thomasson	$K^*$	$\sigma$
Honomanu/Kula Basalt	5129-03	0.25	12.2	13.6	350	370	130	120	1,100	240	270	370	370	320
	5220-01	0.41	16.3	16.3						530	590	930	680	210
	5230-03	0.51	33.2	35.8	510	710	210	180	210	270	300	400	350	180
	5317-01	0.46	37.8	41.8	90	90	30	30	540	240	270	330	200	180
	5320-01	0.30	9.8	10.0	1,500	1,600	2,100	1,400	2,000				1,700	290
	5320-02	0.15	5.8	8.6	1,200	1,200	700	580	140	1,100	1,200	1,300	920	410
	5327-10	0.36	12.5	29.9						390	430	290	370	70
	5328-52	0.15	6.1	20.3	160	70	300	190		890	990	470	440	370
	5329-15	0.15	6.1	14.0						380	420	290	360	70
	5329-19	0.25	9.1	11.1						580	640	860	690	140
	5329-20	0.25	9.1	12.6						200	220	260	230	30
	5329-21	0.36	6.1	11.0						170	190	210	190	20
	5417-01	0.15	4.6	23.7	170	210	720	540					410	270
	5419-01	0.30	12.2	13.8						1,400	1,500	2,100	1,700	390
	5420-01	0.20	6.4	7.7						2,300	2,600		2,400	190
	5420-02	0.30	10.4	14.7						830	930	1,100	940	120
	5424-08	0.15	4.3	4.5	80	140	210	120	700				250	260
	5424-09	0.15	6.1	7.2	40	50	30	20	20				30	10
	5426-01	0.15	2.7	9.4					20				20	
	5427-01	0.51	36.3	67.2						340	370	290	330	40
	5429-02	0.20	18.3	24.3	1	4	2	2		4	4	4	3	1
	5515-04	0.10	6.1	34.7	60	90	420	310					220	170
	5517-02	0.15	6.7	9.2	370	420	150	140	120				240	140
	5517-05	0.15	6.1	7.9	2,600	1,800	1,100	920	270				1,300	890
	5523-01	0.15	2.7	13.7	70	70	260	180	80				130	80
	5615-06	0.15	6.1	12.5					40				40	
	5616-02	0.10	6.1	13.6	40	60	130	90					80	40
	5616-05	0.15	6.5	9.2					30	280	310	340	240	140
	5617-05	0.15	6.4	8.3			2,300	2,000	1,100				1,800	660
	5620-04	0.15	6.7	8.6	2	2	3	2					2	1
	5620-05	0.15	5.8	9.4					290	380	420	410	370	60
	5620-06	0.15	6.1	7.5					130				130	

**Table A.1. (Continued)** Hydraulic conductivity estimates (m/d) of individual wells

Formation	Well No.	$r$	$b$	$L$	Theis	Cooper–Jacob	Harr $t = 10^4$	Harr $t = 10^6$	Recovery	Zangar	Polubarinova	Thomasson	$K^*$	$\sigma$
Sediment	4527-10	0.61	2.1	2.4	40	40	30	20					30	10
	4527-14	0.15	8.8	23.9	2	20	30	20	3				10	10
	5240-07	0.15	4.2	4.2	40	50	30	20	300	110	120	200	110	100
	5529-02	0.20	11.0	20.9	120	90	420	200					210	150
	5530-04	0.30	21.3	25.3					80	10	20	20	30	30
	5332-05	0.36	42.1	80.3	6	20	4	4	8	4	5	3	6	5
Dike Zone	4527-10	0.61	2.1	2.4	40	40	30	20					30	10

## 9. References

- Ahmed, S., and G. de Marsily. 1987. Comparison of geostatistical methods for estimating transmissivity using data on transmissivity and specific capacity. *Water Resources Research* 23, no. 9: 1717-1737.
- Ahmed, S., G. de Marsily, and A. Talbot. 1988. Combined use of hydraulic and electrical properties of an aquifer in a geostatistical estimation of transmissivity. *Ground Water* 26, no. 1: 78-86.
- Bissell, E.G., and S.S. Aichele. 2004. Geostatistical analysis of effective vertical hydraulic conductivity and presence of confining layers in the shallow glacial drift aquifer, Oakland County, Michigan. U.S. Geological Survey Scientific Investigations Report 2004-5167, 19 p.
- Brown, J., A. Collig, D. Park, J. Phillips, R. Dave, and J. Wright. 1989. *Waves, Tides and Shallow-Water Processes. The Open University Course Team*. Oxford: Butterworth and Heinemann, 187 p.
- Burbey, T.J. 2006. Three-dimensional deformation and strain induced by municipal pumping, Part 2: Numerical analysis. *Journal of Hydrology* 330, no. 3-4: 422-434.
- Butler, J.J. 2005. Hydrological methods for estimation of spatial variations in hydraulic conductivity. In *Hydrogeophysics*, ed. Y. Rubin and S. Hubbard. The Netherlands: Springer, p. 23-58.
- Caldwell, P.C. 2005. Validity of north shore, Oahu, Hawaiian Islands surf observations. *Journal of Coastal Research* 21, no. 6: 1127-1138.
- Carr, P.A., and G. Van der Kamp. 1969. Determining aquifer characteristics by the tidal method. *Water Resources Research* 5, no. 5: 1023-1031.

- Cartwright, N., T.E. Baldock, P. Nielsen, D.-S. Jeng, and L. Tao. 2006. Swash-aquifer interaction in the vicinity of the water table exit point on a sandy beach. *Journal of Geophysical Research* 111: C09035, doi:10.1029/2005JC003149.
- Chao, Y.Y., L.D. Burroughs, and H.L. Tolman. 2003. Wave forecasting for the Eastern North Pacific and adjacent waters. NWS/NCEP Technical Procedures Bulletin 491.
- Choi, B.S. 1999. [Determination of aquifer characteristics from specific capacity data of wells in Cheju Island]. *Journal of the Korean Society of Ground Water Environment* 6, no. 4: 180-187.
- Chuang, M.-H., and H.-D. Yeh. 2006. An analytical solution for the head distribution in a tidal leaky confined aquifer extending an infinite distance under the sea. *Advances in Water Resources* 30, no. 3: 439-445.
- Clark, I., and W.V. Harper. 2000. *Practical Geostatistics 2000*. Columbus, Ohio: Ecosse North America, 442 p.
- Clark, L. 1977. The analysis and planning of step-drawdown tests. *Quarterly Journal of Engineering Geology and Hydrogeology* 10, no. 2: 125-143.
- Clark, W.E. 1967. Computing the barometric efficiency of a well. *Journal of the Hydraulics Division, American Society of Civil Engineers* 93, no. HY4: 93-98.
- Coastal Data Information Program. 2005. CDIP Station 106, Set p1 - WAIMEA BAY, HI BUOY, <http://cdip.ucsd.edu/?sub=data&nav=historic&pub=public&stn=106&stream=p1> (accessed Dec. 12, 2005).

- Cooper, H.H., and C.E. Jacob. 1946. A generalized graphical method for evaluating formation constants and summarizing well-field history. *American Geophysical Union Transactions* 27, no. 4: 526-534.
- Cruz, J.V., and M.O. Silva. 2001. Hydrogeologic framework of Pico Island, Azores, Portugal. *Hydrogeology Journal* 9: 177-189.
- Dale, R.H. 1974. Relationship of groundwater tides to ocean tides: A digital simulation model. Ph.D. diss, Department of Geology and Geophysics, University of Hawaii, Honolulu, Hawaii, 150 p.
- Doherty, J.L. 2004. PEST: Model-independent parameter estimation, user manual: 5th edition. Watermark Numerical Computing, 336 p.
- Eagon, H.B., and D.E. Johe. 1972. Practical solutions for pumping tests in carbonate-rock aquifers. *Ground Water* 10, no. 4: 6-13.
- Eden, R.N., and C.P. Hazel. 1973. Computer and graphical analysis of variable discharge pumping tests of wells. *Civil Engineering Transactions, The Institution of Engineers, Australia*: 5-11.
- El-Kadi, A.I., and W. Brutsaert. 1985. Applicability of effective parameters for unsteady flow in heterogeneous aquifers. *Water Resources Research* 21, no. 2: 183-198.
- El-Kadi, A.I., and J.E.T. Moncur. 2006. The history of groundwater management and research in Hawaii. Proceedings of the Jeju-Hawaii Water Forum, July 21-22, 2006, Jeju, Korea, p. 222-241.
- Erskine, A.D. 1991. The effect of tidal fluctuation on a coastal aquifer in the UK. *Ground Water* 29, no. 4: 556-562.
- Fabbri, P. 1997. Transmissivity in the geothermal Euganean Basin: A geostatistical analysis. *Ground Water* 35, no. 5: 881-887.

- Ferris, J.G. 1951. Cyclic fluctuations of water level as a basis for determining aquifer transmissibility. *Association of International Hydrological Science* 2: 148-155.
- Fetter, C.W. 2000. *Applied Hydrogeology*. 4th ed: Prentice Hall, 691 p.
- Fierstein, E., and C.H. Fletcher. 2004. Hawaii. In *The World's Coasts: Online*, ed. E.C.F. Bird: Springer Publications, p. 42-50.
- Flater, D. 1998. XTide 2: Harmonic tide clock and tide predictor, <http://xtide.org/xtide> (accessed Oct. 12, 2005).
- Furumoto, A.S., J.F. Campbell, and D.M. Hussong. 1970. Seismic studies of subsurface structure in the Ewa coastal plain, Oahu, Hawaii. *Pacific Science* 24, no. 4: 529-542.
- Gibbs, A.E., B.M. Richmond, C.H. Fletcher, and K.P. Hillman. 2001. Hawaii beach monitoring program. U.S. Geological Survey Open-File Report 01-308, Version 1.0.
- Gingerich, S.B. 1999a. Estimating transmissivity and storage properties from aquifer tests in the southern Lihue basin, Kauai, Hawaii. U.S. Geological Survey Water-Resources Investigations Report 99-4066, 33 p.
- Gingerich, S.B. 1999b. Ground-water occurrence and contribution to streamflow, Northeast Maui, Hawaii. U.S. Geological Survey Water-Resources Investigations Report 99-4090, 69 p.
- Gingerich, S.B., and D.S. Oki. 2000. Ground water in Hawaii. U.S. Geological Survey Fact Sheet 126-00, 6 p.
- Gourlay, M.R. 1992. Wave set-up, wave run-up and beach water table: Interaction between surf zone hydraulics and groundwater hydraulics. *Coastal Engineering* 17: 93-144.

- Gourlay, M.R. 1994. Wave transformation on a coral reef. *Coastal Engineering* 23, no. 1: 17-42.
- Gregg, D.O. 1966. An analysis of ground-water fluctuations caused by ocean tides in Glynn County, Georgia. *Ground Water* 4, no. 3: 24-32.
- Guo, Q., H.L. Li, M.C. Boufadel, Y.Q. Xia, and G.H. Li. 2007. Tide-induced groundwater head fluctuation in coastal multi-layered aquifer systems with a submarine outlet-capping. *Advances in Water Resources* 30: 1746-1755, doi:10.1016/j.advwatres.2007.01.003.
- Guza, R.T., and E.B. Thornton. 1981. Wave set-up on a natural beach. *Journal of Geophysical Research* 86, no. C5: 4133-4137.
- Halford, K.J., W.D. Weight, and R.P. Schreiber. 2006. Interpretation of transmissivity estimates from single-well pumping aquifer tests. *Ground Water* 44, no. 3: 467-471.
- Hamm, S.-Y., J.-Y. Cheong, S. Jang, C.-Y. Jung, and B.-S. Kim. 2005. Relationship between transmissivity and specific capacity in the volcanic aquifers of Jeju Island, Korea. *Journal of Hydrology* 310: 111-121.
- Harbaugh, A.W., E.R. Banta, M.C. Hill, and M.G. McDonald. 2000. MODFLOW-2000, the U.S. Geological Survey modular ground-water model – User guide to modularization concepts and the ground-water flow process. U.S. Geological Survey Open-File Report 00-92, 121 p.
- Hardy, A.T., and I.R. Young. 1996. Field study of wave attenuation on an offshore coral reef. *Journal of Geophysical Research* 101, no. C6: 14311-14326.
- Harr, M.E. 1962. *Groundwater and Seepage*. New York: McGraw-Hill, 315 p.

- Hegge, B.J., and G. Masselink. 1991. Groundwater-table response to wave run-up: An experimental study from Western Australia. *Journal of Coastal Research* 7, no. 3: 623-634.
- Holman, R.A., and A.H. Sallenger, Jr. 1985. Setup and swash on a natural beach. *Journal of Geophysical Research* 90, no. C1: 945-953.
- Hunt, C.D., Jr. 1996. Geohydrology of the Island of Oahu, Hawaii. U.S. Geological Survey Professional Paper 1412-B, 54 p.
- Huntley, D., R. Nommensen, and D. Steffey. 1992. The use of specific capacity to assess transmissivity in fractured-rock aquifers. *Ground Water* 30, no. 3: 396-402.
- Izuka, S.K., and D.S. Oki. 2002. Numerical simulation of ground-water withdrawals in the Southern Lihue Basin, Kauai, Hawaii. U.S. Geological Survey Water-Resources Investigations Report 01-4200, 54 p.
- Jacob, C.E. 1940. On the flow of water in an elastic artesian aquifer. *American Geophysical Union Transactions* 2: 574-586.
- Jacob, C.E. 1947. Drawdown test to determine effective radius of artesian well. *Transactions of the American Society of Civil Engineers* 112, no. paper 2321: 1047-1064.
- Jacob, C.E. 1950. Flow of ground water. In *Engineering Hydraulics*, ed. H. Rouse. Hoboken, New Jersey: John Wiley, p. 321-386.
- Jalludin, M., and M. Razack. 2004. Assessment of hydraulic properties of sedimentary and volcanic aquifer systems under arid conditions in the Republic of Djibouti (Horn of Africa). *Hydrogeology Journal* 12, no. 2: 159-170.

- Jeng, D.-S., D.A. Barry, B.R. Seymour, P. Dong, and L. Li. 2005. Two-dimensional approximation for tide-induced watertable fluctuations in a sloping sandy beach. *Advances in Water Resources* 28, no. 10: 1040-1047.
- Jeng, D.-S., L. Li, and D.A. Barry. 2002. Analytical solution for tidal propagation in a coupled semi-confined/phreatic coastal aquifer. *Advances in Water Resources* 25: 577-584.
- Jiao, J.J., and Z. Tang. 1999. An analytical solution of groundwater response to tidal fluctuation in a leaky confined aquifer. *Water Resources Research* 35, no. 3: 747-751.
- Kollet, S.J., and V.A. Zlotnik. 2005. Influence of aquifer heterogeneity and return flow on pumping test data interpretation. *Journal of Hydrology* 300: 267-285.
- Kruseman, G.P., and N.A. de Ridder. 1991. *Analysis and Evaluation of Pumping Test Data*. 2nd ed. Wageningen, The Netherlands: International Institute for Land Reclamation and Improvement, 377 p.
- Langenheim, V.M., and D.A. Clague. 1987. The Hawaiian-Emperor volcanic chain, Part II, Stratigraphic framework of volcanic rocks of the Hawaiian Islands, Chap. 1. In *Volcanism in Hawaii*, ed. R.W. Decker, T.L. Wright and P.H. Stauffer. Washington: U.S. Geological Survey Professional Paper 1350, vol. 1, p. 55-84.
- Lau, L.S., and J.F. Mink. 2006. *Hydrology of the Hawaiian Islands*. Honolulu: University of Hawaii Press, 274 p.
- Lebbe, L., and W. De Breuck. 1995. Validation of an inverse numerical model for interpretation of pumping tests and a study of factors influencing accuracy of results. *Journal of Hydrology* 172: 61-85.

- Lennox, D.H. 1966. Analysis and application of step-drawdown test. *Hydraulics Division, Proceedings of the American Society of Civil Engineers* HY6: 25-48.
- Li, G., and C.-H. Chen. 1991. Determining the length of confined aquifer roof extending under the sea by the tidal method. *Journal of Hydrology* 123: 97-104.
- Li, H.L., and J.J. Jiao. 2001. Tide-induced groundwater fluctuation in a coastal leaky confined aquifer system extending under sea. *Water Resources Research* 37, no. 5: 1165-1171.
- Li, H.L., and J.J. Jiao. 2002. Analytical solutions of tidal groundwater flow in coastal two-aquifer system. *Advances in Water Resources* 25: 417-426.
- Li, H.L., and J.J. Jiao. 2003. Influence of the tide on the mean watertable in an unconfined, anisotropic, inhomogeneous coastal aquifer. *Advances in Water Resources* 26, no. 1: 9-16.
- Li, H.L., J.J. Jiao, M. Luk, and K. Cheung. 2002. Tide-induced groundwater level fluctuation in coastal aquifers bounded by an L-shaped coastline. *Water Resources Research* 38, no. 3: 1024, doi:10.1029/2001WR000556.
- Li, H.L., G. Li, J. Cheng, and M.C. Boufadel. 2007. Tide-induced head fluctuations in a confined aquifer with sediment covering its outlet at the sea floor. *Water Resources Research* 43: W03404, doi:10.1029/2005WR004724.
- Li, L., and D.A. Barry. 2000. Wave-induced beach groundwater flow. *Advances in Water Resources* 23: 325-337.
- Li, L., D.A. Barry, C. Cunningham, F. Stagnitti, and J.-Y. Parlange. 2000. A two-dimensional analytical solution of groundwater responses to tidal loading in an estuary and ocean. *Advances in Water Resources* 23: 825-833.

- Li, L., D.A. Barry, J.-Y. Parlange, and C.B. Pattiaratchi. 1997. Beach water table fluctuations due to wave run-up: Capillarity effects. *Water Resources Research* 33, no. 5: 935-945.
- Liu, C.C.K. 2006. Analytical groundwater flow and transport modelling for the estimation of sustainable yield of Pearl Harbor Aquifer. University of Hawaii, Water Resources Resources Center, Project Report PR-2006-06, 53 p.
- Logan, J. 1964. Estimating transmissibility from routine production tests of water wells. *Ground Water* 2, no. 1: 35-37.
- Longuet-Higgins, M.S., and R.W. Stewart. 1962. Radiation stress and mass transport in gravity waves with application to surf beats. *Journal of Fluid Mechanics* 13: 481-504.
- Longuet-Higgins, M.S., and R.W. Stewart. 1963. A note on wave set-up. *Journal of Marine Research* 21: 4-10.
- Lugo-Fernandez, A., H.H. Roberts, and J.N. Suhayda. 1998. Wave transformations across a Caribbean fringing-barrier coral reef. *Continental Shelf Research* 18, no. 10: 1099-1124.
- Macdonald, G.A., A.T. Abbott, and F.L. Peterson. 1983. *Volcanoes in the sea: The geology of Hawaii*. 2nd ed. Honolulu, Hawaii: University of Hawaii Press, 517 p.
- Mace, R.E. 1997. Determination of transmissivity from specific capacity test in a karst aquifer. *Ground Water* 35, no. 5: 738-742.
- Massel, S.R. 2001. Circulation of groundwater due to wave set-up on a permeable beach. *Oceanologia* 43, no. 3: 279-290.
- McDougall, I. 1964. Potassium-argon ages from lavas of the Hawaiian Islands. *Geological Society of America Bulletin* 75: 107-128.

- Merritt, M.L. 2004. Estimating hydraulic properties of the Floridan aquifer system by analysis of earth-tide, ocean-tide, and barometric effects, Collier and Hendry Counties, Florida. U.S. Geological Survey Water-Resources Investigations Report 03-4267, 70 p.
- Meyer, W., and T.K. Presley. 2000. The response of the Iao aquifer to ground-water development, rainfall, and land-use practices between 1940 and 1998, Island of Maui, Hawaii. U.S. Geological Survey Water-Resources Investigations Report 00-4223, 60 p.
- Meyer, W., and W.R. Souza. 1995. Factors that control the amount of water that can be diverted to wells in a high-level aquifer. In *Water resources and environmental hazards: Emphasis on hydrologic and cultural insight in the Pacific Rim*, ed. R. Hermann, W. Back, R.C. Sidle and A.I. Johnson. Honolulu, Hawaii: Proceedings of the American Water Resources Association Annual Summer Symposium, June 25-28, p. 207-216.
- Mink, J.F. 1981. Determination of sustainable yields in basal aquifer. In *Groundwater in Hawaii - A Century of Progress*, ed. F.N. Fujimura and W.B.C. Chang. Honolulu: University of Hawaii, Water Resources Research Center, p. 101-116.
- Mink, J.F., and L.S. Lau. 1980. Hawaii groundwater geology and hydrology, and early mathematical models. University of Hawaii, Water Resources Research Center Technical Report 62, 74 p.
- Mogg, J.L. 1969. Step-Drawdown Test Needs Critical Review. *Ground Water* 17, no. 1: 28-34.
- National Climatic Data Center. 2005. Unedited local climatological data - OGG Kahului Airport, <http://cdo.ncdc.noaa.gov/ulcd/ULCD> (accessed 25 Jan., 2006).

- National Oceanographic & Atmospheric Administration. 2005. Tides and currents, data retrieval of historic tide data,  
[http://tidesandcurrents.noaa.gov/data\\_menu.shtml?stn=1615680%20Kahului,%20HI&type=Historic%20Tide%20Data](http://tidesandcurrents.noaa.gov/data_menu.shtml?stn=1615680%20Kahului,%20HI&type=Historic%20Tide%20Data) (accessed Mar. 18, 2006).
- Naughton, J.J., G.A. Macdonald, and V.A. Greenberg. 1980. Some additional potassium-argon ages of Hawaiian rocks: the Maui Volcanic Complex of Molokai, Maui, Lanai and Kahoolawe. *Journal of Volcanology and Geothermal Research* 7: 339-355.
- Nichols, W.D., P.J. Shade, and C.D. Hunt, Jr. 1996. Summary of the Oahu, Hawaii, Regional Aquifer-System Analysis. U.S. Geological Survey Professional Paper 1412-A, 61 p.
- Nielsen, P. 1989. Wave setup and runup: An integrated approach. *Coastal Engineering* 13, no. 1: 1-9.
- Oki, D.S. 1997. Modeling the effects of pumping, barometric pressure and ocean tides on ground-water levels in northern Oahu, Hawaii. Ph.D. diss., Department of Geology and Geophysics, University of Hawaii, Honolulu, Hawaii, 321 p.
- Oki, D.S. 1998. Geohydrology of the Central Oahu, Hawaii, Ground-Water Flow System and Numerical Simulation of the Effects of Additional Pumping. U.S. Geological Survey Water-Resources Investigations Report 97-4276, 132 p.
- Oki, D.S. 1999. Geohydrology and numerical simulation of the ground-water flow system of Kona, Island of Hawaii. U.S. Geological Survey Water-Resources Investigations Report 99-4073, 70 p.
- Oki, D.S. 2002. Reassessment of ground-water recharge and simulated ground-water availability for the Hawi area of north Kohala, Hawaii. U.S. Geological Survey Water-Resources Investigations Report 02-4006, 62 p.

- Oki, D.S. 2005. Numerical simulation of the effects of low-permeability valley-fill barriers and the redistribution of ground-water withdrawals in the Pearl Harbor area, Oahu, Hawaii. U.S. Geological Survey Science Investigations Report 2005-5253, 111 p.
- Oki, D.S. 2006. Numerical simulation of the hydrologic effects of redistributed and additional ground-water withdrawal, Island of Molokai, Hawaii. U.S. Geological Survey Scientific Investigations Report 2006-5177, 49 p.
- Pavelko, M.T. 2004. Estimates of hydraulic properties from a one-dimensional numerical model of vertical aquifer-system deformation, Lorenzi Site, Las Vegas, Nevada. U.S. Geological Survey Water-Resources Investigations Report 03-4083, 36 p.
- Pawlowicz, R., B. Beardsley, and S. Lentz. 2002. Classical tidal harmonic analysis including error estimates in MATLAB using T\_TIDE. *Computers and Geosciences* 28: 929-937.
- Peterson, F.L. 1972. Water development on tropical volcanic islands, type example: Hawaii. *Ground Water* 10, no. 5: 18-23.
- Peterson, F.L. 1993. Hydrogeology of volcanic oceanic islands. In *Selected Papers on Environmental Hydrogeology - Hydrogeology, Selected Pap 4, IAH*, ed. Y. Sakura. Hannover: Heise, p. 163-171.
- Polubarinova-Kochina, P.Y. 1962. *Theory of Ground Water Movement*. Princeton: Princeton University Press, 613 p.
- Raubenheimer, B., R.T. Guza, and S. Elgar. 2001. Field observations of wave-driven setdown and setup. *Journal of Geophysical Research* 106, no. C3: 4629-4638.
- Razack, M., and D. Huntley. 1991. Assessing transmissivity from specific capacity in a large and heterogeneous alluvial aquifer. *Ground Water* 29, no. 6: 856-861.

- Razack, M., and T. Lasm. 2006. Geostatistical estimation of the transmissivity in a highly fractured metamorphic and crystalline aquifer (Man-Danane region, western Ivory Coast). *Journal of Hydrology* 325, no. 1-4: 164-178.
- Rorabaugh, M.J. 1953. Graphical and theoretical analysis of stepdrawdown test of artesian well. *Proceedings of the American Society of Civil Engineers* 79, no. separate no. 362: 1-23.
- Rotzoll, K., and A.I. El-Kadi. 2007. Numerical ground-water flow simulation for Red Hill fuel storage facilities, NAVFAC Pacific, Oahu, Hawaii. University of Hawaii & Water Resources Research Center, prepared for TEC Inc., 74 p.
- Serfes, M.E. 1991. Determining the mean hydraulic gradient of ground water affected by tidal fluctuations. *Ground Water* 29, no. 4: 549-555.
- Smith, A.J., and W.P. Hick. 2001. Hydrogeology and aquifer tidal propagation in Cockburn Sound, Western Australia. CISRO Land and Water Technical Report 06/01, 48 p.
- Soroos, R.L. 1973. Determination of hydraulic conductivity of some Oahu aquifers with step-drawdown test data. M.Sc. thesis, Department of Geology and Geophysics, University of Hawaii, Honolulu, Hawaii, 239 p.
- Souza, W.R., and C.I. Voss. 1987. Analysis of an anisotropic coastal aquifer system using variable-density flow and solute transport simulation. *Journal of Hydrology* 92: 17-41.
- Spane, F.A. 2002. Considering barometric pressure in groundwater flow investigations. *Water Resources Research* 38, no. 6: 1078, doi:10.1029/2001WR000701.

- State of Hawaii. 2000. The State of Hawaii data book 2000, a statistical abstract. The State of Hawaii, The Department of Business, Economic Development & Tourism, <http://www.hawaii.gov/dbedt/db00/> (accessed Aug. 30, 2005).
- Stearns, H.T., and G.A. Macdonald. 1942. Geology and ground-water resources of the island of Maui, Hawaii. Hawaii Division of Hydrography Bulletin 1, 344 p.
- Stockdon, H.F., R.A. Holman, P.A. Howd, and A.H. Sallenger, Jr. 2006. Empirical parameterization of setup, swash, and runup. *Coastal Engineering* 53: 573-588.
- Sun, H. 1997. A two-dimensional analytical solution of groundwater response to tidal loading in an estuary. *Water Resources Research* 33: 1429-1435.
- Tait, R.J. 1972. Wave set-up on coral reefs. *Journal of Geophysical Research* 77, no. 12: 2207-2211.
- Takasaki, K.J. 1972. Preliminary report on the water resources of central Maui. Department of Land and Natural Resources, Division of Water and Land Development Circular C62, 59 p.
- Takasaki, K.J., and J.F. Mink. 1982. Water resources of southeastern Oahu, Hawaii. U.S. Geological Survey Water-Resources Investigations 82-628, 89 p.
- Takasaki, K.J., and J.F. Mink. 1985. Evaluation of major dike-impounded ground-water reservoirs, Island of Oahu. U.S. Geological Survey Water-Supply Paper 2217, 77 p.
- Theis, C.V. 1935. The relation between the lowering of the piezometric surface and the rate and duration of discharge of a well using groundwater storage. *American Geophysical Union Transactions* 16: 519-524.
- Thiem, G. 1906. *Hydrologische Methoden*. Leipzig: Gebhardt, J.M., 56 p.

- Thomasson, H.G., F.H. Olmsted, and E.F. LeRoux. 1960. Geology, water-resources and usable ground-water storage capacity of part of Solano County, California. U.S. Geological Survey Water-Supply Paper 1464, 693 p.
- Thompson, E.F., and Z. Demirbilek. 2002. Wave climate and wave response, 2025 plan, Kahului Harbor, Maui, Hawaii. U.S. Army Engineer District, Honolulu Final Report ERDC/CHL TR-02-21, 75 p.
- Thompson, E.F., L.L. Hadley, W.A. Brandon, D.D. McGehee, and J.M. Hubertz. 1996. Wave response of Kahului Harbor, Maui, Hawaii. U.S. Army Engineer Division, Pacific Ocean Technical Report CERC-96-11, 224 p.
- Todd, D.K. 1980. *Groundwater Hydrology*. 2nd ed. New York: John Wiley and Sons, 535 p.
- Todd, D.K., and L.W. Mays. 2004. *Groundwater Hydrology*. 3rd ed. New York: John Wiley and Sons, 656 p.
- Townley, L.R. 1995. The response of aquifers to periodic forcing. *Advances in Water Resources* 18, no. 3: 125-146.
- Trefry, M.G. 1999. Periodic forcing in composite aquifers. *Advances in Water Resources* 22, no. 6: 645-656.
- Trefry, M.G., and E. Bekele. 2004. Structural characterization of an island aquifer via tidal methods. *Water Resources Research* 40: W01505, doi:10.1029/2003WR002003.
- Turcotte, D.L., and G. Schubert. 2002. *Geodynamics*. 2 ed. Cambridge: Cambridge University Press, 456 p.
- Turner, I.L. 1998. Monitoring groundwater dynamics in the littoral zone at seasonal, storm, tide and swash frequencies. *Coastal Engineering* 35: 1-16.

- Turner, I.L., B.P. Coates, and R.I. Acworth. 1997. Tides, waves and the super-elevation of groundwater at the coast. *Journal of Coastal Research* 13, no. 1: 46-60.
- Uhl, V.W.J., V.G. Joshj, A. Alpheus, and G. Sharma. 1975. The application of step-drawdown pumping tests for determining well losses in consolidated rock aquifers. *Hydrology and Water Resources in AZ and the Southwest* 5: 133-146.
- Van der Kamp, G. 1972. Tidal fluctuations in a confined aquifer extending under the sea. *International Geological Congress* 24, no. 11: 101-106.
- Vetter, O.J. 2007. Field observations of setup over two fringing reefs: Ipan reef, Guam and Mokuleia reef, Hawaii. M.Sc. thesis, Department of Oceanography, University of Hawaii, Honolulu, Hawaii, 71 p.
- Visher, F.N., and J.F. Mink. 1964. Ground-Water Resources in Southern Oahu, Hawaii. U.S. Geological Survey Water-Supply Paper 1778, 133 p.
- Weeks, E.P. 1979. Barometric fluctuations in wells tapping deep unconfined aquifers. *Water Resources Research* 15, no. 5: 1167-1176.
- Wentworth, C.K. 1938. Geology and ground-water resources of the Palolo-Waialae district. Board of Water Supply, 274 p.
- Wentworth, C.K. 1951. Geology and ground-water resources of the Honolulu-Pearl Harbor area, Oahu, Hawaii. Board of Water Supply, 111 p.
- Werner, P.W., and D. Norén. 1951. Progressive waves in non-artesian aquifers. *American Geophysical Union Transactions* 32, no. 2: 239-244.
- Whittier, R.B., K. Rotzoll, S. Dhal, A.I. El-Kadi, C. Ray, G. Chen, and D. Chang. 2004. Hawaii Source Water Assessment Program Report. Hawaii Dept. of Health, 103 p.

- Williams, J.A., and T.C. Liu. 1975. Response to tides of coastal aquifers: Analog simulation vs. field observation. University of Hawaii, Water Resources Research Center, Technical Report 86, 67 p.
- Williams, J.A., and R.L. Soroos. 1973. Evaluation of methods of pumping test analysis for application to Hawaiian aquifers. University of Hawaii, Water Resources Research Center, Technical Report 70, 159 p.
- Wolansky, R.M., and M.A. Corall. 1985. Aquifer tests in west-central Florida. U.S. Geological Survey Water-Resources Investigations Report 84-4044, 127 p.
- Wu, C.-M., T.-C.J. Yeh, J. Zhu, T.H. Lee, N.-S. Hsu, C.-H. Chen, and A.F. Sancho. 2005. Traditional analysis of aquifer tests: Comparing apples to oranges? *Water Resources Research* 41, no. W09402: doi:10.1029/2004WR003717.
- Xia, Y.Q., H.L. Li, M.C. Boufadel, and G. Li. 2007. Tidal wave propagation in a coastal aquifer: Effects of leakages through its submarine outlet-capping and offshore roof. *Journal of Hydrology* 337: 249-257, doi:10.1016/j.jhydrol.2007.01.036.
- Yeh, T.C.J. 1989. One-dimensional steady state infiltration in heterogeneous soils. *Water Resources Research* 25, no. 10: 2149-2158.
- Zangar, C.N. 1953. Theory and problems of water percolation. U.S.D.I., Bureau of Reclamation Engineering Monograph No. 8, 76 p.